

Lawrence Berkeley National Laboratory

Recent Work

Title

Berkeley, Proton Linear Accelerator

Permalink

<https://escholarship.org/uc/item/7921w42w>

Authors

Alvarez, L.W.

Bradner, H.

Gordon, H.

et al.

Publication Date

1948-11-30

ULCRL-236

LEGAL NOTICE

This report was prepared as an account of work sponsored by the United States Government. Neither the United States nor the Department of Energy, nor any of their employees, nor any of their contractors, subcontractors, or their employees, makes any warranty, express or implied, or assumes any legal liability or responsibility for the accuracy, completeness or usefulness of any information, apparatus, product or process disclosed, or represents that its use would not infringe privately owned rights.

DISCLAIMER

This document was prepared as an account of work sponsored by the United States Government. While this document is believed to contain correct information, neither the United States Government nor any agency thereof, nor the Regents of the University of California, nor any of their employees, makes any warranty, express or implied, or assumes any legal responsibility for the accuracy, completeness, or usefulness of any information, apparatus, product, or process disclosed, or represents that its use would not infringe privately owned rights. Reference herein to any specific commercial product, process, or service by its trade name, trademark, manufacturer, or otherwise, does not necessarily constitute or imply its endorsement, recommendation, or favoring by the United States Government or any agency thereof, or the Regents of the University of California. The views and opinions of authors expressed herein do not necessarily state or reflect those of the United States Government or any agency thereof or the Regents of the University of California.

0 0 1 0 0 6 0 5 4 7 9

UCRL 236

UNIVERSITY OF
CALIFORNIA

*Radiation
Laboratory*

FOR REFERENCE

NOT TO BE TAKEN FROM THIS ROOM

BERKELEY, CALIFORNIA

UNCLASSIFIED

00100605480

UCRL-236

Administrative-General

Copy 3

UNIVERSITY OF CALIFORNIA

Radiation Laboratory

Contract No. W-7405-eng-48

BERKELEY PROTON LINEAR ACCELERATOR

Luis W. Alvarez, Hugh Bradner, Hayden Gordon,
Wolfgang K. H. Panofsky, Chaim Richman, John R. Woodyard

CAUTION

This document contains information affecting the
National Defense of the United States within the
meaning of the Espionage Laws, Title 18, U.S.C.,
its transmission or the disclosure of its contents
in any manner to an unauthorized person is
prohibited and may result in severe criminal
penalties or application of Federal

Berkeley, California

BERKELEY PROTON LINEAR ACCELERATOR

By Luis W. Alvarez, Hugh Bradner, Hayden Gordon,
Wolfgang K. H. Panofsky, Chaim Richman, John R. Woodyard

November 30, 1948

Radiation Laboratory and Department of Physics
University of California
Berkeley, California

ABSTRACT

A linear accelerator, which increases the energy protons from a 4 Mev Van de Graaff injector, to a final energy of $32.0 \pm .1$ Mev, has been constructed. The accelerator consists of a cavity 40 feet long and 39 inches in diameter, excited at resonance in a longitudinal electric mode with a radio-frequency power of about 2.5×10^6 watts peak at 202.5 mc. Acceleration is made possible by the introduction of 46 axial "drift tubes" into the cavity, which is designed such that the particles traverse the distance between the centers of successive tubes in one cycle of the r.f. power. The protons are longitudinally stable as in the synchrotron, and are stabilized transversely by the action of converging fields produced by focusing grids. The electrical cavity is constructed like an inverted airplane fuselage and is supported in a vacuum tank. Power is supplied by 25 high powered oscillators fed from a pulse generator of the artificial transmission line type. Output currents are 4×10^{-9} ampere average, and 1 μ A peak. The beam has a diameter of 3 mm and an angular divergence of 10^{-3} radians.

TABLE OF CONTENTS

I. Introduction	Page 3
II. Cavity Design	7
III. Beam Dynamics	16
IV. Mechanical Design	24
V. Oscillators	38
VI. Power System	45
VII. Electronic Accessories	50
VIII. Accessory Equipment	61
IX. Performance	64
X. Acknowledgments	65

0 0 1 0 0 6 0 5 4 8 4

BERKELEY PROTON LINEAR ACCELERATOR

by Luis W. Alvarez, Hugh Bradner, Hayden Gordon,
Wolfgang K. H. Panofsky, Chaim Richman, John R. Woodyard

November 30, 1948

I. INTRODUCTION

(1) Historical Summary - There was general agreement among physicists before the war that radio frequency linear accelerators of the Sloan-Lawrence¹⁾ type were of historical interest only. This feeling arose largely because the cyclotron was found to be such a reliable device, with beam intensities far beyond the most optimistic hopes of its originators. At the same time, it was realized that to make a competitive linear accelerator for protons or deuterons would require far higher power than was then available at very short wavelengths. Although r.f. linear accelerators are responsible for our present knowledge of the production of X-rays by high speed heavy ions, they have played no part in increasing our knowledge of the nucleus. (Kinsey²⁾ reports that high speed Li ions impinging on hydrogenous material give the well-known alpha-particles first observed by Cockcroft and Walton.)

Interest in linear accelerators was revived toward the end of the war for several reasons. Pressing military need had led to the development of vacuum tubes capable of producing megawatts of pulsed r.f. power down to the microwave range. The main technical bars to the construction of linear accelerators for electrons and light nuclei were thus removed.

But there would probably have been no great post-war interest in linear accelerators if the availability of the tools had been the only factor involved. It had been apparent for some time that there was an upper energy limit for particles accelerated by a cyclotron. The 184" cyclotron was originally designed with the purpose of extending that limit as far as possible, but the goal was only about 100 Mev deuterons, even though a dee voltage in the neighborhood of 1.5×10^6 was to be used.

Since no significant theoretical limit is apparent for linear accelerators, it was felt that they should be reinvestigated as a means of reaching energies in excess of 100 Mev. Similar reasoning was applied to the electron case, where the betatron was known to have an energy limit only a few times greater than the cyclotron. No electron linear accelerators had been built before the war, but a description of the type now under construction in a number of laboratories was given in 1941 by D. H. Sloan.³⁾ Such accelerators have been treated in detail by several authors,⁴⁾ and as they present quite different problems, they will not be discussed in this article on proton accelerators.

The situation as outlined above was drastically altered in 1945 by the introduction of the synchrotron concept.⁵⁾ In principle this removed the cyclotron upper limit, and raised it considerably in the betatron case to about 1,000 Mev. Clearly the linear accelerator must have had some other apparent advantage to have remained in the picture. Although recent studies have shown that the original arguments for undertaking the construction of a proton linear accelerator were not basic, the state of the art at that time did not allow them to be contradicted in a convincing manner.

The argument was essentially as follows: The cost of a relativistic magnetic accelerator varies roughly as the cube of the energy, so long as the basic design is merely scaled in its linear dimension, proportional to the energy. On the other hand, the cost of a linear accelerator varies directly as the first power of the energy. If these cost vs. energy curves are plotted on logarithmic paper, they will clearly be straight lines with slopes three and one. There will always be an intersection of the two lines and for energies greater than the "cross-over" energy, the cost of a linear machine will be less than that of the circular machine. Since the cost of either machine is quite high in this region, it was felt that even though a linear accelerator might be more complex than a synchro-cyclotron, the design decision might have to be made on economic grounds.

The new consideration which has altered our thinking in this matter is that

beyond a certain energy, the magnetic machines can be changed in basic design. Instead of accelerating with constant field and changing radius, these two conditions are reversed. The important change is that a ring magnet can then be used. This ring-shaped magnetic machine, which is really a proton synchrotron, was proposed by Oliphant in 1944, before the work of Veksler and McMillan, but it was generally felt until recently, in this country, that although Oliphant's plan was most attractive in many ways, so many unsolved and serious problems were involved in its practical realization that other alternative methods of attaining high energy protons should be explored. Within the past year, critical examination of the whole question by two groups in this country has shown that without question, all the problems are solvable. Therefore, both the Radiation Laboratory and the Brookhaven National Laboratory are starting to construct such machines.

To see how this factor alters the economic conclusions originally reached, it can be shown that just as the "magnetic cost line" is about to cross the "linear cost line," the former drops to a much lower cost value for the same energy, and then rises again with slope equal to three. The arguments of dimensional analysis are still theoretically sound; there will still be a crossover at higher energies. But long before this point is reached, the cost of either machine is so high that both are excluded in economic grounds.

In the fall of 1945, we started the design of a "pilot model" proton linear accelerator to explore the possibilities of the method. No plans were made for extending the length of the machine beyond the original 40 feet, but it was assumed that this question would be explored after successful operation of the first section. If at that time it appeared wise to continue on to higher energies, such a decision could then be made. In view of the present status of the proton synchrotron plans, it is obvious that no major extension should now be attempted. But it should be pointed out that at the present time, we know of no technical reason which makes this extension impossible or even difficult.

For the moment, then, we are concentrating on using the 40 foot accelerator as

a research tool. An intensive study of proton-proton scattering is now under way, using the highly collimated, small diameter (3 mm) beam of 32 Mev protons, which is conveniently available outside the accelerator tank.

The proton accelerator is thus at present being used in this laboratory not as a means to reach extremely high energies, but as a research tool, similar to the electrostatic machines at lower energies, which permits experiments to be carried out in which precise collimation of beam, low background and energy homogeneity are desirable.

(2) General Design Characteristics - The general design characteristics pertaining to linear accelerators has recently been discussed in detail by Slater.⁶⁾ In particular, Slater points out that the attainable voltage V of a linear accelerator of length l being fed at a peak power P is given by:

$$V = K P^{1/2} l^{1/2} \lambda^{-1/4} \quad (1)$$

where λ is the free-space wavelength. The constant K depends on the detailed geometrical arrangement and numerical values for the Berkeley accelerator will be discussed later. A linear accelerator contains essentially different types of equipment whose cost is proportional either to: (a) length, (b) peak power, (c) average power, (d) energy per pulse. All these factors affect the choice of wavelength, length of the machine, and duty cycle of operation. The pulse length of a resonant accelerator τ must be of the order of:

$$\tau \propto l \propto \lambda^{3/2} \quad (2)$$

in order to permit full build-up of fields; in terms of energy/pulse U , Eq. (1) therefore becomes:

$$V = K l U^{1/2} l^{1/2} \lambda^{-1}$$

The wavelength dependence of power requirement for a given voltage is therefore small ($\lambda^{1/2}$), but the wavelength dependence of energy per pulse, on which the cost of the pulse equipment depends, is large (λ^2). From the latter point of view particularly, it is therefore desirable to choose a small wavelength. This desire has to be compromised into the physical design of the cavity structure as compared to the expected beam diameter. In this design, a wavelength of $\lambda \approx 150$ cm has

been chosen, partially because of the availability of equipment and partially because of the large geometrical apertures permissible. Even if no equipment limitations existed, wavelengths shorter than 75 cm appear to be unsuited to this type of accelerator, owing to excessively diminished aperture. In addition, it must be remembered that the "electrical length" of the machine for a given length increases with decreasing wavelength and hence the mode separations decrease and tolerances become more stringent.

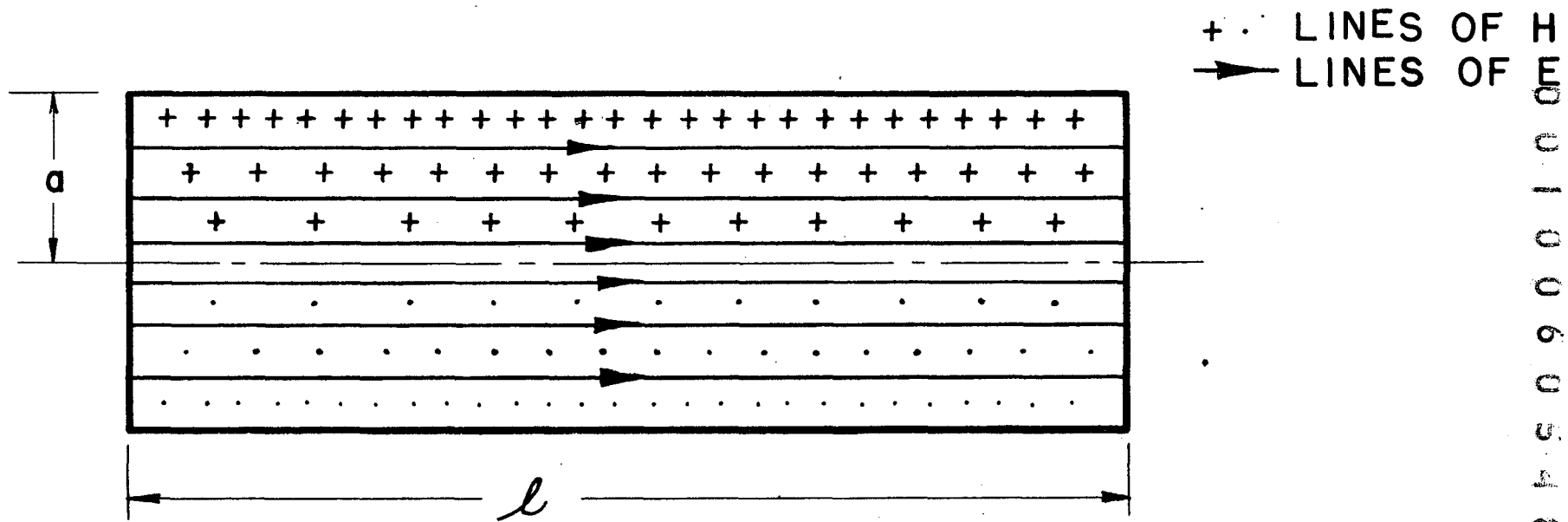
It might appear as if the balance between length and power would be made by matching the cost of the length proportional items and the power (or energy) proportional items. Actually in this and all other machines under design, as much power per unit length is applied as is feasible, compatible with electrical breakdown or available power sources. For a machine of the type discussed here, this limitation permits voltage gains only of about two to three million volts per meter. At high energies, higher energy gains per unit length appear feasible.

The choice of duty cycle is dictated by considerations of power consumption, cavity cooling, and tube power dissipation. Increase in repetition rate will not increase the cost of the pulse equipment; the pulse length is therefore chosen to give a duration of the pulse equal to several "build-up times"; the repetition rate is then chosen in accordance with available power.

The injection energy in the Berkeley accelerator was chosen as 4 Mev. The reason for this choice was twofold: (1) 4 Mev is a reasonable voltage to attain with an electrostatic generator and the construction of such a machine was desirable at this laboratory as a general research tool. (2) At the time of design, it was intended to accomplish focusing by means of thin beryllium foils.⁷⁾ Multiple scattering in these foils⁸⁾ made it necessary to choose a high injection energy. It appears now feasible to consider design at a considerably lower injection energy, possibly in the neighborhood of 500 KV. The lower limit of injection energy is set by limitations of cavity geometry and possible electron multiplication effects.

II. CAVITY DESIGN

(1) Basic Geometry - A linear accelerator for protons starting from low



684509001000

Fig. 1 Long Cylindrical Cavity Excited in Axial Electric 010 (TM_{010}) Mode

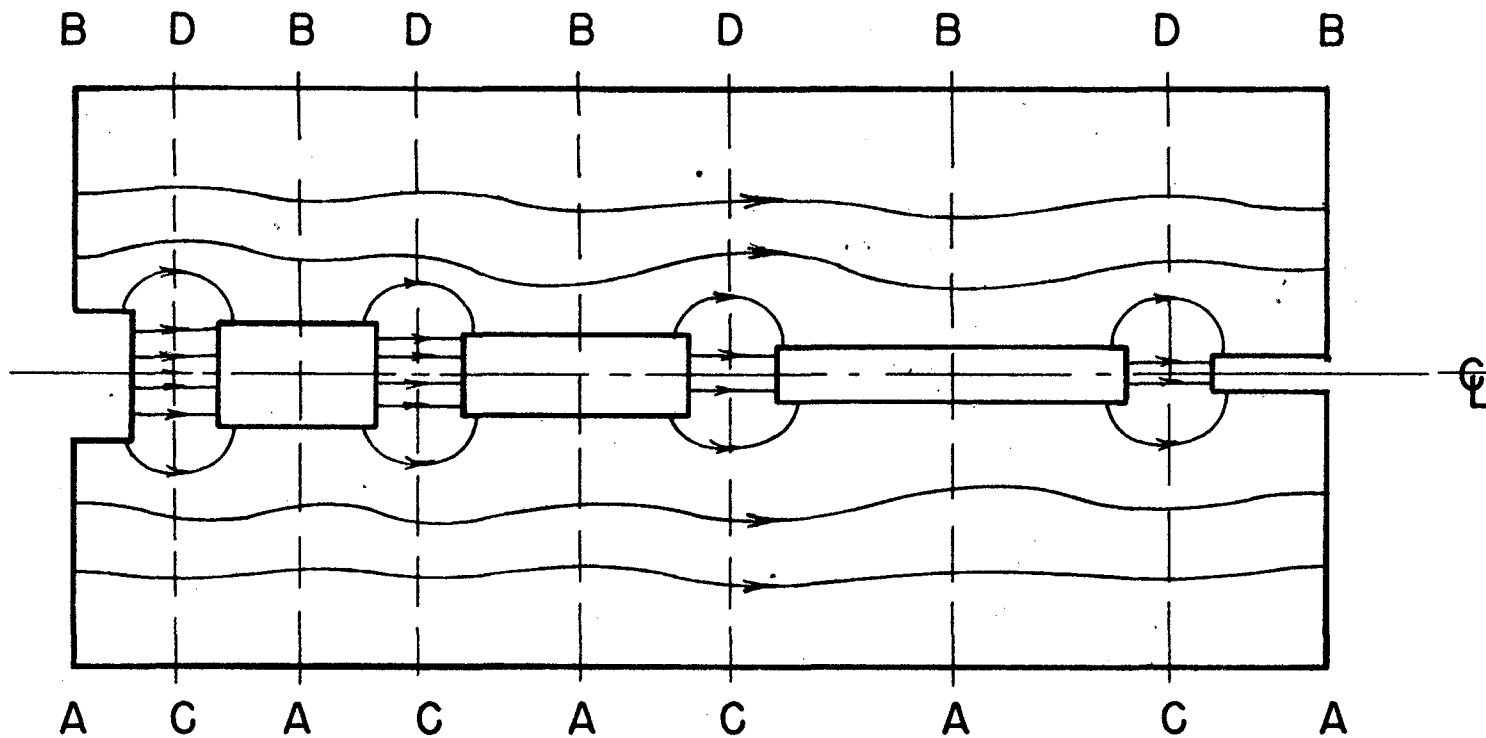
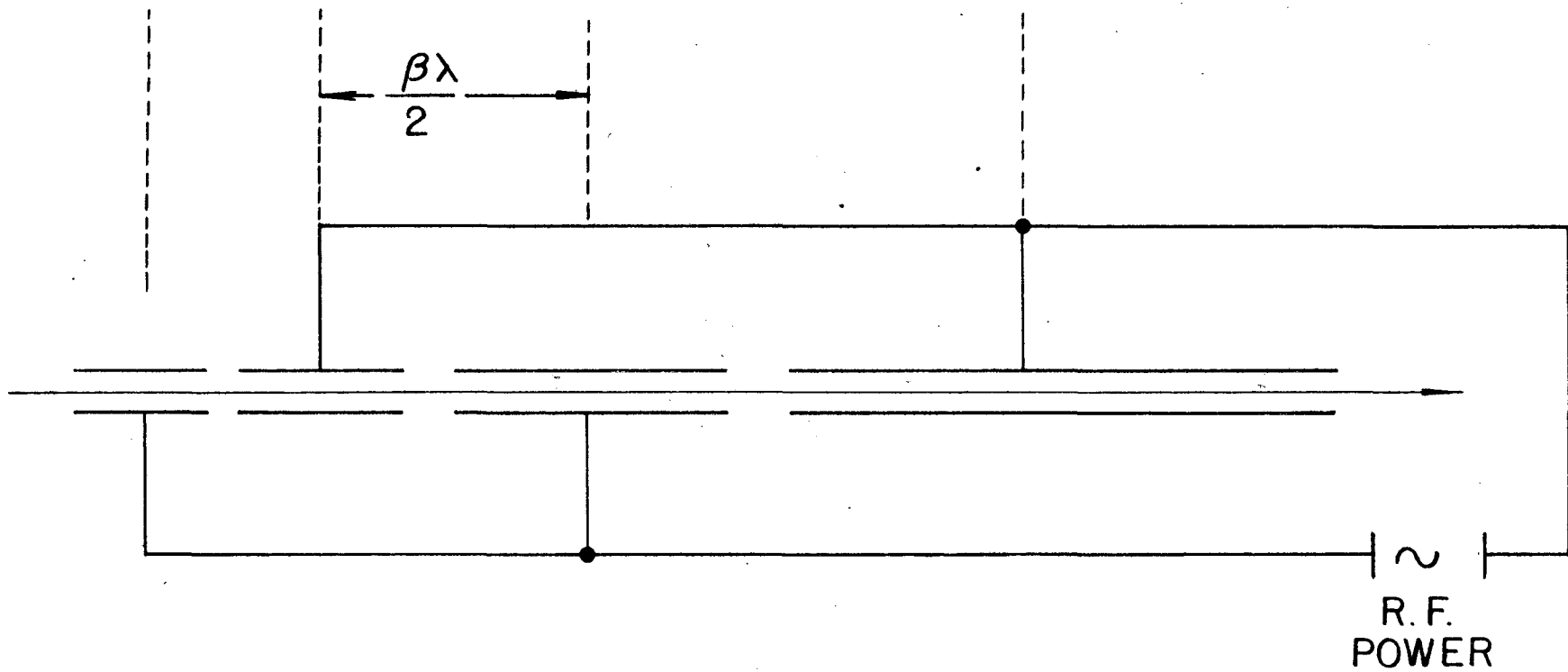


Fig. 2 Linear Accelerator Produced by Introducing Drift Tubes into Cavity, Excited as in Fig. 1. Division into Unit Cells

0645090100



00100605491

Fig. 3 Sloan-Lawrence Linear Accelerator Geometry

velocities ($\beta = v/c = .092$, 4 Mev) cannot be practically constructed on the basis of loaded wave guide geometry as is done for electrons.⁴⁾ Loading which would reduce the phase velocity to this low figure would lead to excessive r.f. power loss. For this reason, loading as such is not used. Instead, the phase velocity is left unchanged, that is, the electric field is everywhere in the same phase, and small hollow conducting "drift tubes" are provided to shield the protons while the field is in the wrong direction. Unfortunately, the drift tubes also cause a small amount of field perturbation which must be taken into account in designing the resonator.

The resonant cavity is essentially a long cylindrical cavity operated in the axial electric (0,1,0) mode, that is, the mode in which an axial electric field without azimuthal or transverse nodes is produced, as shown in Fig. 1. Efficient acceleration in such a cavity is possible only if its axial length is shorter than $\beta\lambda/2$ where λ is the free-space wavelength corresponding to driving frequency, which, excepting for very low voltage machines, is not feasible. For this reason, the drift tubes previously mentioned are introduced coaxially in the cylinder, as illustrated in Fig. 2, with the distance between centerlines AB of successive drift tubes equal to $\beta\lambda$. If the gap g between drift tubes is short compared to $\beta\lambda/2$, the voltage gain of the particle will be equal to the r.f. voltage developed across the gap. Note that the particle spends one r.f. period in each drift tube plus space and that each drift tube is charged oppositely at each end, but each drift tube is excited in phase. In the long wavelength Sloan-Lawrence accelerator¹⁾ (Fig. 3) the drift tubes are alternately plus and minus and each drift tube plus space is only $\frac{\beta\lambda}{2}$ long.

The general field geometry in the "unit cell" ABBA is very nearly the geometry of a doubly re-entrant symmetrical cavity excited in the lowest mode such as is used in klystron resonators, T.R. boxes, etc. The entire accelerator can therefore be considered as being a juxtaposition of such cells repeatedly excited in such a phase that the current flowing on opposite sides of the joining faces AB (see Figs.

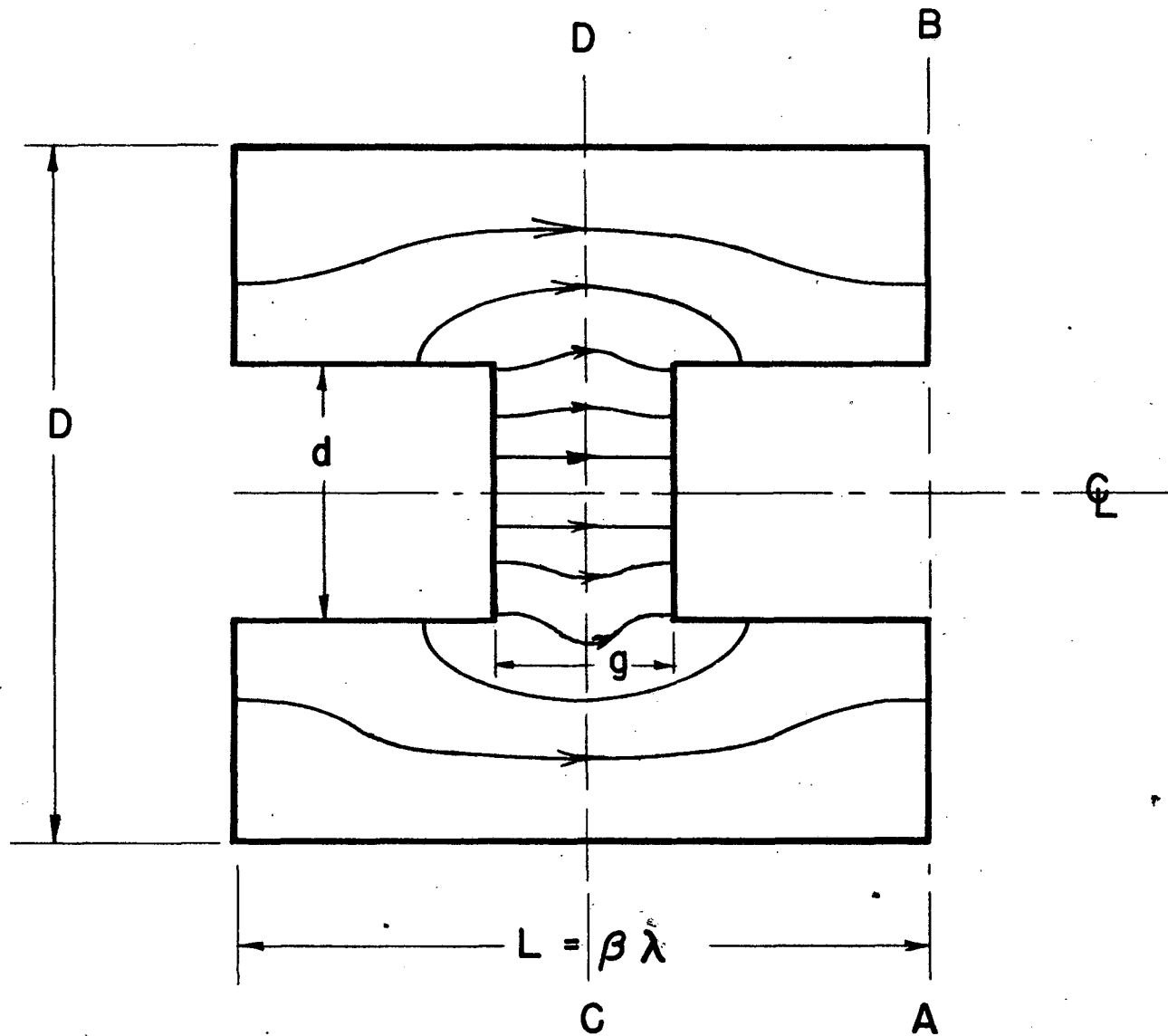
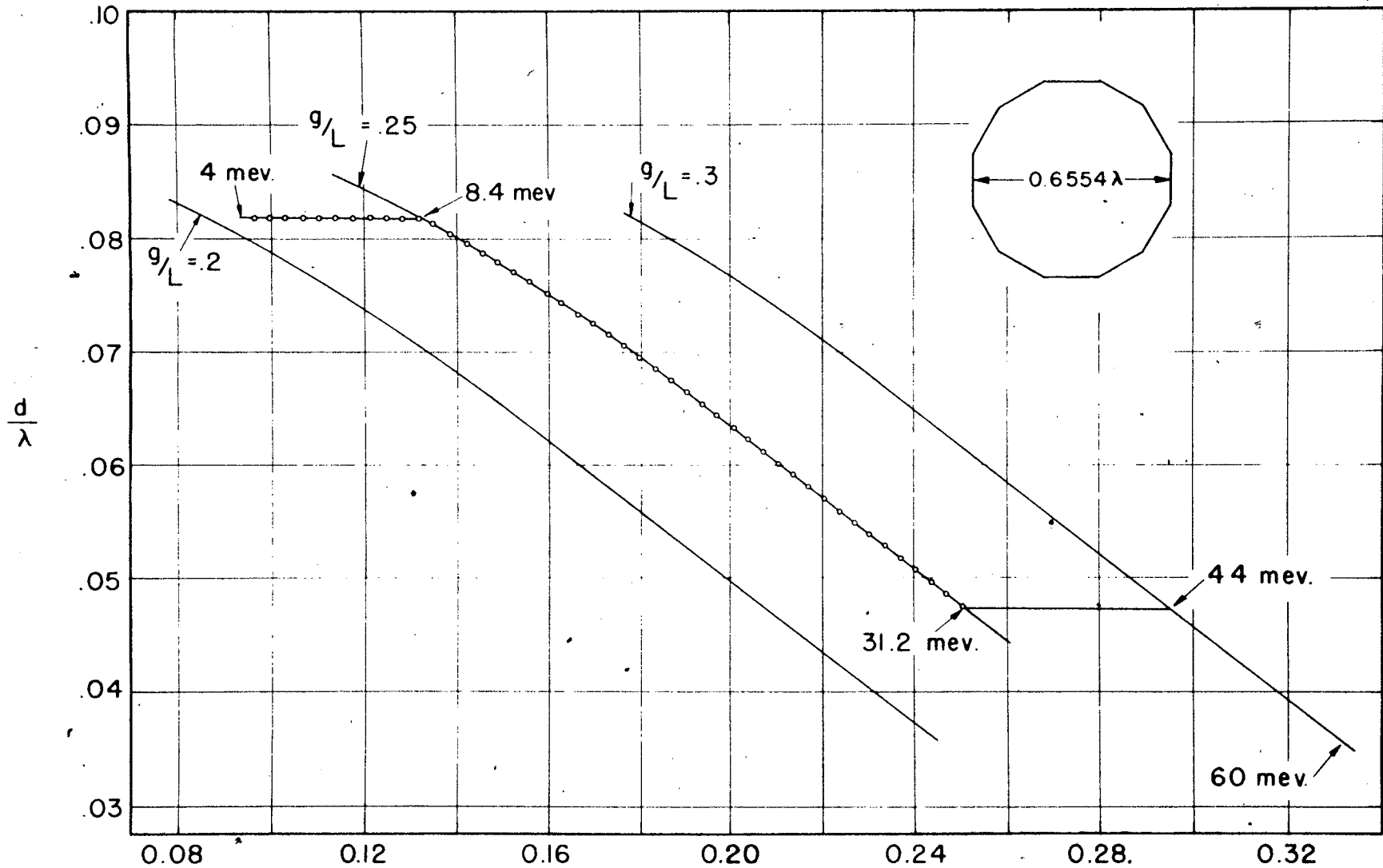


Fig. 4 Fields in "Unit Cell" of Accelerator. Note that a Conductor Across DC Would not Change Distribution

00100605493

00100605494



$$\frac{L}{\lambda} = \beta$$

FIG. 5

RESULTS OF MODEL TESTS ON RESONANT FREQUENCIES OF RE-ENTRANT CAVITIES

2 and 4) cancels. Such a picture would be exact if each successive cell were identical to the previous one; however, due to the progressive change in β corresponding to the gain in energy, the field distribution of the actual accelerator will not be exactly that corresponding to the distribution if the walls AB were actually present. For purposes of design, however, experimental and theoretical data based on single cell structure models are entirely adequate.

The joining of the unit cells is possible if each cell is accurately tuned to the same frequency. The tolerance of the tuning of the individual cell will be discussed later. Published design figures⁹⁾ on the resonant frequency of this type geometry is not of sufficient range to be used here, and also the details of the mechanical support structure of the drift tubes and similar deviations from ideal geometry made it necessary to derive the data pertaining to the resonant frequency of the unit cell from models. The resultant data¹⁰⁾ are shown in Fig. 5, using the notation as indicated in Figs. 2 and 4. The data are plotted in terms of dimensionless ratios to permit easy scaling. These data can be fitted by the empirical equation

$$\frac{g}{L} = (-.877) + (1.63) \frac{D}{\lambda} + (1.096) \frac{L}{\lambda} + (3.58) \frac{d}{\lambda} \quad (4)$$

in the range of application used here.

It is clear that as the energy, and hence β and L/λ increases, the diameter d of the drift tubes decreases; this decrease will eventually lead to a point where the design becomes impractical due to insufficient beam aperture and excessive curvature at the end of the drift tubes with consequent high surface yields. For this reason, the diameter D of the outer cavity must be chosen small enough to conform to this limitation for the highest values of β ; if chosen too small the drift tubes on the low β end will become too large in diameter with consequent increase in losses. In the 40' linear accelerator described here it was possible to compromise between these two extremes by the choice $D/\lambda = .66$. (Note that an unloaded cylindrical cavity is resonant at $D/\lambda = .766$).

(2) Voltage Gain and Input Power - The voltage gain per unit cell is determined

by three factors: (a) geometry, (b) power input, (c) phase of particle transit.

Let N be the crest value of the magnetic flux circulating in the unit cell.* It can then be shown easily that the voltage gain in the unit cell is then given by

$$V = \omega N \cos \phi \frac{\sin \frac{\pi g}{L}}{\frac{\pi g}{L}} \quad (5)**$$

if the electric field is assumed to be uniform across the gap; here ϕ is the transit phase angle relative to the phase of a particle crossing the center of the gap at the time of maximum voltage. On the other hand, ωN is given in terms of the power losses in the walls (and beam loading, here usually negligible) by a relation of the form

$$V_1 = \omega N = \sqrt{2PZ_1} \quad (6)$$

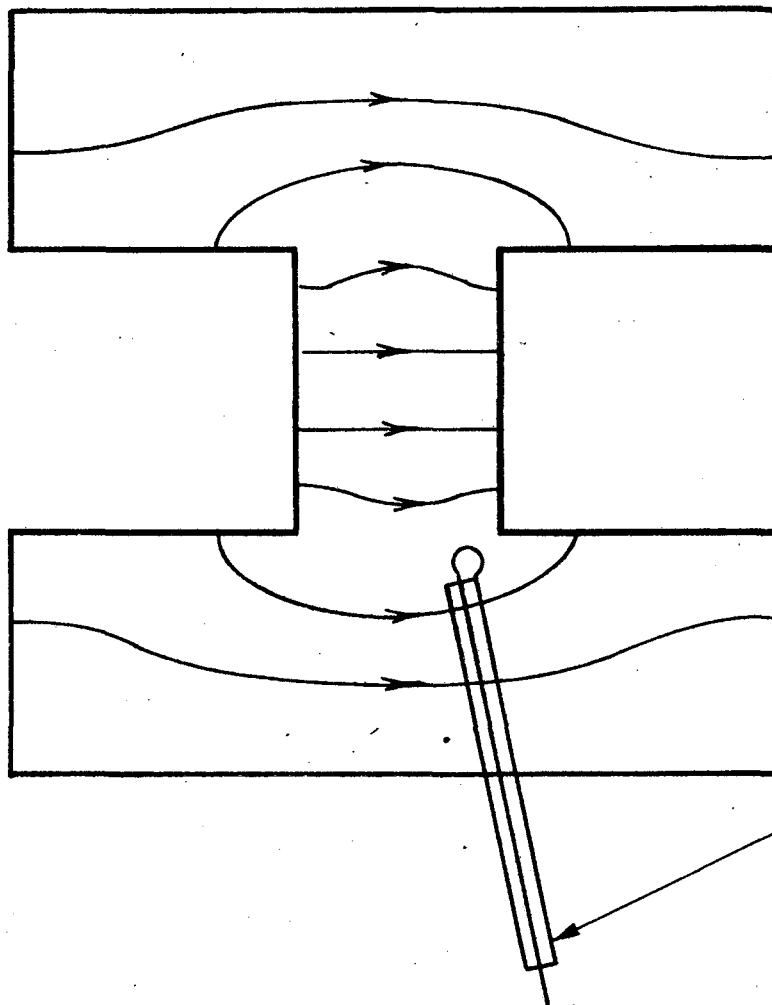
where Z_1 , the shunt-impedance/unit cell, is determined by the geometry and the skin depth of the cavity wall material. For a continuing structure Z_1 is proportional to the length; e.g. for a cylindrical, unloaded cavity of length l excited in the axial electric (0,1,0) mode, the shunt impedance is given by (neglecting end-losses):

$$Z_0 = \frac{491l}{\delta} \sqrt{\frac{\mu_0}{K_0}} = 185 \frac{l}{\delta} = 185 \left(\frac{l}{a}\right) Q_0 \text{ ohms} \quad (7)$$

where $a = \lambda/2.61$ is the radius and $\delta = \sqrt{\frac{2}{\omega\mu_0\sigma}}$ is the skin depth of the walls of conducting σ , and where $Q_0 = a/\delta$ is the conventional Q -value of the cylindrical infinite cavity. To judge the merits of comparative drift tube structures and to estimate the voltage gain as a function of power input, it is therefore necessary to evaluate the shunt impedance per unit length (Z_1/l) of the loaded cavity relative to the similar quantity for the unloaded cylindrical structure as given above. This evaluation was done semi-empirically by mapping the magnetic field B across an azimuthal plane of the cavity by means of an exploring loop as shown in

* Since the magnetic field is everywhere in phase in the mode used here, N can be defined uniquely as the surface integral of the crest value of the magnetic induction.

** MKS units are used throughout.



EXPLORING LOOP
 INTRODUCED APPROXIMATELY
 \perp TO ELECTRIC FIELD

00100605497

Fig. 6 Schematic Diagram Showing Magnetic Field Mapping of the Unit Cell. The Field Maps Permit Evaluation of the Integrals in Eq. (5) and (6)

Fig. 6. The shunt-impedances Z_1 and the Q are then obtained by numerical evaluation of the integrals:

$$Z_1 = \sqrt{\frac{\mu_0}{K_0}} \frac{8\pi}{\lambda \delta} \frac{\left(\int_{\text{Surface}} \frac{B dA}{\text{Field}} \right)^2}{\int_{\text{Surface}} B^2 dA} \quad \sqrt{\frac{\mu_0}{K_0}} \frac{8\pi}{\lambda \delta} \frac{\left(\int_{\text{Surface}} \frac{B dA}{\text{Field}} \right)^2}{\int_{\text{Surface}} B^2 dA} \quad (8)$$

$$Q = \frac{8\pi}{\delta} \frac{\int_{\text{Surface}} \frac{B^2 r dA}{\text{Field}}}{\int_{\text{Surface}} B^2 dA} \quad (9)$$

Typical resultant values* of Q and Z_1 , tabulated relatively to the unloaded cavity values, are given below. (Table I).

Proton Energy (Mev)	$B=L/\lambda$	Z_1/ℓ ohms/meter	Z_0/ℓ ohms/meter	Q	Q_0
50	.315	41×10^6	37.5×10^6	106,000	117,000

Frequency = 148. m.c.

Table I

The resultant values of Z_1 , Z_0 , Q and Q_0 require an additional correction factor of approximately $1/(1 + a/\ell)$ to correct for end losses in the cavity. Note that the shunt impedance/unit length of the loaded cavity as calculated from field plots is actually slightly larger than that of the unloaded cavity, although the difference is probably within the accuracy of the measurements.

The loss values arrived at by the flux plotting method are obviously lower limits, since losses in the drift tube support structure, pumping slots, joints, etc., are not taken into account. However, a simple measurement of the experimental Q of the cavity will give a measurement of the true shunt impedance also, since Z and Q are reduced in the same ratio. The resultant values, arrived at by experimental measurement of Q are given in Table II, computed for the entire accelerator.

* Experimental values are probably accurate to ± 10 percent.

	Q	Z(ohms)	Power for V = 28 Mev* (watts)
From flux plot	106,000	457 x 10 ⁶	1.40 x 10 ⁶
Exp. from Q measurement	72,000	311 x 10 ⁶	2.06 x 10 ⁶

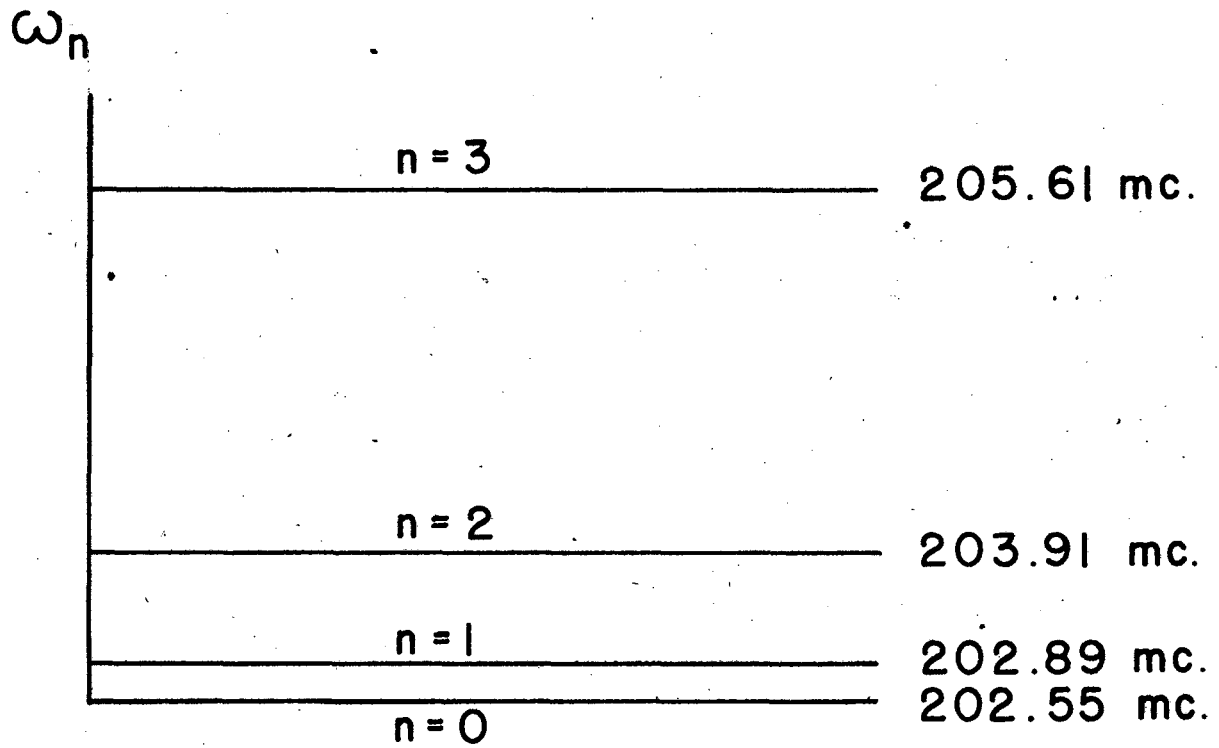
Table II

(3) Modes of a Long Cavity - In designing the accelerator cavity from data pertaining to the unit cells, a definite assumption has to be made pertaining to the voltage gain/cell. In order to join the cells without partition, the wall currents, and therefore the wall magnetic field, must be continuous. Since, as shown by magnetic flux plots, the ratio of total flux per unit length (and therefore voltage gain/unit length) to the magnetic field at the edge varies by only 20 percent from the injection end to the output end of the accelerator, (the ratio being higher at the high voltage end) it was decided to design the accelerator for constant voltage gain/unit length, which results in a 20 percent "taper" of magnetic field along the cavity walls. The constancy of the voltage gain/unit length is of course also desirable in order to equalize the surface gradient along the accelerator and reduce tendency to spark.

In order to assure equality of the mean electric field in a coupled structure involving 47 individual resonators, the individual resonators must have very accurately the same resonant frequency. This can only partially be assured by the model "unit cell" measurements referred to above, since: (a) the extension from unit cells to the long accelerator of varying units is not exact, and (b) slight mechanical changes from the model geometry will interfere with exact transfer of the data, and (c) the accuracy (approximately .05 percent) of the model frequency measurements is not quite sufficient. For this reason it is necessary to adjust the final field distribution to its value required for acceleration by corrections applied to the cavity as a whole.

The behavior of the cavity can best be described by means of its mode

* Taking $\phi = 30^\circ$, $g/L = .25$ (see eq. 5)



00050900100

Fig. 7 Mode Spectrum of Linear Accelerator Cavity

spectrum. The mode used here is on the edge of the pass band of the cavity used as wave guide, and therefore the mode separation varies quadratically as the limit is approached. Specifically, for an unloaded cavity, the spectrum is given by

$$\omega_n = \omega_0 \sqrt{1 + c \frac{n\pi}{\omega_0 L}}^2 \quad (10)$$

where ω_0 is the angular frequency of the lowest mode. The low end of the spectrum applying to the 40' accelerator cavity is plotted in Fig. 7. Owing to the small mode separation (.17 percent) near the limit, two problems have to be considered: (a) the possibility of "mode jumping" to an adjacent mode, and (b) the tolerances in geometry required to assure that the lowest mode has the desired shape. These two problems appear at first sight to be independent, but it will be shown shortly that they are different aspects of the same limitation. The first problem is solvable by proper disposition of the exciting oscillators or by careful tuning and will be discussed later. The second problem can be analyzed by a simple perturbation calculation in which we assume that the actual field distribution excited in a single mode can be expanded in terms of the modes of a cavity whose mode distribution is the desired one,* hereafter called the "ideal" cavity.

Let us consider the variation of the field as a function of the axial coordinate Z only. This is justified provided we are considering modes differing in the number of longitudinal nodes and which are of low order only, which will not overlap with radial and azimuthal modes.

Let $f(Z)$ be the actual field distribution corresponding to the frequency ω_m of the cavity excited in its m^{th} mode. Let $f_n(Z)$ be the distribution of an ideal cavity corresponding to the mode spectrum ω_n . The f obeys the differential equation

* Such an expansion is always possible since the normal modes in a cavity form a complete orthogonal set of functions.

$$\ddot{f}(Z) + \omega^2 f(Z) + \omega Q^{-1} \dot{f}(Z) = 0 \quad (11)$$

The f_n obeys eq. 11 for constant $\omega = \omega_0$. In the actual case ω will be a slowly varying function of Z also, since not all unit cells are accurately adjusted to the same frequency. Therefore we put:

$$\omega^2(Z) = \omega_m^2 \left\{ 1 + \sum_n \varepsilon_n f_n(Z) \right\} \quad (12)$$

and

$$f(Z) = \sum_n A_n f_n(Z) \quad (13)$$

where

$$A_m \gg A_r \text{ for } r \neq m$$

Substituting in (11); dropping higher order terms, noting that $\dot{f}_n(Z) = -\omega_n^2 f_n(Z)$, $\ddot{f}_n(Z) = j\omega_n \dot{f}_n(Z)$, and using the orthogonality of the modes, we obtain:

$$-A_n \omega_n^2 + \omega_m^2 A_n + A_m \omega_m^2 \varepsilon_n + j\omega_m^2 Q^{-1} A_n = 0 \quad n \neq m \quad (14)$$

$$\therefore \frac{A_n}{A_m} = \frac{\varepsilon_n}{(1 - \omega_n^2/\omega_m^2) + j Q^{-1}} \quad (15)$$

Hence the n^{th} Fourier component ε_n of the deviation of the resonant frequency distribution from uniformity as a function of the axial co-ordinate can be deduced from the Fourier components of a measured field distribution. Let the boundary condition at $Z = 0, L$ be that $\frac{\partial f}{\partial Z} = 0$. Then the f_n are given by:

$$f_n(Z) = \cos \frac{n\pi Z}{L} \quad (16)$$

If the mode separation is large compared to the mode width (as in the case here), and if ω_m refers to the lowest mode, then (15) reduces to:

$$\frac{A_n}{A_0} = \frac{\varepsilon_n}{n^2} \cdot \left(\frac{\omega_0 L}{\pi c} \right)^2 \quad (17)$$

Relations (16) and (17) can be used directly to correct the cavity empirically as follows: The longitudinal field distribution is measured with pick-up loops feeding bolometers along the cavity edge. The distribution is then Fourier analyzed by conventional methods and the Fourier coefficient of the frequency error function calculated from Eq. (17). The frequency error function is then

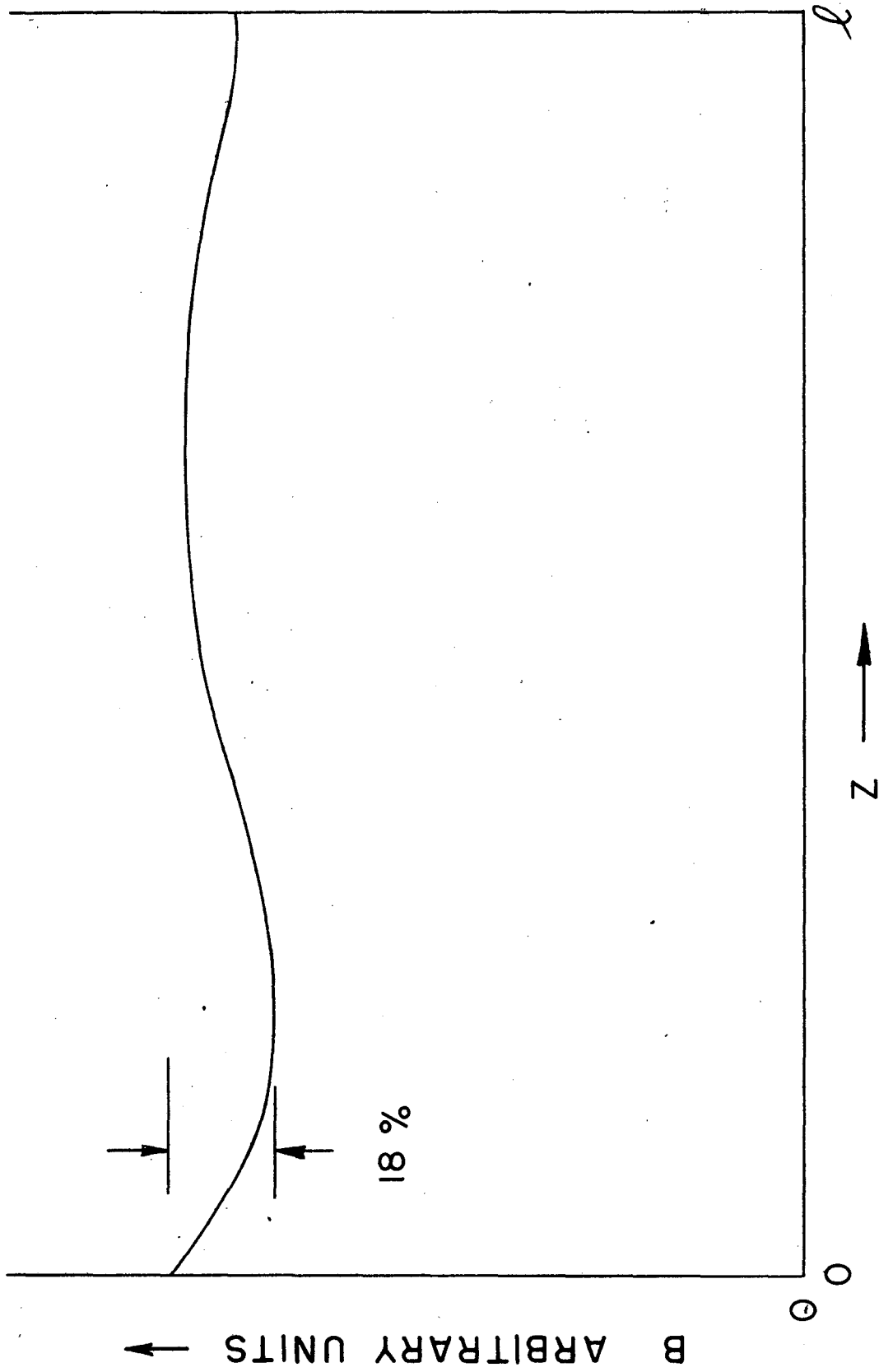


Fig. 8a Effect of Fourier Analysis in Correcting Cavity

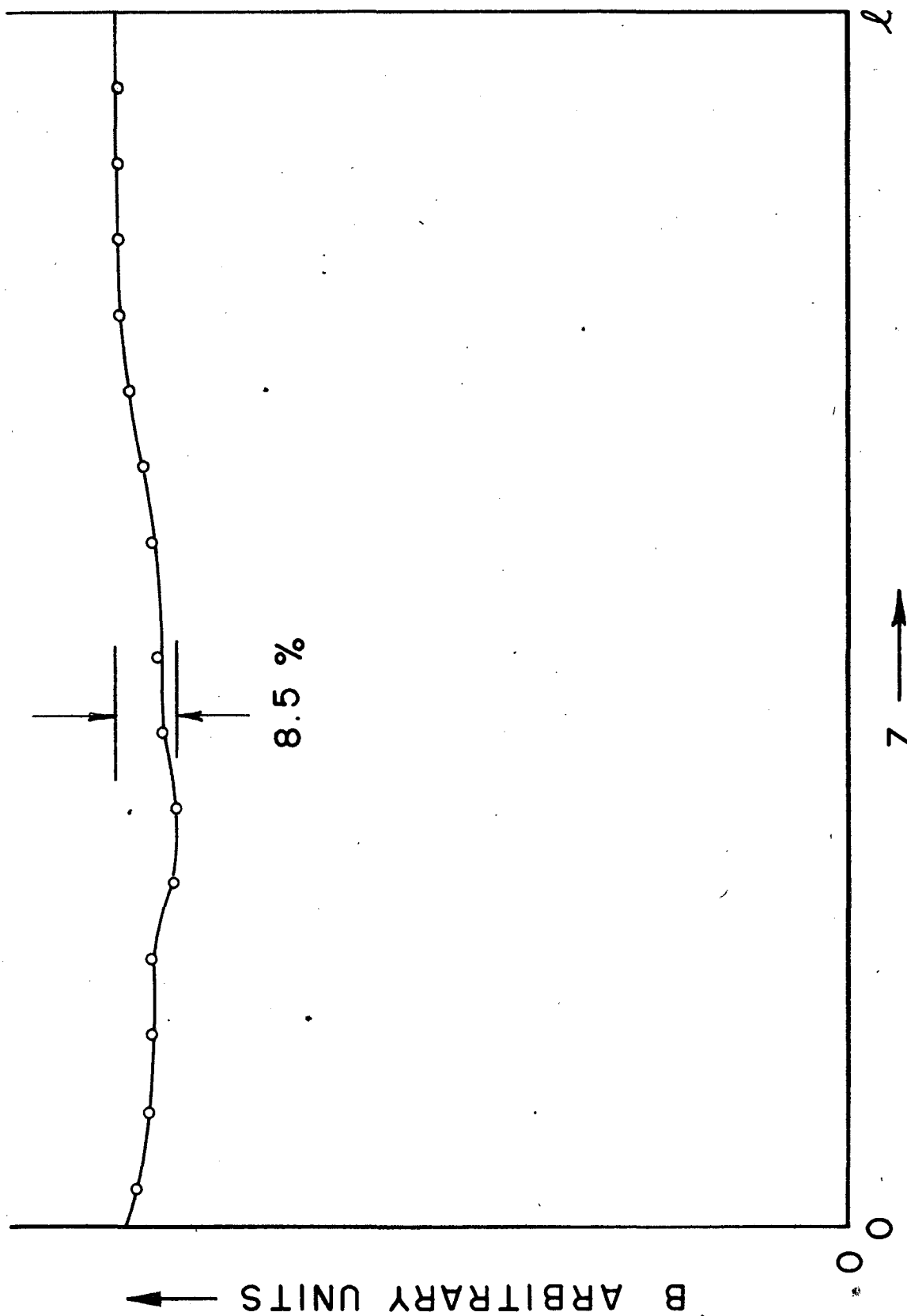


Fig. 8b Effect of Fourier Analysis in Correcting Cavity

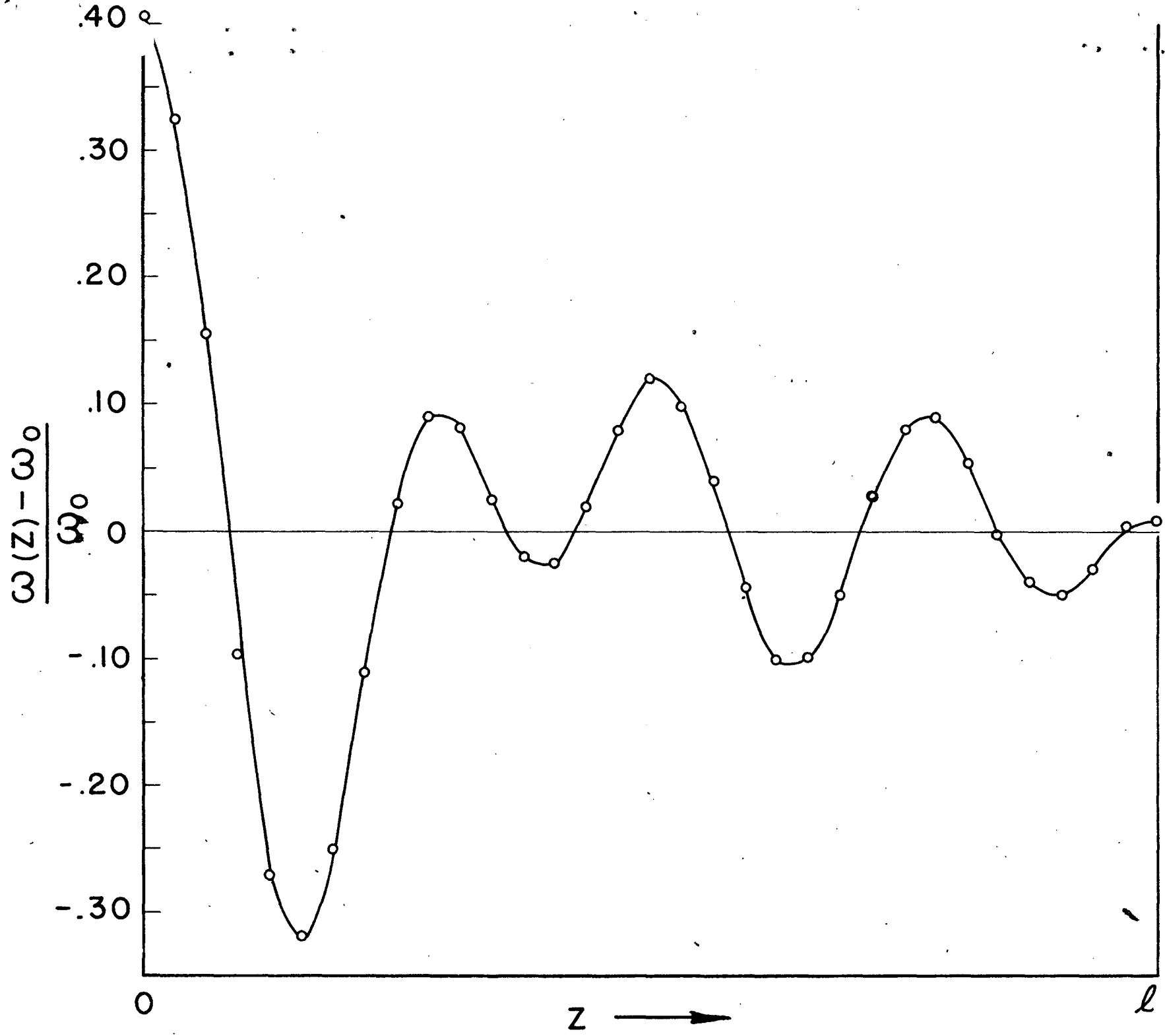
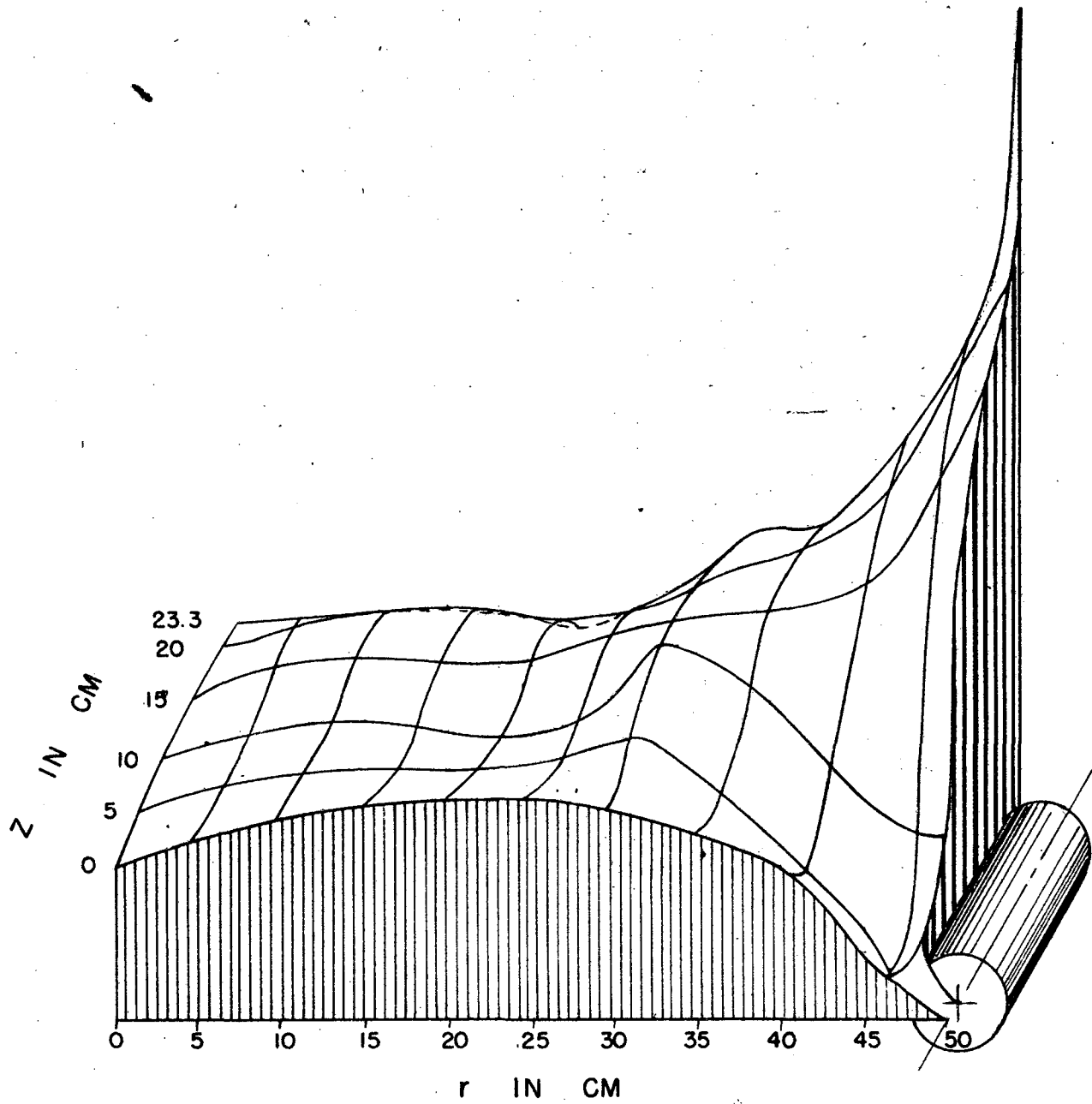


Fig. 8c Effect of Fourier Analysis in Correcting Cavity

00100605305



MAGNETIC FIELD CONTOURS IN CAVITY WITH DRIFT TUBES

$$\beta = .31$$

PROTON ENERGY ~ 50 MEV

Fig. 9 Contour Plot of Magnetic Field in Typical Cavity Section

90550900100

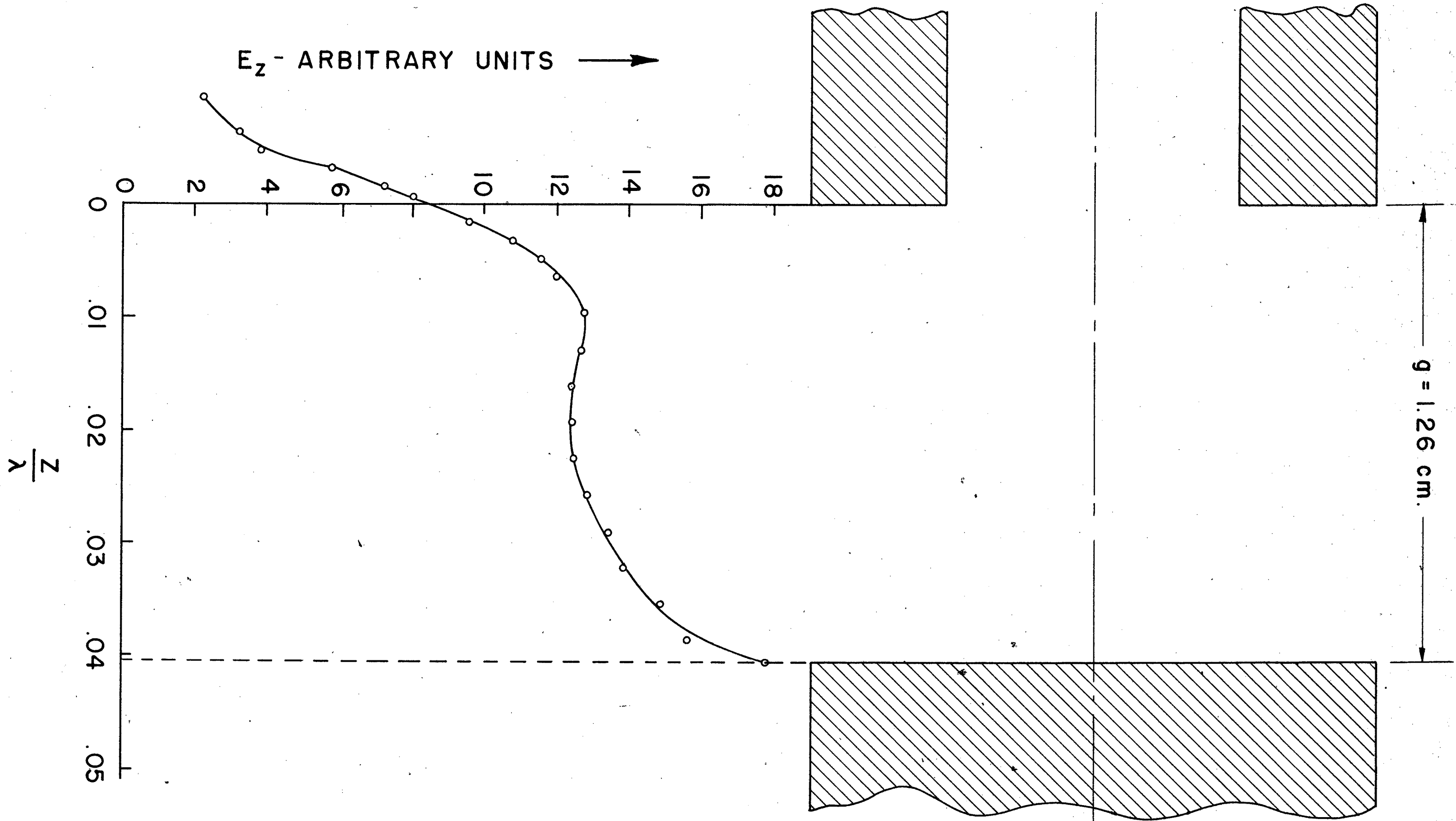


Fig. 10 Typical Axial Electric Field Plot Along Drift Tube Axis

FIG. 10
13-7-64

synthesized. Shims, corresponding to the calculated frequency errors, and calculated from Eq. (4) are then introduced into each drift tube to adjust the gap. Fig. 8 shows the effect of this procedure.

It should be noted that the sensitivity of the distribution to errors in resonant frequency distribution decreases with the inverse square of the order of the harmonic. Therefore the effect of random variations is considerably less than systematic deviations from correct adjustment. E.g., in order to hold the distribution to 5 per cent of the correct value, the variation in frequency of the individual cavities which is systematic in the 1st harmonic must be kept to less than 2×10^{-4} , or about $\pm .0015''$ in drift tube length. For random variations (considered as $\sim \sqrt{47} \sim 7^{\text{th}}$ harmonic) a tolerance of $\pm .075''$ is sufficient. The first and last drift tubes have been made adjustable by outside control in order to permit adjustment of the 1st harmonic externally.

(4) Experimental Field Plots - A three dimensional picture of the complete field plot as obtained by the magnetic loop method is shown in Fig. 9. Note that the resultant fields are a mixture of fields of the co-axial type ($1/r$ dependence near the drift tubes) and the TM_{01} type [$J_1(kr)$ dependence in the gaps].

For use of transit time and focusing calculations, the electric field $E(z)$ along the axis is needed. As will be explained later, the entrance of each drift tube is closed with a focusing grid while the exit end is open. For this reason, theoretical analysis of the field is difficult and an experimental procedure is used. This procedure consists in measuring the frequency shift produced by placing a small metallic object of volume δV at various points in the field. The disturbed frequency is given by⁽¹¹⁾

$$\omega^2 = \omega_0^2 \left\{ 1 + \int_{\delta V} (H^2 - E^2) dv \right\} \quad (18)$$

where H^2 and E^2 are normalized to unity over the total volume of the cavity. If the measurement is made along the axis, $H = 0$ and

$$\omega^2 - \omega_0^2 = - \frac{\int E^2 dV}{\int_{\text{total cavity}} E^2 dV} \sim \frac{E^2 \delta V}{\int_{\text{total}} E^2 dV} \quad (19)$$

An axial field plot for a typical drift tube geometry is shown in Fig. 10. These data were taken on a 1000 mc scale model using a heterodyne frequency measuring method.

III. BEAM DYNAMICS

(1) General Lateral and Longitudinal Stability Considerations - Consider a charged particle traveling near the axis of an electric field of cylindrical symmetry. The total radial momentum while traveling from a to b at a fixed small distance r from the axis is given by

$$\Delta p_r = e \int_a^b \frac{1}{V} E_r dz \quad (20)$$

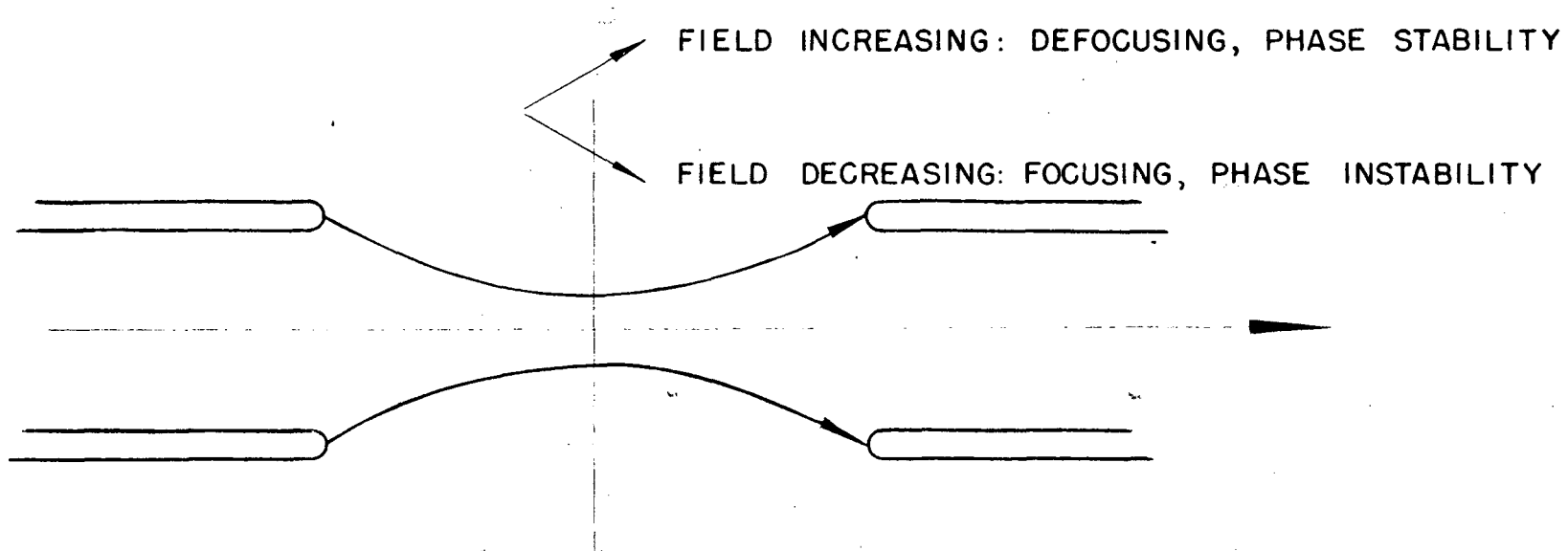
If the velocity is essentially constant in the range a - b, then

$$\Delta p_r \sim \frac{e}{2\pi r V} \int_a^b 2\pi r E_r dz = \frac{e \Phi_r}{2\pi r V} \quad (21)$$

where Φ_r is the total radial electric flux. If V is not constant, then so-called second order focusing effects will occur; these, although important in d.c. accelerators, are negligible here, since the fractional energy gain per accelerating section is small.

If no charge is contained within the beam, then Φ_r will be positive or negative depending as to whether the field is increasing or decreasing while the particle is crossing the gap; if the field is constant $\Phi_r = 0$; i.e., there is no "first order" focusing. Lateral stability therefore requires an accelerating field which is decreasing as the accelerating gap is crossed.

This requirement is exactly opposite to the requirement of longitudinal or phase stability.⁵⁾ For phase stability, a "late" particle must meet a stronger



0010060905509

Fig. 11 Diagram Showing Incompatibility of Focusing and Phase Stability

field and vice versa; i.e., the field must be increasing. This incompatibility between phase stability and focusing is shown graphically in Fig. ~~17~~. 11.

It will be shown that this difficulty cannot be overcome by any arbitrary re-arrangement of gaps, lenses, etc., excepting by:

- a) Introducing charge into the beam
- b) Using an external magnetic field
- c) Depending on the very small phase range of second order focusing

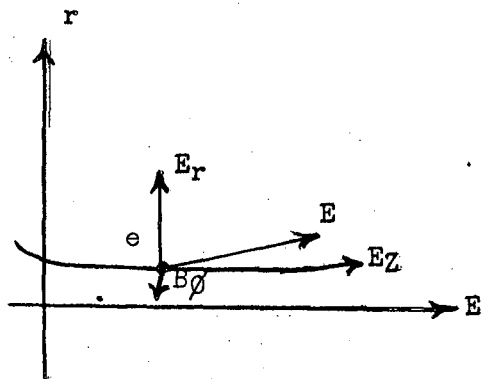
The general nature of this statement can be shown as follows: The fact that radial stability and phase stability are in general incompatible in the absence of charge in the beam can be shown as follows:

$$\text{Let } E_z = f(Z, t) \quad (22)$$

be the longitudinal field component of an axially symmetrical field. The radial force acting on a particle of charge e moving parallel to the Z axis at a distance r from the axis with a velocity v is given by:

$$F_r = e(E_r - vB_\phi) \quad (23)$$

$$\text{But, since } \nabla \cdot \mathbf{E} = \frac{\partial E_z}{\partial Z} + \frac{1}{r} \frac{\partial}{\partial r} (rE_r) = 0$$



we have, for small r ,

$$E_r = -\frac{r}{2} \frac{\partial E_z}{\partial Z} \quad (24)$$

$$\text{and, since } (\nabla \times \mathbf{B})_r = \frac{\partial B_\phi}{\partial Z} = \frac{1}{c^2} \frac{\partial E_r}{\partial t} = \frac{r}{2c^2} \frac{\partial^2 E_z}{\partial Z \partial t}, \text{ we have}$$

$$B_\phi = \frac{r}{2c^2} \frac{\partial E_z}{\partial t} \quad (25)$$

Let the subscript a denote differentiation of $f(Z, t)$ with respect to the first argument and b differentiation with respect to the second.

The radial momentum gained by a particle in transit across a gap starting from field-free space and ending in field-free space (or moving in a spatially periodic

field across a spatial period) is given by:

$$P_r = \frac{1}{v} \int F_r dZ = 1 \frac{re}{2v} \left\{ \int f_a(Z, t + Z/v) dZ + v/c^2 \int f_b(Z, t + Z/v) dZ \right\} \quad (26)$$

where t is the time of passage across an arbitrary point in the field. Integrating the first term by parts, this becomes, dropping out the integrated term due to the above specification on the path of integration,

$$P_r = +\frac{re}{2v^2} (1 - \beta^2) \int f_b(Z, t + Z/v) dZ \quad \beta = v/c \quad (27)$$

The longitudinal gain in momentum is

$$P_z = e/v \int f(Z, t + Z/v) dZ \quad (28)$$

The phase stability condition is (later particle gains more momentum):

$$\frac{\partial P_z}{\partial t} > 0 \quad (29)$$

or

$$\int f_b(Z, t + Z/v) dZ > 0 \quad (30)$$

The radial stability condition is, from (27),

$$\int f_b(Z, t + Z/v) dZ < 0 \quad (31)$$

(30) and (31) are incompatible.

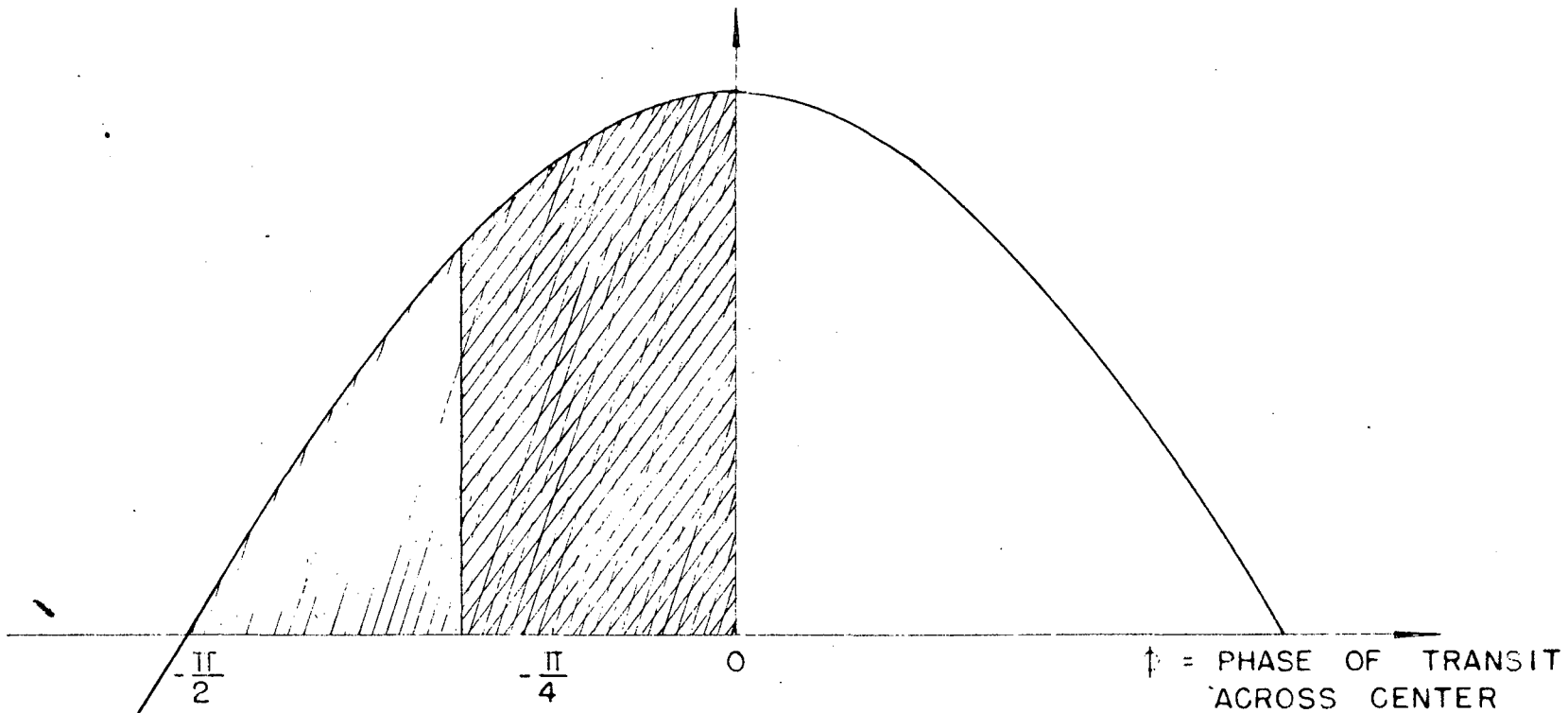
The only assumptions involved in this proof which are not general are: (1) that the velocity across the gap is constant, which neglects the effect of so-called second order focusing; (2) that there is no charge in the beam. The second assumption can be violated by focusing by means of grids, foils, space charges,¹²⁾ etc.

In the case of highly relativistic conditions, such as in electron acceleration, at even moderately high energies, this situation still pertains, but only to such a small degree that the beam diverges only logarithmically.

(2) Focusing Oscillation in Grid-focused Accelerator - At non-relativistic velocities focusing compatible with phase-stability is therefore possible only if charge is introduced in the beam.* If we introduce a grid or foil across the

* The use of a d.c. focusing field is not practical here.

ELECTRIC FIELD AT CENTER OF GAP



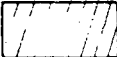
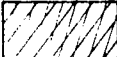
-  PHASE STABLE AND DEFOCUSING
-  PHASE STABLE AND FOCUSING FOR $g/L = \frac{1}{4}$

Fig. 13 Phase Diagram Indicating Definition of ϕ and Regions of Stability in Grid Focused Operation

001000905013

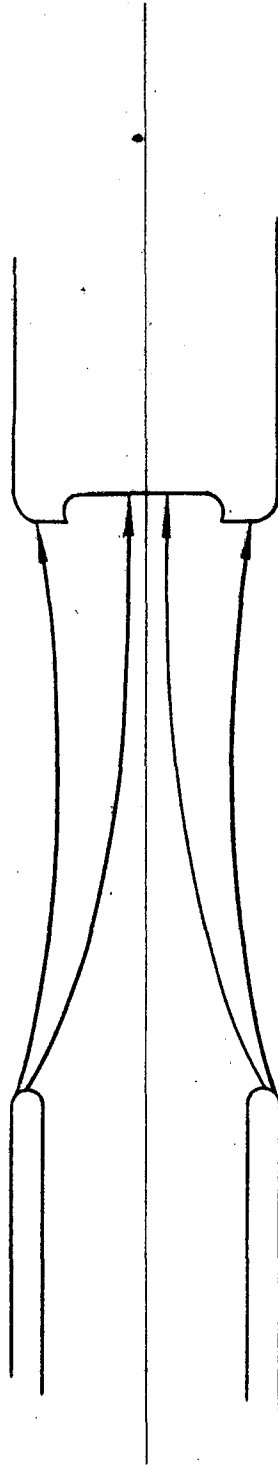


Fig. 12 Grid and Foil Focusing

entrance end of a drift tube (see Fig. 12) then the beam would cut across radial flux even in the static case, and first order focusing would result. In the general case we have, integrating from Eq. (27), using a sinusoidal time variation:

$$-\frac{\Delta p_r}{r} = (1 - \beta^2) \frac{e}{2V} \left\{ \cos \left(\frac{\pi g}{L} + \phi \right) E_0 \left(\frac{g}{2} \right) + \frac{2\pi}{L} \int_{-g/2}^{g/2} \sin \left(\frac{2\pi z}{L} + \phi \right) E_0(z) dz \right\} \quad (32)$$

in the notation of Fig. 13, where $\frac{L\phi}{2\pi V}$ is the time* of transit across the center of the gap, relative to the time the crest of the field is reached.

These integrals can be evaluated numerically, using the field plots obtained by the frequency shift method described in Section II. In general, it is sufficient to take the field to have the constant value E_0 across the gap; this gives:

$$-\frac{\Delta p_r}{r} = (1 - \beta^2) \frac{eE_0}{2\beta c} \cos \left(\frac{\pi g}{L} - \phi \right) \quad (33)$$

The energy gain per gap is

$$\Delta U = e \int_{-g/2}^{g/2} E_z dz = \frac{LeE_0}{\pi} \cos \phi \sin \frac{\pi g}{L} \quad (34)$$

Let us number the drift tubes with number $n = 0, 1, 2$, starting from zero velocity.

Then:

$$\Delta p_r = \frac{dp_r}{dn} = \frac{d}{dn} \left(\mu \frac{dr}{dt} \right) = \frac{\omega}{2\pi} \frac{d}{dn} \left(\mu \frac{dr}{dn} \right) \quad (35)$$

where μ is the mass of the particle. Hence, non-relativistically,

$$-\frac{1}{r} \frac{d^2 r}{dn^2} = \frac{1}{2\beta} \eta \frac{E}{L} \cos \left(\frac{\pi g}{L} - \phi \right) \quad (36)$$

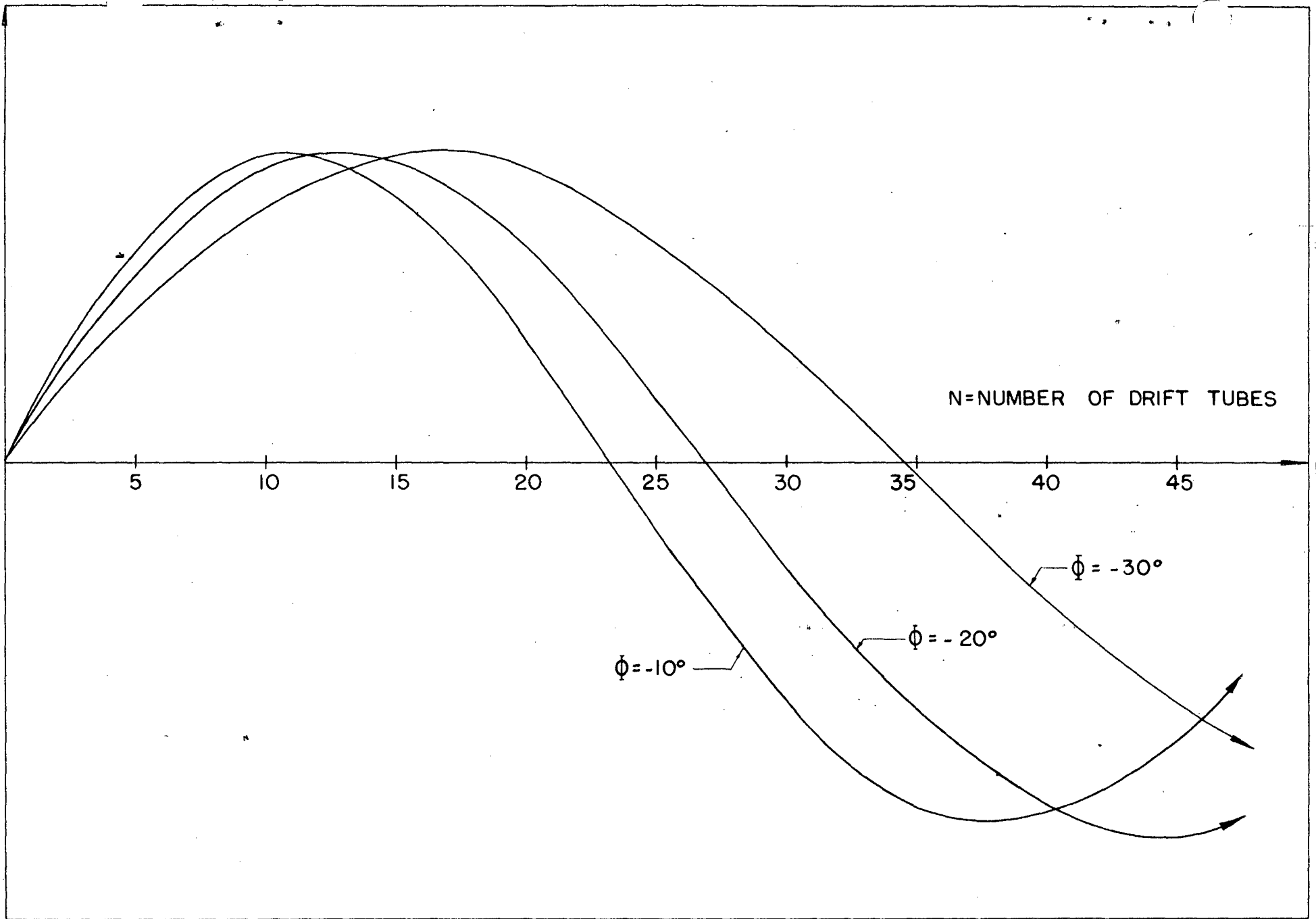
where η is the mean voltage/wave length in the accelerator measured in rest energy units of the accelerated particle. Also, non-relativistically, from Eq. (34)

$$\begin{aligned} \frac{d}{dn} \left(\frac{1}{2} \mu c^2 \beta^2 \right) &= \frac{\beta \lambda e E_0}{\pi} \cos \phi \sin \frac{\pi g}{L} \\ \frac{d\beta}{dn} &= \left(\frac{\lambda e E_0 L}{\mu c^2 g} \right) \cos \phi \sin \frac{\pi g}{L} \end{aligned}$$

$$\beta = \eta \left(\cos \phi \frac{\sin \frac{\pi g}{L}}{\frac{\pi g}{L}} \right) n \quad (37)$$

* Note that $\phi \ll 0$ for phase stability.

RADIAL DISPLACEMENT



00100100
51525215

Fig. 14 Particle Trajectory for Injection into Linear Accelerator from Focal Point at Entrance. Transit Phase Angles 10° , 20° and 30°

Note that the velocity increase per drift tube is constant, while the energy gain is proportional to the length of the drift tube. Therefore the differential equation for focusing oscillations is:

$$\frac{d^2 r}{dn^2} + \frac{K}{2n} r \quad (38)$$

where

$$K = \cos \left(\frac{\pi g}{L} - \phi \right) \cdot \frac{\pi g}{\sin \frac{\pi g}{L} L} \quad (39)$$

Hence focusing is stable with a period of

$$N_r = 2 \sqrt[4]{\frac{2n}{K}} \quad (40)$$

which increases as the fourth root of the energy, and an amplitude which increases as $n^{1/4}$ corresponding to the eighth root of the energy.*

The 40' linear accelerator has only one or two internal foci if protons are injected from a focal point of an electrostatic accelerator. A typical particle trajectory for $g/L = .25$, is shown in Fig. 14, computed from Eq. (41),

$$\phi = -10^\circ, -20^\circ, -30^\circ$$

Note that the focusing force vanishes at an equilibrium phase angle of:

$$-\phi = \frac{\pi}{2} \left(1 - \frac{2g}{L} \right) \quad (42)$$

In the 40' linear accelerator this corresponds to a limiting phase angle of 45° .

It is of course not necessary to have a radial restoring force so large as to produce several nodes in the length of the accelerator. The only requirements are: (1) to limit the maximum radial excursions after injection, and (2) to locate a node close to the output of the accelerator. Fig. 14 shows that focusing is actually

* This variation corresponds rigorously to the asymptotic solution of Eq. (38) only. In the 40' accelerator, this assumption is not yet valid since only a small number (1 or 2) focusing oscillations occur in the accelerator. The precise solution of Eq. (38) is

$$r = \sqrt{n} \left\{ A J_1 \left[2 \sqrt{Kn} \right] + B Y_1 \left[2 \sqrt{Kn} \right] \right\} \quad (41)$$

with A and B adjusted to fit the injection conditions.

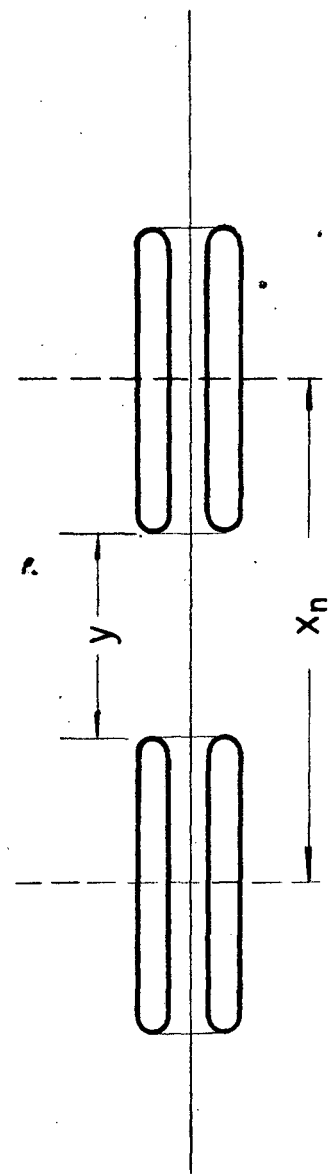


Fig. 15 Definition of Repeat Length x_n and Gap g

somewhat stronger than required. The focusing can be weakened by: (1) leaving out a certain number of grids, and (2) weakening the field at the grids by recessing them slightly into the drift tube. The first solution, although leading to an apparent gain in transmission, is a poor one, since the gridless gaps give actually a defocusing impulse rather than a weakly focusing one. The result is that the critical phase angle of radial stability is no longer given by Eq. (41), but by

$$\tan(-\phi) = \frac{f}{2-f} \cot \frac{\pi g}{L} \quad (43)$$

if only a fraction f of grids is present. For instance, if $1/3$ of all grids are omitted, the limiting phase angle of stable operation is reduced to 26.6° . It is therefore advantageous to reduce the focusing by recessing the grids or by similar means; this will weaken the field at the grid and will therefore permit a more open grid without excessive field at the grid wires. Recessing will decrease the effective limiting aperture of the device owing to fringing of some of the field lines outward toward the rim of the grid.

The exact location of the node is very difficult to predict in practice owing to the fact that the equilibrium phase angle is usually unknown and may be variable throughout the machine, depending on the degree of perfection to which the field adjustments have been achieved.

(3) Phase Stability - We will now study the phase stability of the linear accelerator a little more closely. To do this let us consider the n^{th} repeat length which we measure from the middle of one drift tube to the middle of the next. Let its length be x_n , and let the length of the gap be g , as shown in Fig. 15. In this machine, $g \approx 1/4 x_n$. We can in a study of the question of phase stability speak of the proton crossing center of the gap at a certain phase ϕ of the r.f. field. This phase ϕ for the machine to be phase stable, is in the shaded region of Fig. 13. We again define ϕ/ω as the time after the crest of the field at which the proton crosses the center of the gap, i.e., $\phi < 0$ for phase stability. Yet the machine is so designed that the proton crosses each gap at a phase ϕ_0 . If the maximum energy gain (i.e. gain at zero phase) per unit length is W_0 , then the design value of the energy

gain in the n^{th} gap is $W_0 \cdot \cos \phi_0 \cdot x_n$. The kinetic energy that the proton has after crossing the n^{th} gap is denoted by W_{n+1}^0 and its velocity is β_{n+1}^0 . We have therefore for a proton which is out of phase from the design value ϕ_0 at the n^{th} gap by the amount ϕ_n :

$$W_{n+1} - W_n = W_0 \cdot \cos (\phi_0 + \phi_n) x_n \quad (44)$$

for all n , where $x_n = \frac{\beta_{n+1} + \beta_n}{2}$. We will now study the phase oscillations that the proton undergoes as it moves through consecutive gaps. Let us write

$$W_n = W_n^0 + W_n^1 \quad (45)$$

where W_n^0 will represent the energy that the proton has after crossing the n^{th} gap if it had always been in phase. W_n^1 is then the amount of excess energy the proton has over the "in phase" proton energy. Similarly we have

$$\beta_n = \beta_n^0 + \beta_n^1 \quad (46)$$

We have first of all from (44) and (45)

$$W_{n+1}^1 - W_n^1 = W_0 \lambda (\cos (\phi_0 + \phi_n) - \cos \phi_0) \beta_n^0 \quad (47)$$

Secondly, we have, if we neglect second order terms in β^1 :

$$W_{n+1}^1 - W_n^1 = Mc^2 (\beta_{n+1}^0 \beta_{n+1}^1 - \beta_n^0 \beta_n^1) \quad (48)$$

Equating (47) to (48) and introducing differentials instead of differences, we have

$$\frac{d}{dn} (\beta_n^0 \beta_n^1) = \frac{W_0 \lambda}{Mc^2} [\cos (\phi_0 + \phi_n) - \cos \phi_0] \beta_n^0 \quad (49)$$

It follows furthermore from the phase advance due to deviation from the design velocity that:

$$\frac{d\phi_n}{dn} = - 2\pi \frac{\beta_n^1}{\beta_n^0} \quad (50)$$

and from design of the accelerator:

$$\beta_n^0 = \frac{W_0 \lambda}{Mc^2} \cos \phi_0 \cdot n \quad (51)$$

If these are now substituted into our differential equation we have

$$n \frac{d^2 \phi_n}{dn^2} + 2 \frac{d\phi_n}{dn} = - 2\pi [\cos (\phi_0 + \phi_n) - \cos \phi_0] / \cos \phi_0 \quad (52)$$

This is the final differential equation describing the phase oscillation in the linear accelerator.

Suppose now that the phase oscillations are small, i.e., $\phi_n \ll 1$. Then the

0 0 1 0 0 6 0 5 5 2 0

POTENTIAL FUNCTION
(ARBITRARY ORIGIN
AND UNITS)

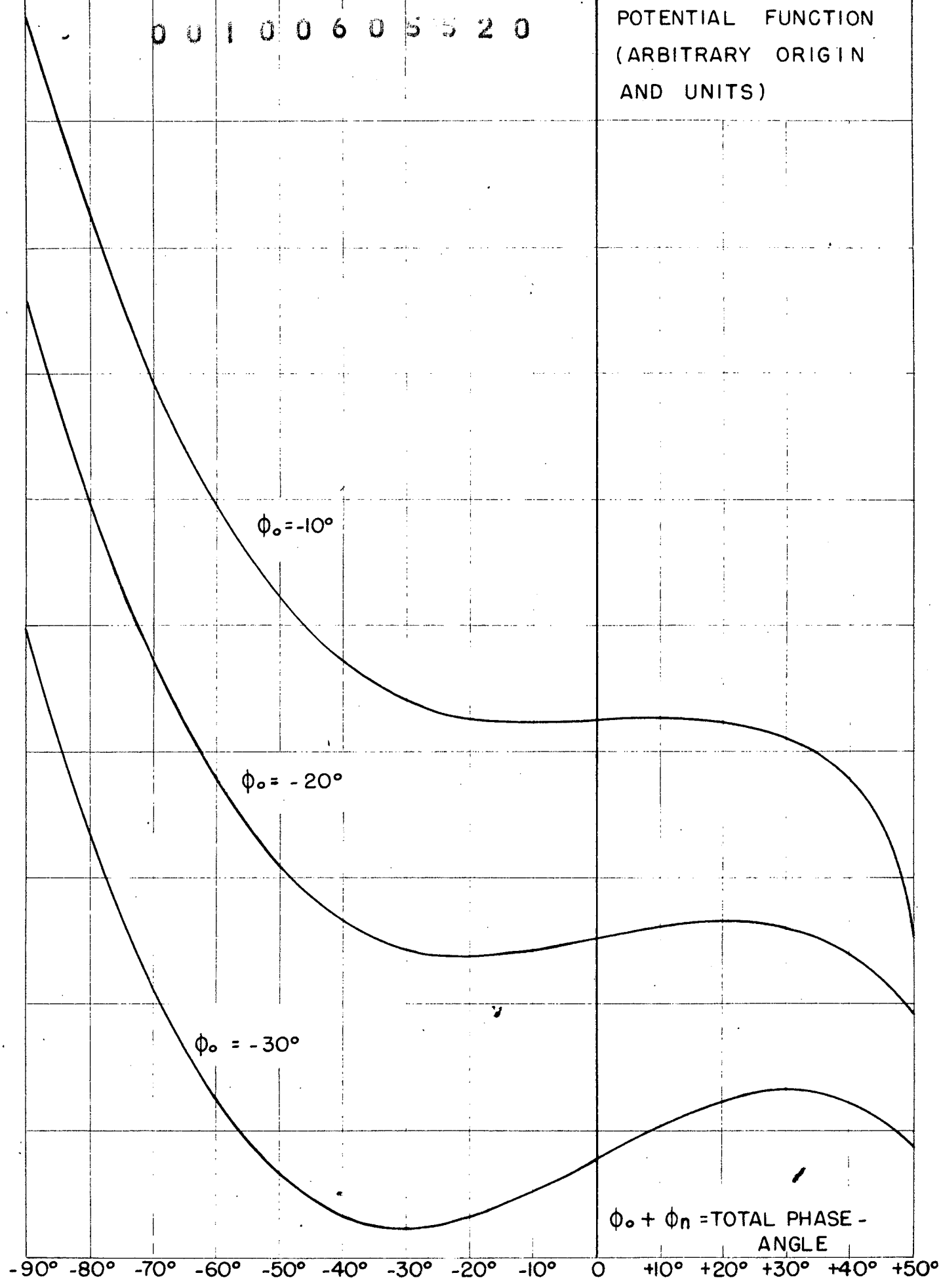


Fig. 16 Effective Potential Function of Protons Plotted for Various Equilibrium Phase Angles ϕ_0 as a Function of Total Phase Angle $\phi_n + \phi_0$

equation takes on the following form:

$$\frac{d}{dn} \left(n^2 \frac{d\phi_n}{dn} \right) + a^2 n \phi_n = 0 \quad (53)$$

where $a^2 = -2\pi \tan \phi_0$. This equation is a form of a Bessel equation and it possesses the asymptotic solution

$$\phi_n \approx A n^{-3/4} \sin(2an^{1/2} + \delta), \quad (54)$$

where A and δ are constants determined by the initial conditions. We see therefore that the phase oscillations are damped out as $n^{-3/4}$ or as $W^{-3/8}$. Furthermore the number of drift tubes required for one oscillation goes up to $n^{1/2}$ or $W^{1/4}$. Using our design numbers, one easily calculates that a proton undergoing small phase oscillations about $\phi_0 = 30^\circ$ would undergo ≈ 2 complete phase oscillations in going down the 40' accelerator.

For large oscillations about equilibrium a precise solution of Eq. (52) would be necessary which in general is difficult. We can, however, answer the important question of the amplitude of ϕ_n which is permitted if the machine is operated at a design phase angle ϕ_0 . Eq. (52) can be written in the form:

$$\frac{d}{d\nu} \left[\nu^{3/2} \frac{d\phi_n}{d\nu} \right] + \frac{\pi}{2} (\cos \phi_n - 1 - \sin \phi_n \tan \phi_0) = 0 \quad (55)$$

where $\nu = n^2$. This is the same as the equation of motion of a particle of mass proportional to $\nu^{3/2}$ and under the influence of a potential function:

$$V = -\phi_n + \sin \phi_n + \cos \phi_n \tan \phi_0 + \text{constant} \quad (56)$$

If the protons are injected at the design energy, which is very closely possible, then the range of stable phase angles is essentially defined by the stable range of the potential energy functions (Eq. (56)). This function is plotted in Fig. 16 for equilibrium phase-angles of $\phi_0 = -10^\circ$, -20° , and -30° . Note that the acceptable phase angle is slightly larger than $3\phi_0$, since even protons entering at positive ϕ (i.e. early protons) up to $\phi = \phi_0$ will be stable. Also note that the limit of stability is reached at approximately

$$\phi_n = -2\phi_0 \quad (57)$$

and that the depth of the potential well varies as ϕ_0^3 .

IV. MECHANICAL DESIGN

(1) Tank - The resonant cavity of the accelerator is housed in a vacuum tank 40 feet $6 \frac{1}{2} + \frac{1}{4}$ inches long and $48 \frac{1}{2} + \frac{1}{4}$ inches diameter (inside dimensions) made of welded $\frac{1}{2}$ inch boiler plate, with flat steel ends $1 \frac{1}{4}$ inches thick. The tank is divided longitudinally 4 inches above center, and the top lid is hinged at four points along the north side to permit the lid to be opened for access. Provisions for vacuum seal of the lid are described in Section IV-(3) of this report. Opening of the lid is accomplished by a pair of hydraulic cylinders mounted near the middle of the lid, and anchored to the pump manifold which is a protuberance from the bottom half of the tank, on the north side. The entire tank is supported on two pads, each $\frac{1}{4}$ of the way from an end of the tank. The east end pad rests on a 2-foot long, 2-inch diameter steel bar which can roll east-west on a steel plate that in turn is fastened to the concrete floor. The west end pad rests on two similar bars which give some rotational stability to the tank. The 2-foot long bars are sufficient to keep the tank from falling over, but additional stability against rotation is provided by resting the pump manifold on the floor. The tank is thus mounted so that it can expand freely with temperature changes.

The resonant cavity is also mounted so that it is free to expand and contract with temperature changes independently of the steel tank. In the southeast and southwest corners of the tank, groove pads with the groove pointed east-west are mounted at the height of the middle of the liner. In the north center of the tank there is a similar pad with its groove oriented north-south. The liner is not sufficiently rigid to be supported at just these three points, so 15 spring loaded pads with hardened flat ground surface are equally spaced around the sides of the tank to distribute the support points. On the liner there are $\frac{3}{8}$ inch bolts with hardened steel balls soldered to the ends so that the resonant cavity is supported at 18 points, of which three constrain its position and motion. This elaborate mounting was installed after it was noticed that the steel vacuum tank warped in places as much as $\frac{1}{2}$ inch when the lid was raised and lowered. Methods of accommodating for this warp

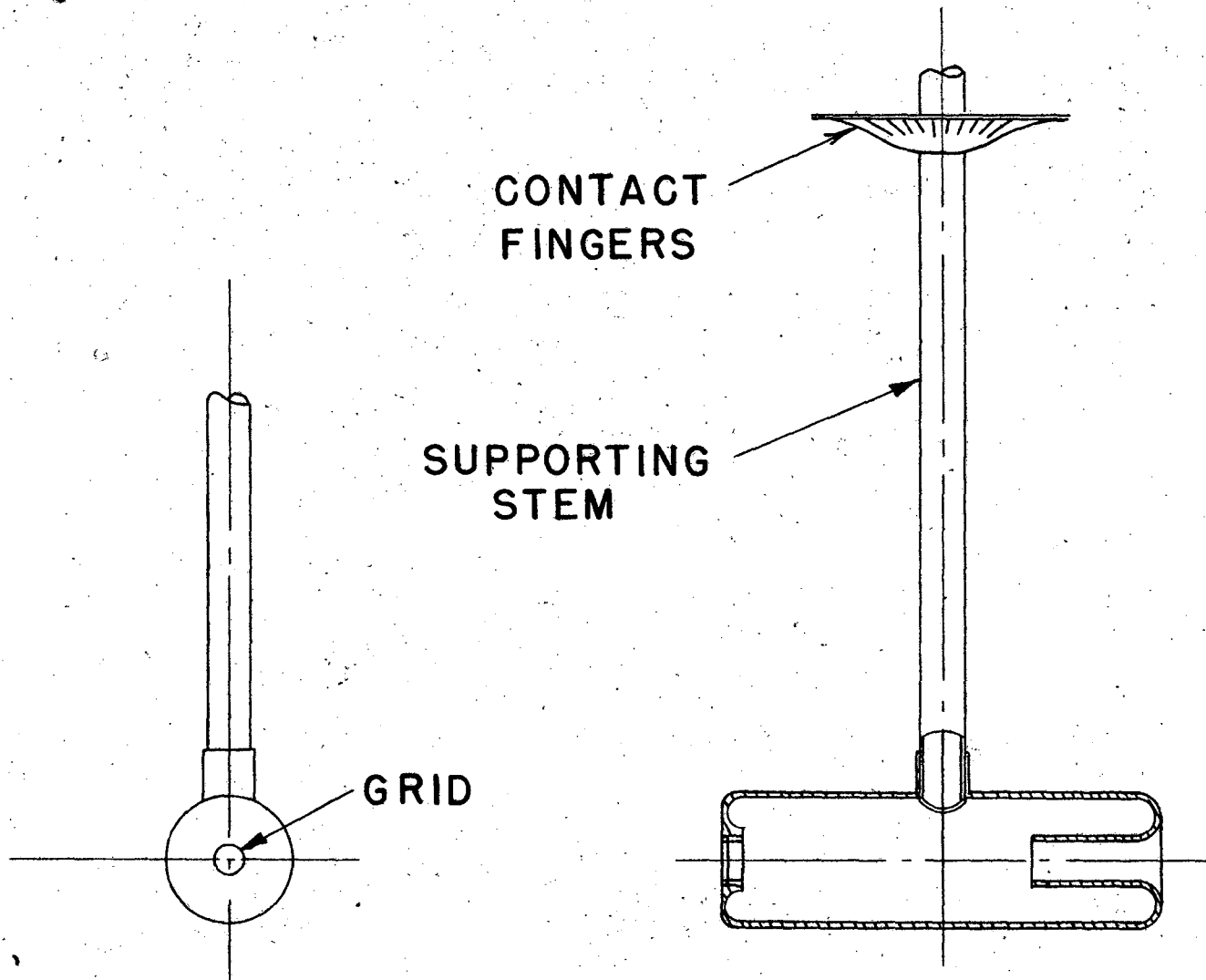
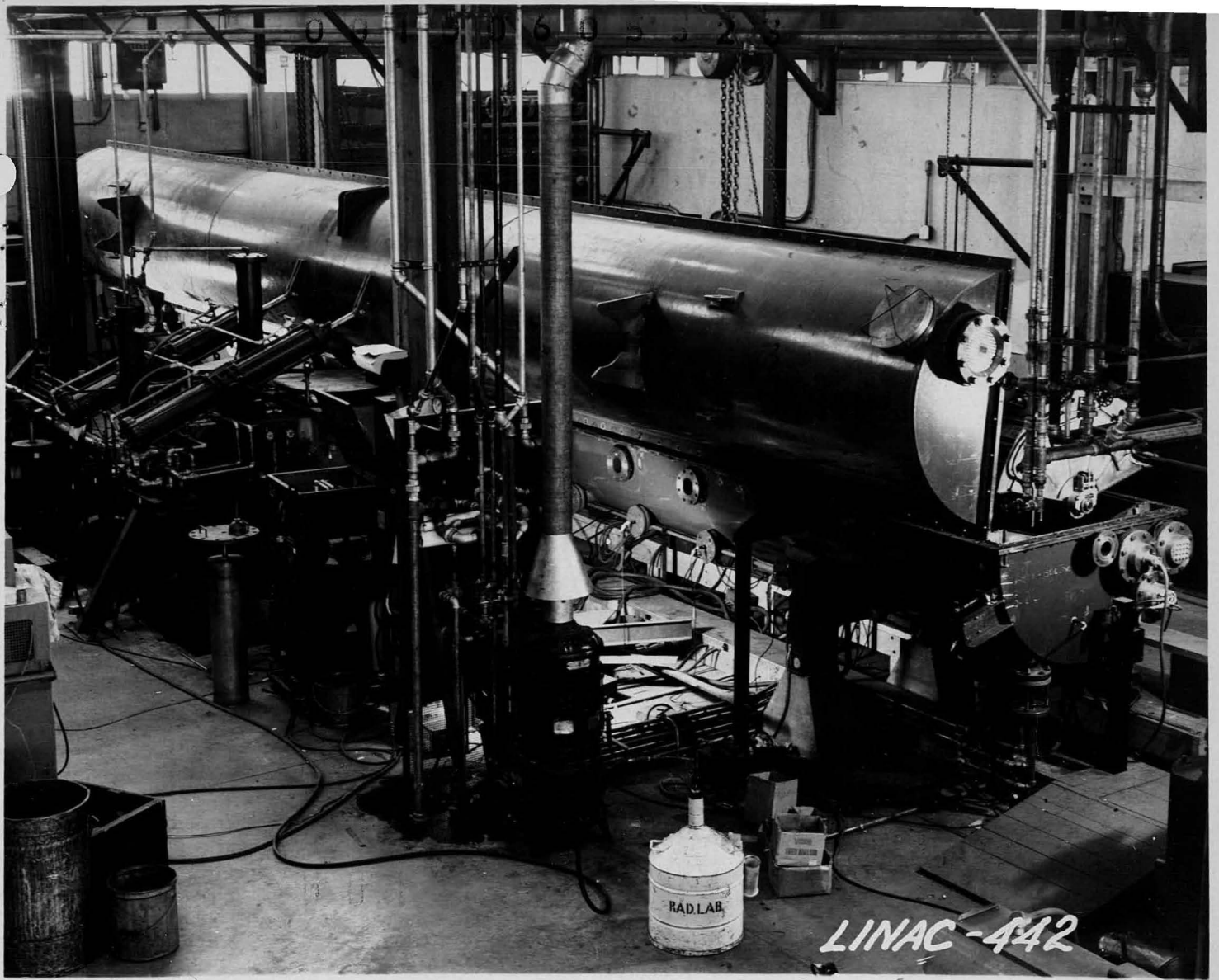


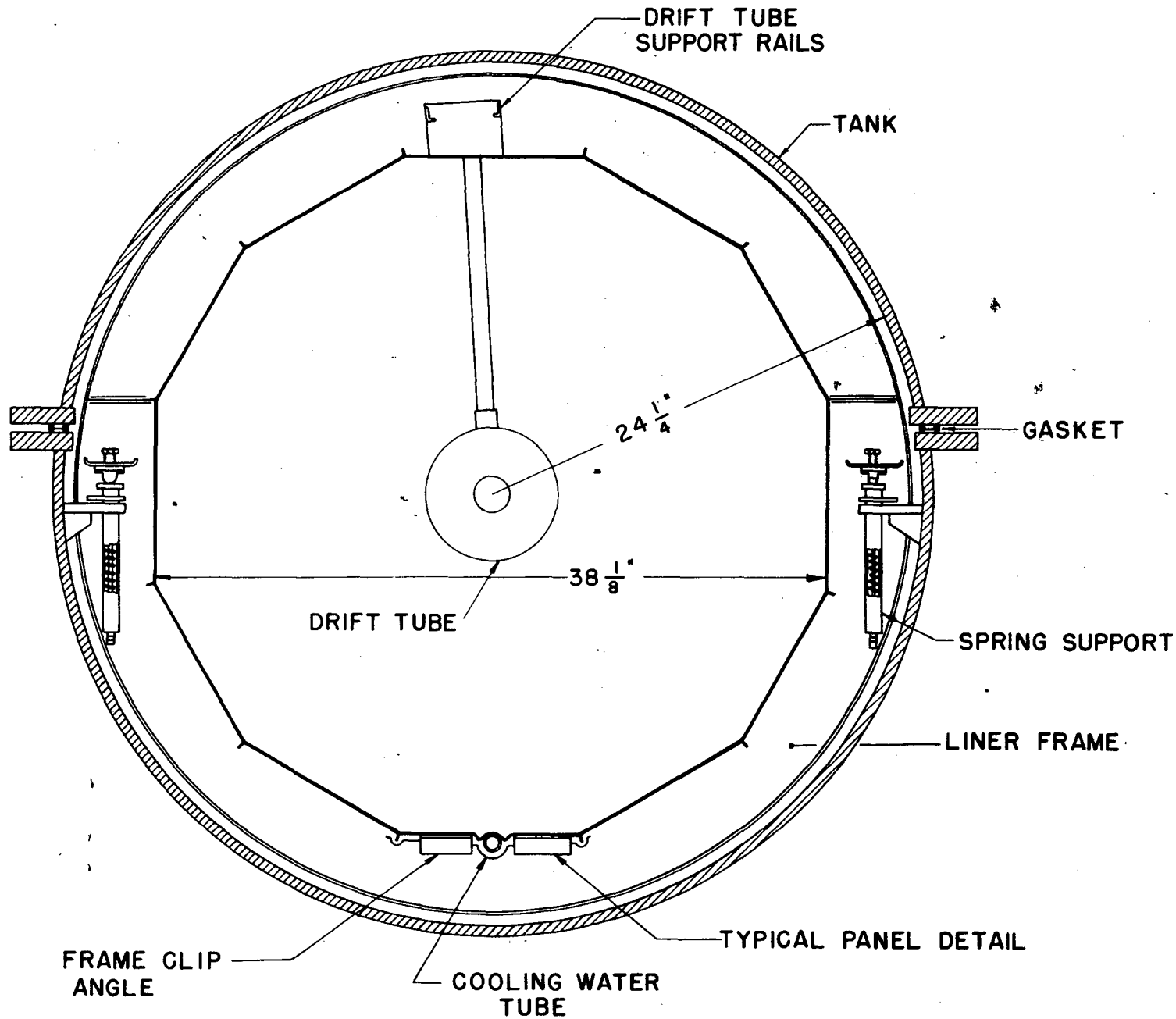
Fig. 21 Outline Drawing of Drift Tube

001000605333



PHOTOGRAPH OF TANK OPENED FOR RECEIVING LINER
FIG 17

02-267



100100605524

FIG. 18

DIAGRAM SHOWING DISPOSITION OF TANK & LINER

COGN-1-2-1-1

2-2

in the attachments between liner and tank, i.e., r.f. transmission lines, water cooling lines, and end tuning motors, are indicated elsewhere in this report.

The tank, opened by the hydraulic lifts, is shown in Fig. 17.

(2) Liner Design - With the decision to separate the mechanical and electrical functions of the linear accelerator resonant cavity came the need for the design of an accurate, rigid, and light weight tubular lining for the vacuum tank. This "liner" became a structure basically similar to a monocoque airplane fuselage of frame, stringer and sheet construction save that the sheet surfaces were on the inside. Since it was desired to avoid circumferential joints in the sheet surfaces, and since the cross section was constant, it became practicable to roll copper strip stock into panels of the length of the liner, with flanges and corrugations to serve as longitudinal stringers. By using die-formed circumferential frames with a polygonal inside cross section, the longitudinal panels could be flat and the necessary dimensional tolerances could be more easily maintained. The cross section of the liner as situated in the tank is diagrammed in Fig. 18.

The specifications were consequently set for a liner of dodecagon cross section of 38 1/8 inch dimension across flats, 480 inch length and split longitudinally into two unequal parts, of 150° and 210°, to permit support of the lower part along the horizontal centerlines. Provisions for cooling of the liner and support and cooling of the drift tubes were to be made. To permit access for accurate adjustment and alignment of the drift tubes it would be necessary to provide for a uniformly spaced separation of the lower and upper parts of the liner by means of integral extensions of the upper part of the frames which could be rested upon the corresponding lower part by moving the upper part longitudinally by the thickness of the circumferential frame. Provisions for handling the complete liner assembly, as well as the upper part, separately, and for clamping the two parts rigidly together were also needed.

To permit measurement of the resonant frequencies of the cavity both with and without drift tubes it was decided to procure a 45-inch-long prototype of the liner. The prototype was to be partially hand made, including forming of the copper panels on

a power brake with maple dies. This would also enable the design details to be tested before completion of the production tooling.

Since the liner had become essentially an aircraft type of structure, arrangements were made to obtain the services of the Douglas Aircraft Company for the preparation of shop drawings and fabrication of the prototype and production liners. This arrangement proved eminently satisfactory in both the quality of the finished product and the expedition with which the job was completed.

(3) Liner Construction - The longitudinal copper panels were rolled from an .032 inch thick by 13 inch wide by 60 foot long copper strip to have a flange turned up at each edge and to have a semicircular channel in the center to receive a 5/8 inch copper cooling-water tube. The channel was raised above the surface in order that the inside surface of the finished panel would remain essentially flat. Since only soft copper strip was available for the rolling it was necessary to stretch the strips on a hydraulic stretch bench both before and after the rolling as well as after the cooling tube was soft soldered into its channel to work harden and flatten the copper. The cooling tube was also stretched to straighten it as it was supplied in 50 foot coils. After the panels were given the final stretching, sets of slots for pump-out openings were cut through the panels in such a pattern that slots were arrayed between alternate sets of frames in alternate panels in five of the lower panels in the general area of the vacuum manifold. A total of 40 slots one-half inch wide by 12 inches long were used, with the slots strapped every four inches. Thirty-three circumferential frames were made in two parts from .072 inch 24 ST aluminum alloy. The flanging of the frames was done in a hydropress by the Douglas Guerin process. The internal flange, to which the copper attached, was made of short lengths of extruded angle riveted to the frame in a separate sub-assembly jig. This enabled the dimensions of the inside of the liner to be held within the specified uniformity tolerance of .005 inches. Clearance cutouts for the cooling tubes and drift tube supports were provided and reinforced where necessary by attached angles. The frames were finished with an aircraft zinc chromate primer.

SUPPORT RAILS
OF LINER

CLAMP SCREWS

UPPER CLAMP
PLATE

ADJUSTING SCREWS

LOWER CLAMP PLATE

ADJUSTMENT
SPRING

SPHERICAL WASHER

DRIFT TUBE
COOLING LEADS

DRIFT TUBE
STEM

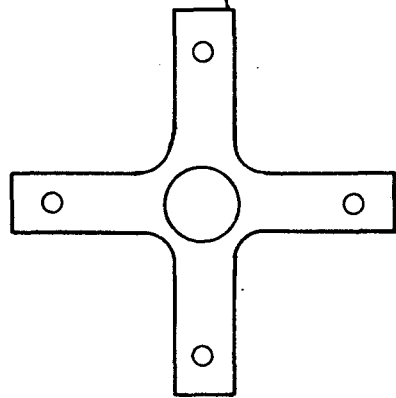


Fig. 19 Drift Tube Clamps and Arrangement

00100605527

The liner end plates were hydropress formed from .045 inch thick hard copper. A typical end plate was designed for the lower part of the liner with integral flanges on all edges. This same 210° plate was then hand trimmed to 150° and provided with riveted flanges for the upper part of the liner. Additional spare sets of end plates were obtained for use at the Radiation Laboratory as movable diaphragms for measurement of the frequencies of each section of the liner during installation of the drift tubes. These diaphragms were provided with phosphor bronze spring contacts around their periphery and reinforced with an aluminum frame so that they could be moved along the liner as the measurements progressed.

Support rails for the drift tubes ran from end to end of the liner through cutouts in the frames. These rails were interrupted every 30 inches to allow for differential thermal expansion. Openings for the drift tube stems could then be cut through the copper panel at any point without interference with frame position. These openings, as well as those for transmission lines, probes, and other purposes, were subsequently cut with chassis punches. Support of the drift tube was accomplished by two clamp plates that were placed on each side of the salient flange of the angles that formed the rail. (Fig. 19)

Three inch diameter holes are punched in the end and the side of the liner, opposite glass viewing ports in the vacuum tank. This enables one to observe sparking and other related phenomena in the liner.

Vertical aluminum braces are attached between the end of the liner and the "end tuner" structure, to provide rigidity to the tuner. An end tuner consists of a drift tube extending into the resonant cavity from the end of the liner, with length controllable by a worm gear which is driven by a flexible shaft leading to a motor outside the vacuum tank. Electrical contact is made between this drift tube and the end of the liner by means of a tight fitting slotted collar of silver-plated steel, fitting around the drift tube, and bolted to the liner. The west end (entrance) tuner drift tube is 4.750 inches diameter, and adjustable in length from 2 inches to 4 inches. The east end tuner drift tube is 2.750 inches diameter and 4 inches to 7

inches long. Nominal settings are 2.97 inches and 5.60 inches respectively.

The liner was supported by means of leveling screws at nine uniformly spaced stations along each side of the liner. An intercostal member between pairs of frames was provided with a plate type self locking nut through which the leveling screw passed. These intercostals were formed by flanging .091 inch 24 ST aluminum alloy sheet. The leveling screws were provided with spherical ends which rested in turn upon the spring supported pads of the main tank as previously described.

The spacing legs to permit the upper part of the liner to be supported at a fixed distance from the lower part, within a tolerance of .005 inch, as was required when adjustments were being made, were formed from aluminum alloy sheet as a channel and riveted to the upper part of the circumferential frame. Holes were provided in the flanges at the open end of each circumferential frame and each spacing leg for the installation of dowels in the upper part to mate with holes in the lower part for both the case where the liner was closed and when in position on the spacing legs.

Assembly of all of the component parts was accomplished in a jig approximately 20 feet long which located the copper panels and the circumferential frames in the proper positions. Aluminum alloy rivets were inserted from the inside through the copper panels and frame flanges and headed on the outside of the flange. These rivets were brazierhead aircraft rivets that were dipped in zinc chromate paste before installation. Zinc chromate paste was also used between the faying surfaces of the frames and copper panels. This paste minimizes electrolytic action between the aluminum and copper due to atmospheric moisture although it was felt that this condition would not be serious since the liner generally remained in the vacuum tank. The extended ends of the copper panels were temporarily supported on a wooden framework during the assembly of the first 20-foot section. When this was completed the liner was moved along the assembly jig for a progressive assembly of the succeeding frames. An overlap was maintained to permit accurate indexing of parts and the overhang of the assembled portion was also supported on a wooden frame. This assembly procedure was accomplished with each part of the liner turned with its open side downward and the workmen working

0 0 1 0 0 6 0 5 5 3 0



LINAC-438

LINER SUPPORTED ON LIFTING FIXTURES
FIG. 20

from the inside towards the outside. After the lower part of the liner was completed it was rolled over on felt pads on the floor and the upper part of the liner was then placed on the lower. Attachment of the upper and lower parts both in service and for shipment from the factory to the laboratory was accomplished by means of Cleco fasteners through holes in the flanges of the mating surfaces of both the copper panels and end plates at a spacing of 5 inches. In service the gaps between the panel flanges were checked by feeler gages and maintained at less than .020 inch to reduce high frequency leakage. Flanges on the aluminum frames were also temporarily clamped together during shipment.

Handling of the two parts of the liner and of the completed liner was accomplished at the factory by means of a fixture consisting of a 40 foot long steel tube with clips for attaching ties which were then in turn fastened to each circumferential frame of the liner. This fixture was replaced by a pair of lightweight steel tube frames fabricated at the Radiation Laboratory when it became necessary to handle the liner in service. These lightweight frames each attached to four points on the liner circumferential frames at stations ten feet apart and symmetrically placed with respect to the ends and centerlines. These attachment points were provided on both the upper and lower parts of the liner so that the upper part could be lifted off the lower when the latter was installed in the tank to permit access to the drift tubes. By attaching the lifting fixtures to the attachment points on the lower part of the liner the entire liner could be lifted from the tank. Fig. 20 shows the completed liner supported by these fixtures.

Each lightweight fixture was supported by an overhead crane through a manually operated worm gear hoist. It was found by service experience that electric hoists and spur gear hoists were unsatisfactorily rough in operation since it was necessary to start and stop the liner motion smoothly and to be able to lower it by minute increments when placing it upon the supports.

A shipping fixture was made in the form of an enclosing rectangular frame fabricated by welding from heavy steel angles. Removable transverse members on the top of

this frame permitted the liner to be lowered vertically through the frame to where it rested on padded supports and was clamped in place with additional padded supports placed against the top of the liner.

(4) Drift Tube Construction and Support - The drift tubes were basically a cylinder of variant length and diameter supported by a single stem perpendicular to the liner axis at the center line of each drift tube. The drift tube diameter varied from $4 \frac{3}{4}$ inches to $2 \frac{3}{4}$ inches, the first eleven drift tubes being constant at $4 \frac{3}{4}$ and the remaining 35 drift tubes diminishing to $2 \frac{3}{4}$ in steps of approximately sixty-thousandths of an inch. The drift tube lengths varied from about $4 \frac{3}{8}$ for the first drift tube to 11 inches for the last drift tube. The drift tube body was made of a copper tube with the end at the beam exit made from a copper plate hard soldered into the tube and with a threaded ring in the opposite end. Into this threaded ring screwed a cap which in turn received a grid holder. The exit end of the drift tube had a re-entrant opening formed by a brass tail tube about 3 inches in length and varying from 1 inch inside diameter to $1 \frac{1}{2}$ inches inside diameter for the range of drift tube sizes. All external edges were uniformly rounded with a radius of $\frac{3}{8}$ inch. The external dimensions were obtained by machining; the entire surface of the drift tube to a tolerance on diameter and length of plus or minus two one-thousandths of an inch. The threaded cap was originally designed to be screwed into the drift tube body after the grid holder had been inserted from the inside. On the initial runs serious sparking was found to have occurred across the contact surface between the drift tube cap and body even though special effort had been taken to insure high contact pressures at this point. Thus it became necessary to solder the drift tube cap to the body with a low temperature eutectic alloy and to redesign the grid holder so that it could be inserted from the front of the drift tube. The threaded construction, however, did permit final adjustment of drift tube length to be made after voltage distribution measurements were completed.

The drift tube stems were made of one inch diameter brass tubing soft soldered into a reamed boss on the transverse center line of the drift tube. Through this stem

was passed a quarter inch diameter copper tube that made a loop around the inside of the drift tube body to which it was soft soldered and then returned through the stem for circulation of cooling water. It was subsequently found necessary to silver plate the drift tube body and stem to reduce r.f. losses in the brass stem and tail tube. The drift tube stem was closed by a plug which carried a threaded extension. The drift tube components are diagrammed in Fig. 21.

The drift tubes were supported (see Fig. 19) by a pair of plates which clamped on the salient flanges of the drift tube support rails supported by the liner frames. One of these clamp plates had a large clearance hole while the other was provided with a seat for a spherical washer and with four tapped holes uniformly spaced about the seat. The threaded extension of the drift tube stem passed through a cross of steel, heat treated to a spring temper, thence through a hemispherical washer and was terminated with a nut. With the hemispherical washer resting in the seat provided in the clamp plate and with four cap screws through the threaded holes bearing against the arms of the cross, the drift tube was held firmly in position and could be adjusted along the three coordinate axes by means of the two pairs of screws on opposite sides of the stem and by means of the nut on the threaded extension.

(5) Liner and Drift Tube Cooling - A semi-circular distribution manifold was soldered to the end plates of the liner on both top and bottom parts. From this manifold radial tubes led to fittings on the ends of the 40 foot tubes soldered to each liner panel; thus, the panels were cooled by water flowing through these long tubes in parallel in circuits that came through the tank at one end, through the distribution manifold, along the panels into the collection manifold and out through a discharge lead at the opposite end of the tank. Separate circuits were maintained for the upper and lower parts of the liner.

The drift tubes were also cooled in parallel by a third water cooling circuit. Two tubes were supported in openings in the liner frames with one tube serving as supply header and the other as collection header. These tubes had nipples hard soldered to them adjacent to each drift tube into which the 1/4 inch copper tube



PHOTOGRAPH OF VARIOUS TYPES OF SLAT GRIDS AND BERYLLIUM FOILS MOUNTED IN HOLDERS

FIG. 22

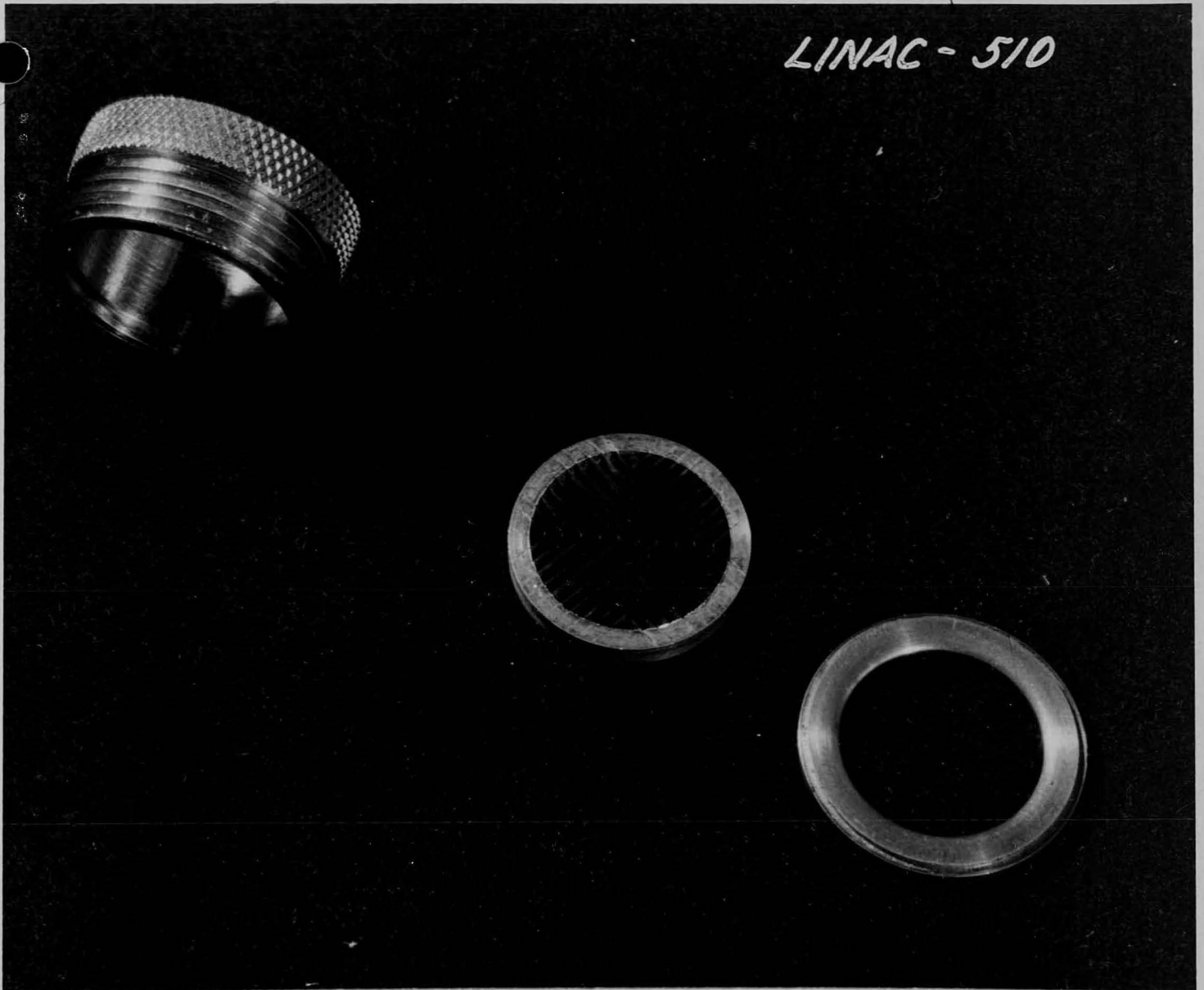
passing through the drift tube stems were soldered. By introducing the water at one end of the tank and removing it from the other the cooling water pressure drop through each parallel flow path was maintained the same. Checks upon the operation of the parallel flow system were made by putting hot water through the lines and feeling all the tubes to see that they were receiving their quota of water and that no obstructions existed in the individual circuits.

(6) Grids - As was shown in Section III of this paper, phase focusing and phase stability can only be achieved in the machine by introducing charge within the beam; e.g., by arranging the entrance end of drift tubes so that electric field lines terminate within the beam. This was first done by putting 3×10^{-5} inch thick beryllium foils across the entrance of each drift tube. However, sparking in the tank destroyed them, and grids were used instead. There is, of course, greater field concentration on grids than on flat foils. To a first approximation, if one considers a grid to be merely a foil with many holes punched out, the field is increased by a factor equal to the ratio of the total area to the area occupied by conductors, since the same number of lines of force end on the conductor, but on a smaller area.

The ratio of aperture to field strength can be improved by using a slat grid of structure similar to a klystron grid instead of a perforated plate, since some of the field line will terminate on the flat sides of the slats. Fig. 22 shows several grid shapes which have been used and also the beryllium foils.

Grids were fabricated from .002 x 1/16 inch tungsten ribbon. A 95° bend was put in short sections of this strip by means of modified vise-grip pliers. Brass rings mounted on a carbon mandrel were slit by a multiblade saw to a depth of 72 mils. The bent strips were put into these slots and hard soldered around the rim which was then given a finishing lathe cut. The grids were polished to approximate the theoretical shape by immersing in 2 molar NaOH and passing 5 amps. a.c. for 5 seconds between the finished grid and a tungsten rod. They were next soldered with pure tin into copper holders which hid the brass ring, and could be screwed into the entrance end of the drift tubes. Grids were given a thorough visual inspection through 30x stereo-

LINAC - 510



GRIDS OF THE TYPE NOW USED IN THE LINEAR ACCELERATOR
FIG. 23

scopic microscope, and sharp points were removed. Then they were tested by photometering the transmission of a beam of parallel light from a tungsten strip filament lamp. The optical path was: pin hole over strip filament lamp, collimating lens, grid, focusing lens, .010 inch diameter pinhole, photronic cell. It is interesting to note that this was a "good geometry"* experiment, so that an aperture of, say, 90 percent the total opening gave a photocell reading of 80 percent.

The final test of the grids was made by investigating their behavior in vacuum under d.c. field equal to the r.f. field of the linear accelerator. If the cold emission was less than 50 μ a after the grids had been given up to 5 minutes run-in time, they were accepted. The final grid in its mounting is shown in Fig. 23.

In practice, we do not believe that the etching procedure was necessary. We tested several grids electrically which had not been etched, and could not find any significant difference from the normal ones.

The 15 cycle r.f. pulses produce fields of 10^7 volts/meter between the drift tubes, or 4 gm/cm² on the drift tube ends. This pulsed force was sufficient to loosen the grid holders, so set screws were used to lock them into the drift tubes.

(7) Drift Tube Alignment - In order to align the drift tubes in the tank, the top half of the liner was placed on its legs on the bottom half which was in position in the vacuum tank (Fig. 24). Then after aligning roughly so that a beam of light would pass clear through all drift tubes, cross-hairs were inserted in both ends of each of the end tuners. The tuners and the liner were next adjusted so that they were in line and horizontal, as seen through a 24x precision engineer's level. Accuracy of measurement at the far (west) end of the liner was \pm 50 mils, and at the near end it was \pm 10 mils. Cross-hairs were then put in the entrance and exit end of No. 1 (the west end) drift tube, and brought into coincidence with the tuner cross-hairs by the drift tube support adjustments. A level was used to check that the drift tube stem was perpendicular to the liner axis, and the axial position of the drift tube center was checked by steel scale measurement to the end of the liner. A similar procedure was used to align No. 2 drift tube, and in addition the gap between No. 1 and No. 2 was

* i.e. the diffracted component of the beam is not recorded by the photocell.



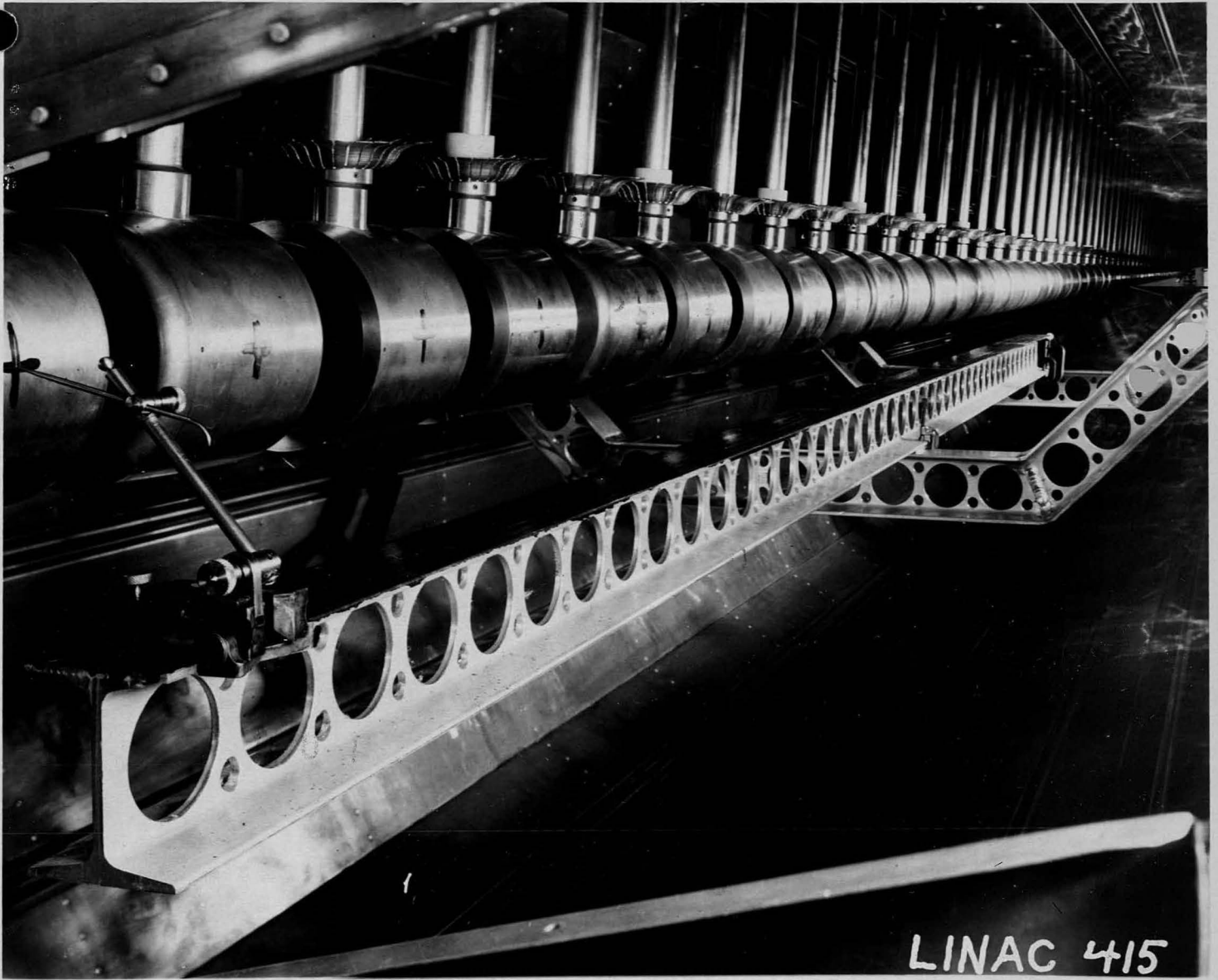
LINER OPENED UP AND STANDING ON EXTENSION LEGS TO PERMIT DRIFT TUBE ALIGNMENT

FIG. 24

micrometered at four points between drift tube faces to check alignment and position. A similar procedure was used for the rest of the drift tubes, except that the steel scale was replaced by a 10 foot long aluminum I beam upon which the accurate positions of drift tube centers had been scribed. A surface gauge was employed to transfer the scribed positions to the centers of the drift tube surface (Fig. 25). After alignment of drift tubes, the grids were carefully installed without disturbing drift tube positions. It is thought that this initial alignment was accurate to ± 25 mils. Later experience has shown that such accuracy is not required. A twist of 3° in drift tube No. 25, so severe that the beam area is reduced to half, reduced the beam of the linear accelerator by no more than a factor of 2.5. Axial displacement of a drift tube by $1/2$ inch did not affect the beam measurably, nor did $1/4$ inch axial displacement of four drift tubes, though this latter condition did make tuning of the pre-exciter more critical than normal and made the r.f. envelope fuzzy; i.e., other modes were excited noticeably. Present method of checking drift tube alignment consists of sighting by eye down the outside of the line of tubes to check axial position and alignment, and checking the distances between drift tubes with inside calipers to see that the lengths of successive gaps increase by approximately constant increments. It is to be noted that this relative lack of sensitivity to lack of proper alignment is true only after the initial adjustments of the lower harmonics have been made, as described in Section II. All the disturbances referred to here are presumably high harmonic perturbation to which the fields are relatively insensitive.

(8) Radiation Shielding - The stray radiation around the linear accelerator has been investigated to determine its sources and energies. The radiation comes practically entirely from x-rays produced by electron bombardment of the drift tube ends. The electrons arise from ion and electron cascading on the drift tube ends and gas between drift tubes. These sources were determined by exposing x-ray plates through an iron slat collimator "telescope" laid on top of the accelerator. The energies of the x-rays near the exit end of the accelerator were found by absorption measurements to be up to 2 Mev corresponding to electrons passing through one or two gaps between

00100605540



LINAC 415

AXIAL DRIFT TUBE ALIGNMENT PROCEDURE USING LENGTH STANDARD
AND SURFACE GAUGES

FIG. 25

07-265

No. 45 drift tube and the end of the liner.

One-half inch of lead shielding hung on frames near the sides and top of the linear accelerator has reduced the x-ray level, measured two feet from the machine, to ~ 10 MR/hr. The shielding has many openings such as holes for the transmission lines, and four-foot wide space below the Pb, so that there is scattered radiation throughout the room. The level 30 feet from the machines is ~ 5 MR/hr.

Note from Fig. 26 that the x-ray level increases by a factor of 3 per kilovolt d.c. in the operating region of the machine, the normal operating level being 10 kv d.c.

Three inches of lead glass are provided over the tank windows through which the inside of the liner can be viewed.

After the tank has been let down to air and re-evacuated, the radiation level is higher by a factor of 2 to 5, but improves quickly with running of the r.f. which serves to outgas the system. Outgassing can also be speeded by running hot water through the liner cooling lines, though that has very seldom been done.

(9) Vacuum System - The basic requirements of the linear accelerator vacuum system are, first, a base pressure 10^{-5} mm or less and, second, a pump-down and bake-in time of reasonable length, say, 8 hours. To fulfill these conditions in a steel tank 40 feet long, of 15,000 liters capacity, containing about 500 vacuum seals and joints and several hundred feet of polyethylene cable, it was obviously necessary to provide a fast pump and keep leaks and outgassing to a minimum. That this has been done successfully can be seen from the fact that at present the base pressure is about 2×10^{-6} mm, the rate of pressure rise with the pumps closed off is as low as 10^{-7} mm/sec., and bake-in times as short as 4 hours have been recorded.

Pumps - The pumps used are a 30 inch three-stage diffusion pump with a pumping speed of 7000 liters/sec. and an 8 inch two-stage diffusion pump in series, backed by two 43 c.f.m. Kinney rotary mechanical pumps in parallel. The diffusion pumps use Litton oil, which is effectively kept out of the tank by a thorough refrigerated baffling system. The pumping speed measured inside the liner is 2,500 liters/sec.,

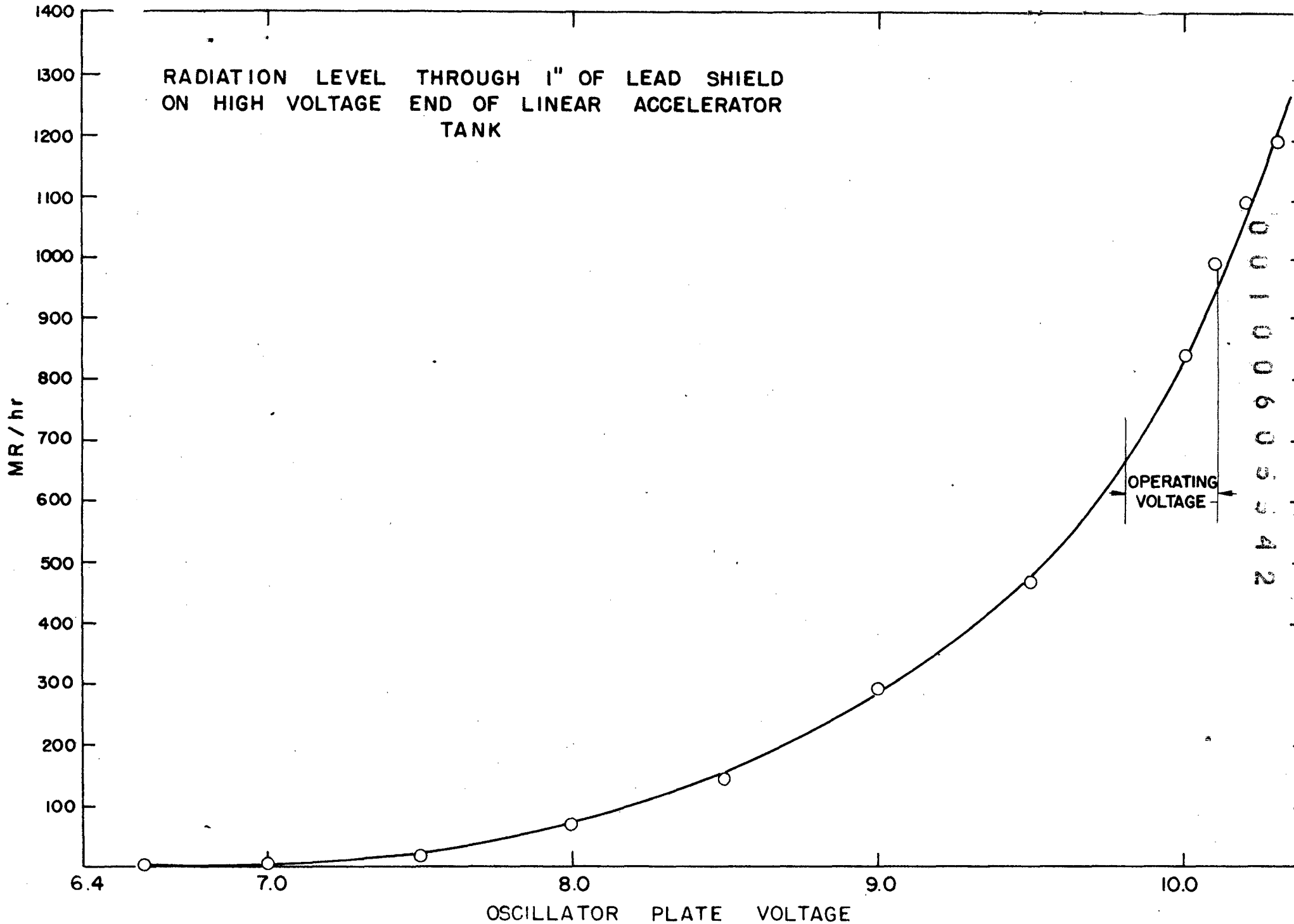


Fig. 26 X-ray Level Near Output End of the Linear Accelerator as a Function of Operating Voltage

which is considered a reasonable fraction of the speed of the pump alone.

For the first stages of pumping down there is a three inch pipe line about 250 feet long connecting the linear accelerator fore-vac system to a 750 c.f.m. Beach-Russ mechanical pump in the 184" cyclotron building. The pumping speed of this line becomes low around 500 microns and at this point the two 43 c.f.m. Kinney pumps take over. The 8 inch diffusion pump will operate against a back pressure of 125 microns, and the usual operating pressure of the Kinney pumps is between 10 and 20 microns.

In order to remove condensible vapors from the tank and prevent pump oil from entering it, a water-cooled baffle, (see Fig. 27) a refrigerated baffle, and a liquid nitrogen trap have been employed. The trap will hold almost 40 liters and consumes 200 liters of liquid nitrogen per day. Recent experiments indicate that it is possible to run without this trap, after the initial outgassing. The refrigerated baffle is cooled by a small freon refrigerator to a temperature of about -30° C and has been very effective in stopping the oil vapors from the pump.

Seals and Joints - A very wide variety of seals is used on the linear accelerator. Besides the usual types, such as soft and hard solder joints, gaskets, and arc-welded seams, there are Wilson seals, sylphon seals, aircraft-type spark plugs, and even certain standard r.f. connectors which have been found to be vacuum-tight.

Perhaps the most noteworthy of the gasket seals is the main tank gasket, which runs completely around the tank and is almost 90 feet long. To eliminate the expense of machining a flange 40 feet long it was decided to use a molded rubber gasket held to the flange with special screws and retained by a 1/4 inch square strip of steel tack-welded to the flange along the vacuum side (see Fig. 28). Despite the un-machined flange, the performance of this gasket has exceeded our expectation. Three bolts on each side suffice to hold the flanges together and when the pumps are started, the external air pressure exerts ample force to complete the seal. The heads of the screws act to separate the flanges and prevent them from damaging the gasket.

Another problem is encountered in making vacuum-tight the coaxial lines that transmit power from the oscillators to the cavity. The requirements for this part

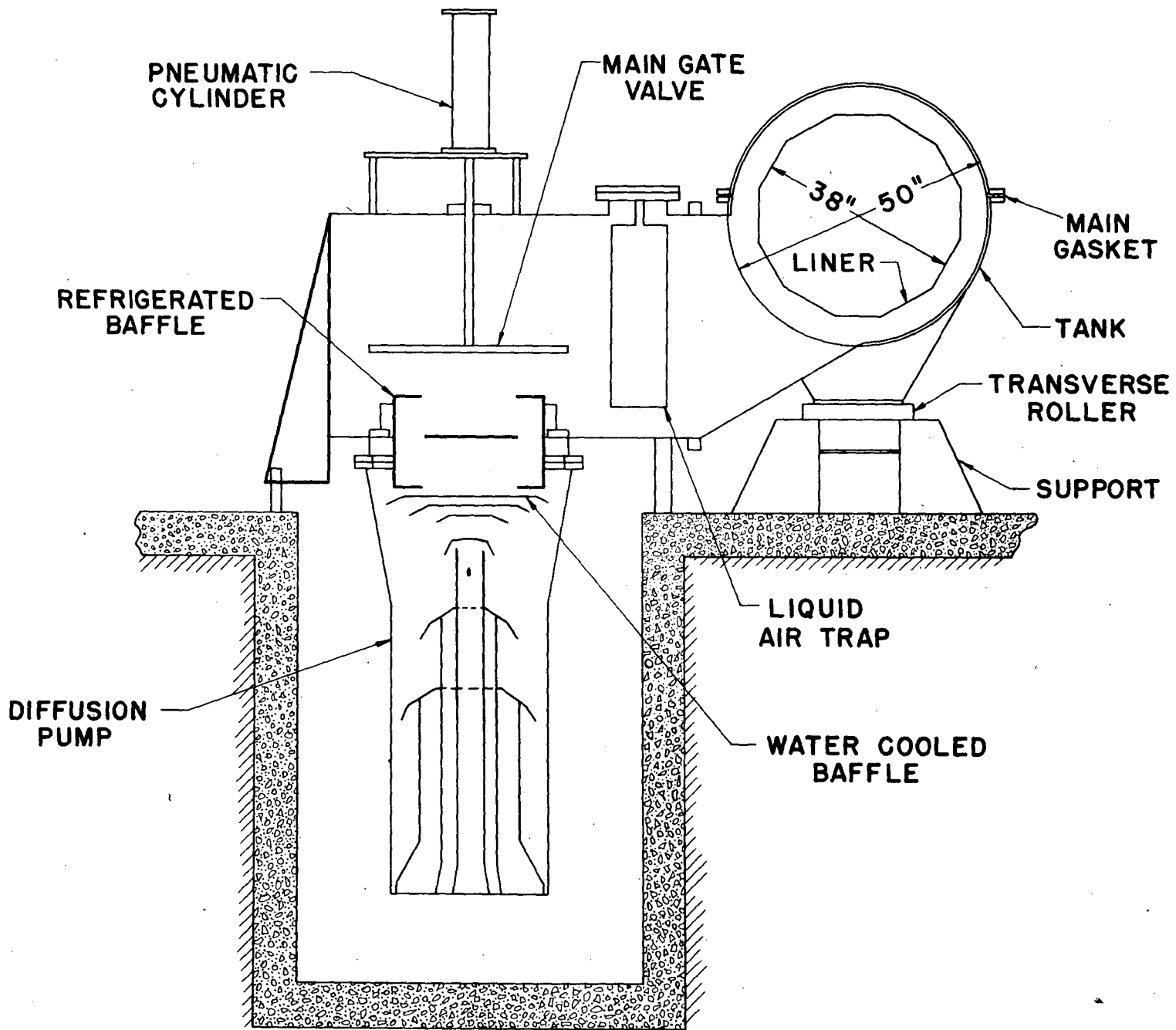


FIG. 27

OUTLINE DRAWING OF PUMPING SYSTEM

00100605344

STEEL

0-311

0 0 1 0 0 6 0 5 5 4 5

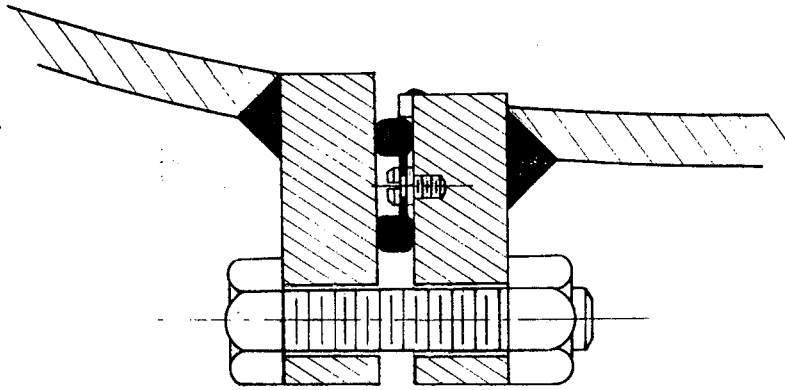


Fig. 28 Cross Section of Main Tank Gasket

were that it be vacuum tight, that the dielectric losses be small, that it make good electrical connections inside the tank, that it be capable of installation and removal without opening the tank, and that without impairing the seal, it could swing slightly from side to side and vertically to allow for motion of the liner inside the tank. A line utilizing a Housekeeper, glass-to-copper seal was tried and discarded as too fragile for the purpose. The design finally adopted is illustrated in Fig. 29. It will be noted that the inside of the inner conductor is evacuated, while the space between the two conductors is at atmospheric pressure. In spite of their complexity, careful fabrication and thorough pre-testing have made it possible to use these lines with a minimum of trouble.

The inner conductor is fastened to the coupling loop inside the liner by means of a captive screw which is reached with a long screw driver through the pipe-threaded hole at the other end of the inner conductor. The whole line is held against the external pressure by a retaining ring which permits some freedom of rotation of the axis of the transmission line about lines in the plane of the molded rubber gasket.

It has been found that the standard r.f. fitting RG-98U is satisfactory for bringing low power leads into the vacuum. The liner and drift tube water-cooling pipes are brought out of the tank through a rubber compression seal of conventional type.

The stems of most of the valves used on this tank are sealed with Wilson seals, and have given little or no trouble. Some sylphons have been used, both in valves and elsewhere, with spotty results. Most of them gave no trouble in use, while others repeatedly failed.

It is a policy of this laboratory to use double gasket seals wherever possible, and to provide a "pump-out" passage connecting the space between the gaskets with the open air. The pump-out is particularly important in that it gives a check point to determine the "tightness" of the whole inner gasket, regardless of small leaks in the outer gasket. It is also possible in emergencies to evacuate the space between the two gaskets until a more permanent repair can be made. The use of this arrangement

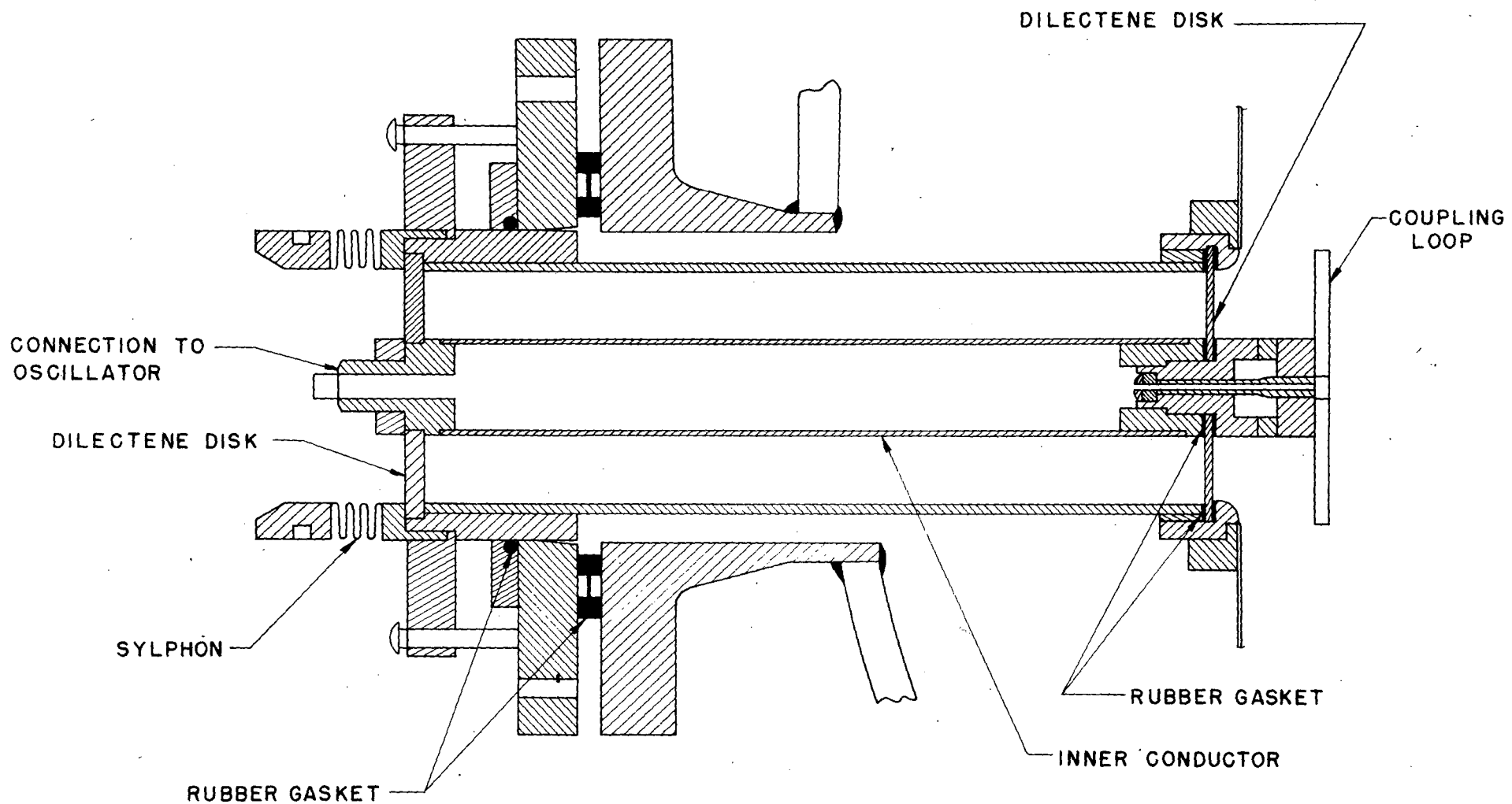


FIG. 29

OUTLINE DRAWING OF RADIOFREQUENCY TRANSMISSION LINE

00100603647

has enabled us to find quickly many leaks which otherwise would have been very insidious and hard to locate. All components are pre-tested before installation.

The inside surfaces of our tank have been painted with glyptal as a rust preventive measure. The first time the tank was evacuated there was heavy outgassing of the glyptal solvent, but in a few days this was over and much subsequent outgassing has thereby been avoided.

It was feared that the ceramic accelerating tube in the Van de Graaff generator might some day fail under pressure and raise the pressure inside the linear accelerator to 100 p.s.i. or so. To prevent this, a "blow-off" plate was installed which is held onto its gasket only by its weight and the external pressure. It is expected to relieve any internal pressure over one p.s.i. Both entrance and exit valves to the machine have been converted to solenoid controlled pneumatic valves interlocked to an ionization gauge protective relay which turns off the ionization gauge filament power and closes both valves whenever the pressure reading rises off scale.

V. OSCILLATORS

One of the major developmental problems in connection with a linear accelerator is the production of the large peak high frequency power required. The present machine is designed to operate with an average voltage gradient of .90 megavolts per foot or a total voltage of 36 million overall. This differs from the energy gain (28 Mev) of the particles due to operating phase angle and transit time loss. The shunt impedance of the cavity at resonance on the fundamental mode is 316 megohms. From these numbers one arrives at a required peak power of approximately 2.5 megawatts. The machine is pulsed on fifteen times per second with an "on" time of 300 microseconds, or a duty cycle of 225. This gives an average power input of approximately 10 KW.

While the average power requirements are quite moderate, the peak power could not be delivered by any single oscillator or tube in existence when the machine was planned. It was obvious that initial operation would have to be with a multiplicity of oscillators coupled into the resonator.

The original planning called for the use of surplus 200 mc radar transmitters

(BC-677) in essentially unaltered form. Several difficulties developed. One was the low efficiency of the oscillators, but the limiting difficulty was their coupling system. It proved impossible to couple these oscillators into the resonant cavity without the inclusion of a large resistive element in the coupling system to prevent the oscillators from jumping to frequencies determined by the coupling system and their own multiplicity of resonant circuits instead of the resonant frequency of the cavity.

With this large loss, the efficiency from d.c. power "in" to r.f. power "out" was in the neighborhood of 12 percent. This coupling system was inherently a loose coupled system, so that the oscillators had a very narrow turning range over which they would lock into the accelerator frequency, necessitating very careful tuning adjustments.

When it was realized that the BC-677 oscillators would be a definite weak link in the machine, a program was initiated to investigate possible modification of the units. From a standpoint of economy, it was desired to use as much of the original surplus equipment as possible. A quick series of tests determined that the tubes (GL-434-A) used in the BC-677 were not a limitation on efficiency and on this basis it was decided to use these same tubes in any new oscillator. In addition the following rough specifications were set up:

1. The frequency of the oscillator should be determined primarily by the linear accelerator cavity.
2. The oscillator should have reasonable overall efficiency.
3. The oscillators must be easy to maintain.

If the first two of these specifications are considered, they lead quite naturally to an oscillator in which the linear accelerator resonator is effectively the tank circuit of the oscillator. Such an oscillator would be capable of oscillating only on a frequency to which the main cavity was resonant, and would need no large loss element to damp modes associated with its own resonant circuits, for there need not be such circuits.

This type of construction suggests an oscillator tube of some sort mounted directly on the inside of the liner and having very low inductance loops coupling its input and

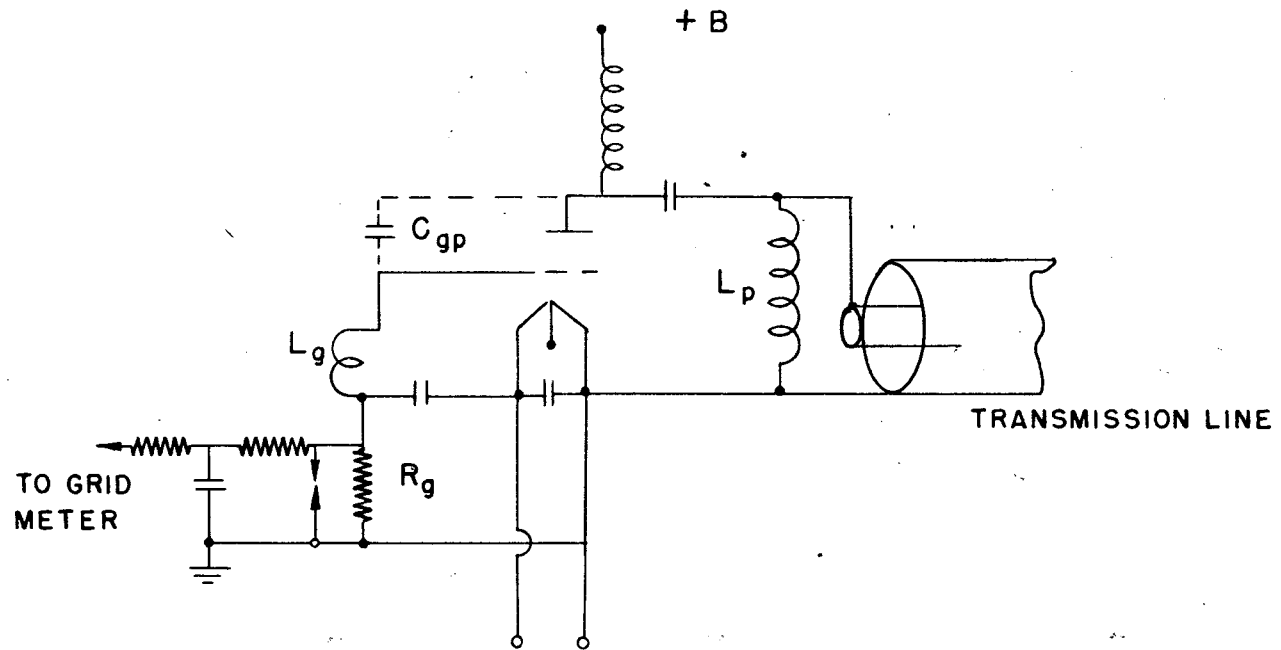


Fig. 30 Schematic Diagram of Oscillator

1 5 5 5 0 9 0 0 1 0 0

output circuit to the fields inside the tank. It brings with it the unfortunate requirement of developing a tube which could be so used, as well as cooling and maintenance problems.

A practical modification of this ideal scheme consists of using low inductance, tightly coupled loops in the cavity, but bringing them electrically outside of the vacuum tank by means of a transmission line an integral number of half wavelengths long. Such a line has the property of presenting at the sending end exactly that impedance which is connected at its receiving end. This scheme made it possible to have a pair of terminals outside of the vacuum system which for electrical purposes were as good as a direct connection to the loop inside, provided the standing wave ratio on the line differs considerably from unity.

The remaining problem was to design an oscillator which could use these tightly coupled terminals without sacrificing all of the tightness in the coupling to the tubes, in order to make the oscillator frequency and phase be controlled by the accelerator cavity.

From this concept, the oscillator design shown in Fig. 30 evolved. A short cylindrical cavity is used in which four tubes are placed symmetrically. The anodes of the tubes are connected to the bottom of the resonator (for r.f.) and the cathodes are connected directly to the top of the resonator. The resonator is tuned roughly to resonance by the capacity between the tube elements. In order to keep the oscillator free from circuits resonant near the desired operating frequency, the grid receives energy from the plate through the grid-plate capacity, with only a very small inductance inserted from grid to ground to determine the magnitude and phase of the grid signal.

In this construction, the r.f. fields of the output (plate-cathode) circuit are totally enclosed in the resonator as shown in Fig. 30. From this drawing it is seen that a co-axial line can be brought into the resonator in such a way as to link virtually all of the magnetic flux. In other words, it is possible to secure a connection to the output circuit with low series impedance. It therefore follows that the oscillator voltage will follow closely voltage developed across the loop in the

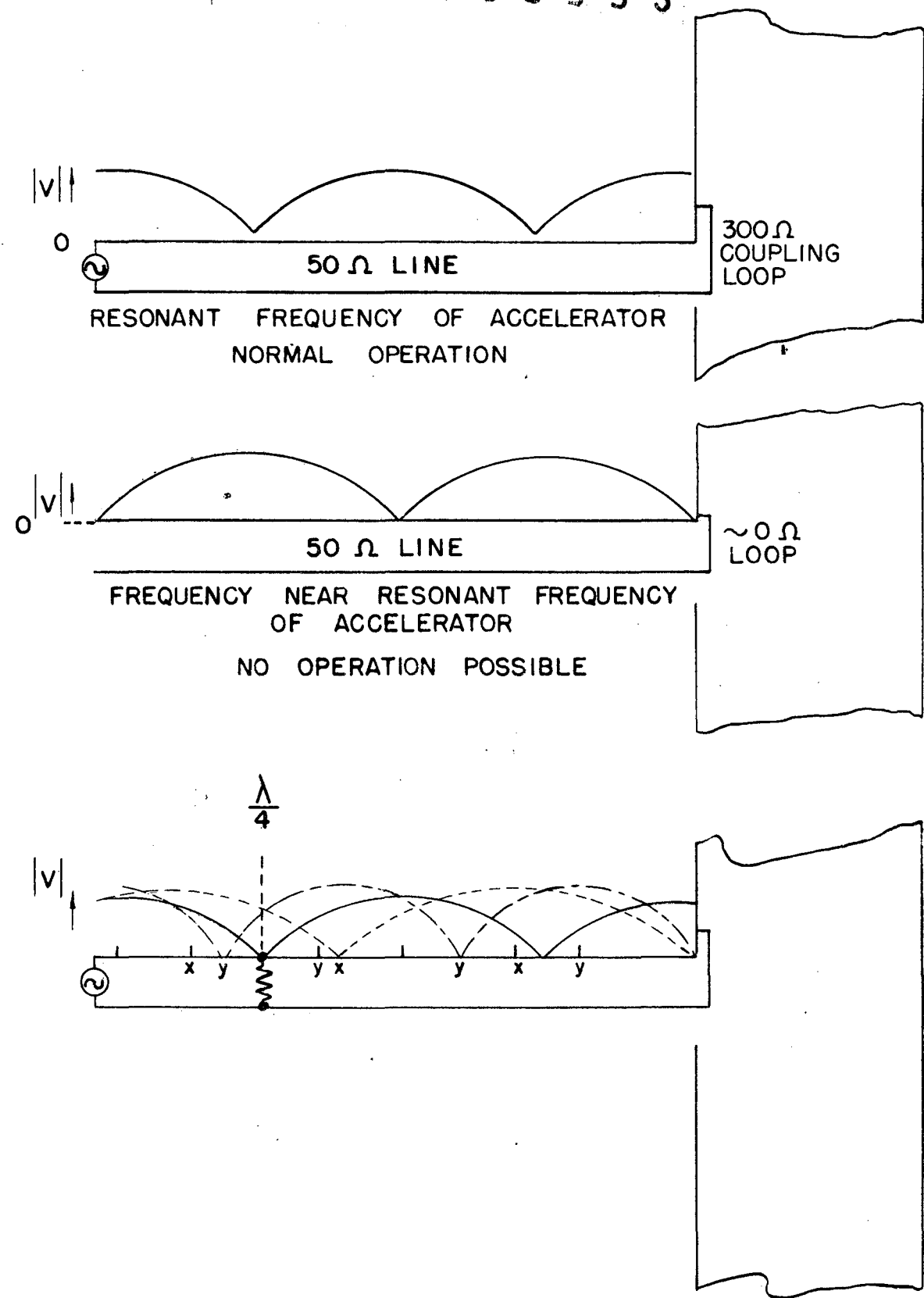


Fig. 31 Voltage Distribution Along Transmission Line for Correct and Incorrect Modes of Operation

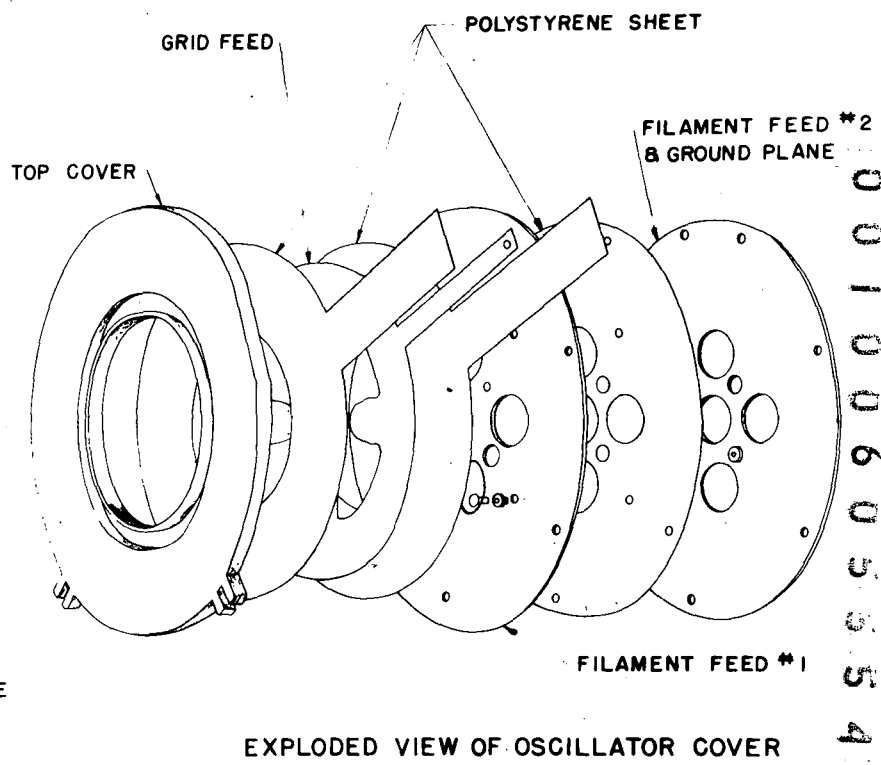
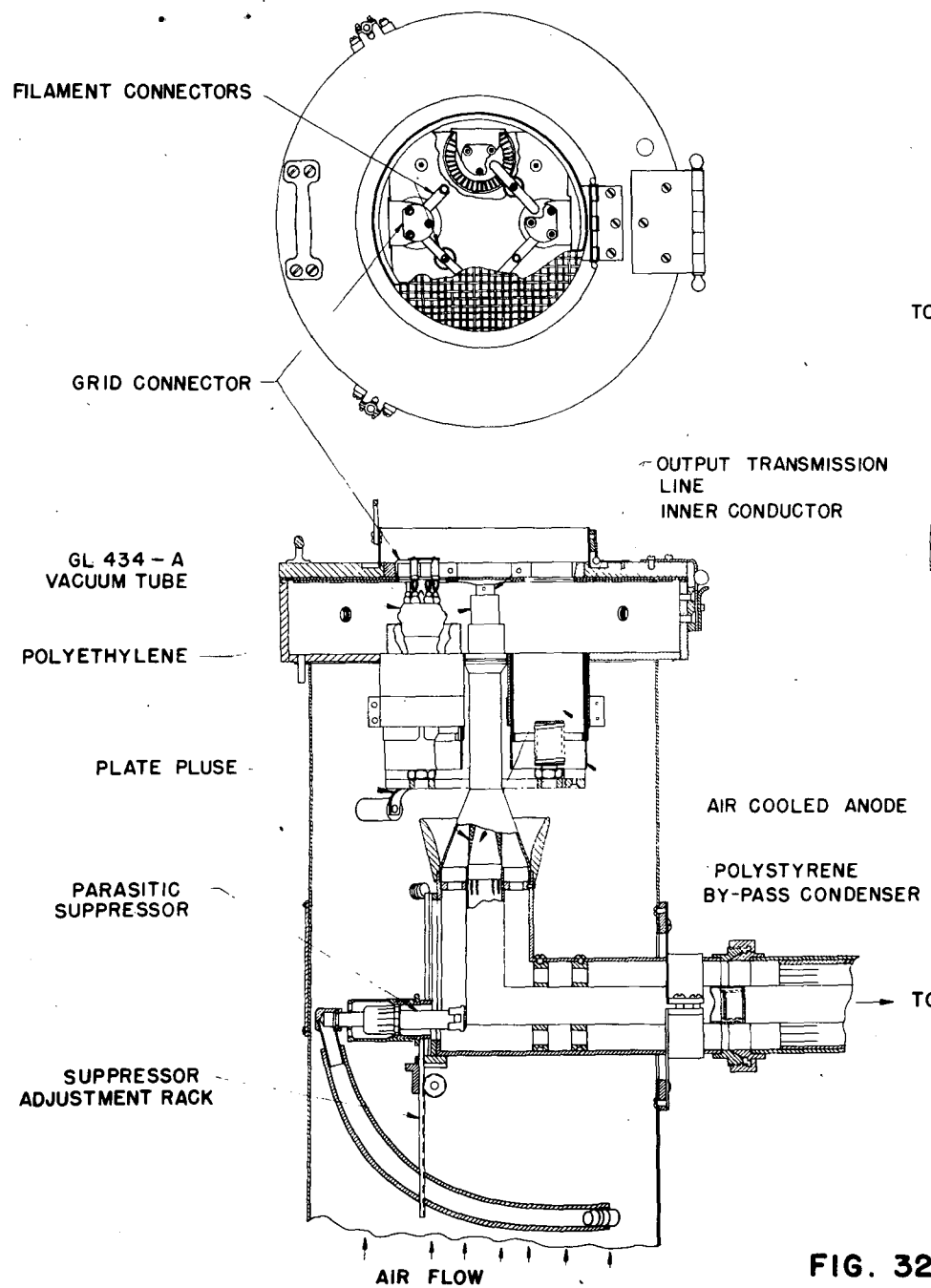


FIG. 32

OUTLINE DRAWING OF RADIOFREQUENCY OSCILLATOR

0010060554

main cavity. By unconventional design, it is possible to make the self inductance of this loop so small that the coupled impedance of the accelerator cavity at resonance dominates. These loops are copper plates approximately 3 inches by 4 inches located $3/4$ inch from the cavity wall, having an inductive impedance of approximately 15 ohms at 200mc. The coupled impedance at resonance of the cavity is 300 ohms.

Examination of the overall system shows one remaining problem, once again the matter of spurious modes. Looking at Fig. 31 which shows the impedance of the transmission line and loop system for various frequencies, it is seen that no mode can exist which is very close to but not on the correct frequency, since the coupling loop would present a very low impedance to such a frequency, and this would be reflected by the transmission line across the oscillator output. In addition oscillations differing by more than 50 percent from the correct frequency will not exist because the grid drive scheme is sufficiently selective to eliminate them. In tests, two frequencies other than the desired one did appear. One of these was about 20 percent higher in frequency, and the other 20 percent lower. The voltage distribution for these two frequencies and the desired frequency is shown in Fig. 32.

It is seen that there is a voltage node on the line for the fundamental frequency, $\lambda/4$ wavelengths from the oscillator. Since the line is terminated in a load only on a frequency to which the accelerating cavity is resonant and is short-circuited for other frequencies, there would be a large voltage on the line at the $\lambda/4$ point if such frequencies existed. If a resistor is placed across the line at that point it will have a large damping effect on the spurious frequencies without appreciably affecting the correct one. In practice it turns out to be possible to eliminate these undesired frequencies completely with a 700 ohm resistor at this point. The amplitude of the desired frequency at this point is only 1000 volts, which gives a loss in the resistor of approximately 2 percent of the transmitted power.

The choice of characteristic impedance of the transmission line from the loop to the oscillator is determined by the desired voltage at the node, which is approximately $1/6$ of the oscillator voltage. This leads to a value of 50 ohms, which also represents

the best ratio of inner diameter to outer diameter from a flashing standpoint.

Examination of Fig. 7 which gives the spectrum of frequencies to which the accelerator is resonant, shows that there exists very close to the desired frequency, other resonances, which to the oscillator will appear just as good as the correct one. The problem of keeping the high power oscillators from running on one of these other modes at first seemed formidable.

It developed in the course of the oscillator design that the oscillators would not build up when connected to a cavity by themselves, if the grid circuit was adjusted for optimum output at high level. Building up was prevented by the low power-gain of the tubes for small signals and the large energy storage or "fly-wheel effect" of the cavity. It proved possible to force the oscillators to build up by exciting the cavity to about 10 percent of the final voltage (1 percent power) by means of a loosely coupled oscillator pulsed on 100 microseconds ahead of the main oscillators.

This eliminated the problems of mode selection. All that is needed is to provide a low-power free running oscillator loosely coupled to the cavity. This oscillator can be manually tuned to the desired mode and the main oscillators will build up and run only on that frequency. In practice three pre-exciter are used to provide the power needed to start the main system of 25 oscillators.

The construction of an individual oscillator is shown in Fig. 32. The tube anodes are bypassed to the bottom of the oscillator tank with concentric polystyrene sheet capacitors for the purpose of d.c. plate voltage isolation. Since no r.f. fields exist outside the oscillator cavity, the d.c. can be applied directly to the bottom of the tubes. The grid and filament connections and associated bypass condensers are assembled on the top or lid, which is hinged to provide easy access to the tubes. All connections to the oscillator, including the r.f. output, are of the plug-in type permitting the entire oscillator to be disconnected quickly in case of failure. In practice a defective oscillator can be located, replaced and the machine restored to operation in two minutes.

The base, in which the transmission line from the accelerator to the oscillators

terminates, serves primarily as a support for the oscillator and as a cabinet for the filament transformer, motor blower and other accessory equipment.

The only metering provided for the individual oscillators at the control desk consists of meters reading d.c. grid current. These meters give a small constant reading whenever the filament of an oscillator is on, read slightly higher due to grid rectification when the pre-exciter is operating, and are inversely proportional to oscillator loading when the main oscillators are on. By noting the distribution of readings with respect to the individual oscillator positions along the tank when the pre-exciter is on, it can be ascertained whether the pre-excitation is on the correct frequency. This metering scheme has proved very satisfactory, and seems to represent the maximum information per meter.

For protection of the oscillators against tube flashes, each oscillator has a fast overload relay in its plate circuit which is arranged to shut the main pulse system off before the next pulse. The entire energy stored in the pulse system is prevented from appearing in any one tube flash by having resistors built into the base of each oscillator which are connected in series with the high voltage lead. With this protection, it is found that a single tube spark in general does no serious damage to a tube, and the machine can be immediately restored to operation.

The oscillators are limited in output primarily by the internal resistance of the tubes, and not by power dissipation in plate or grid. They are therefore loaded to operate at 50 percent d.c. to r.f. efficiency which gives the maximum r.f. power output.

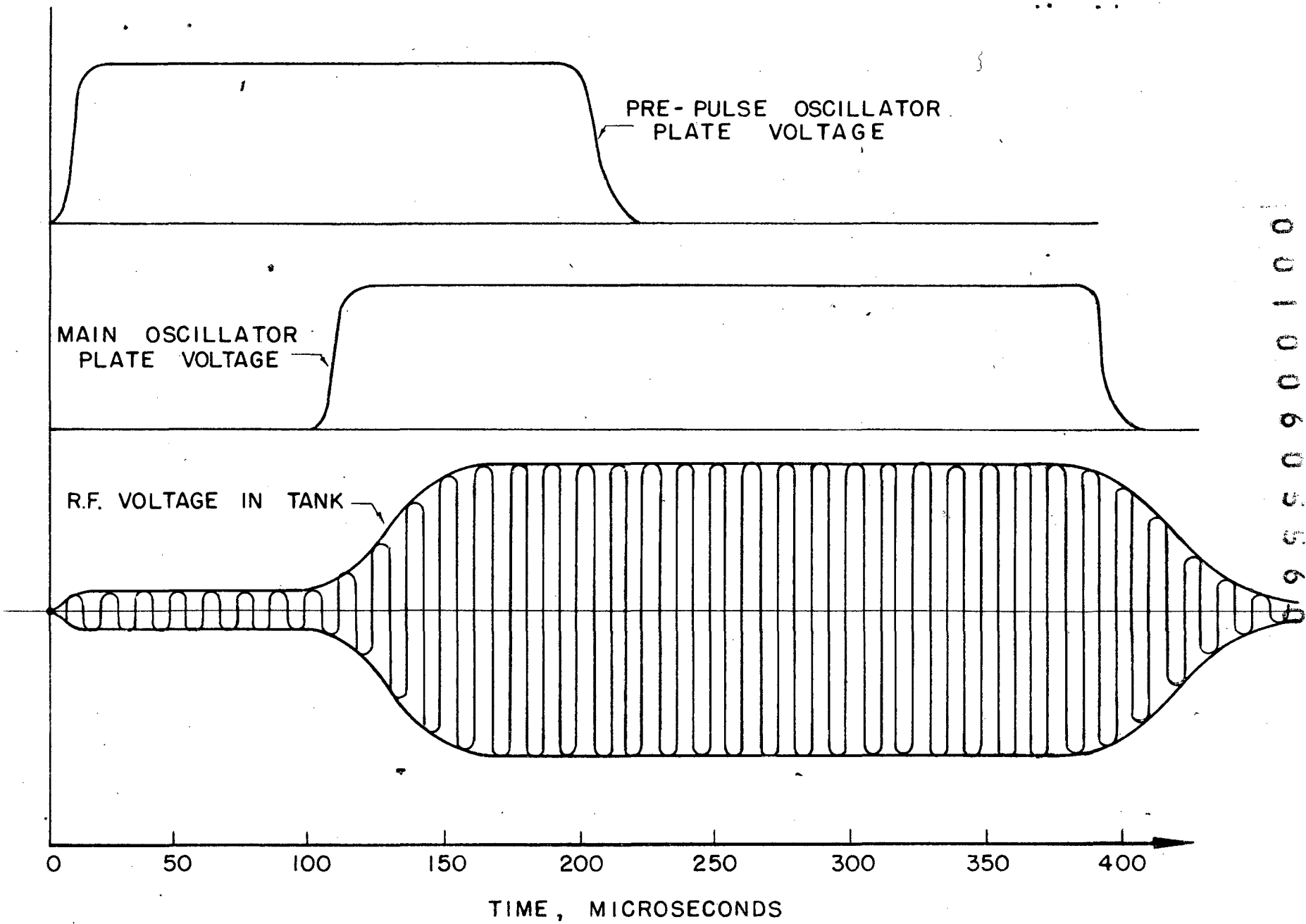
One problem almost universally met in devices using high voltage r.f. in a vacuum is "multipactor" action. This is a secondary electron multiplication process which can produce severe loading at low power levels, but once the system is above that level it disappears. The mechanism of this discharge can be illustrated as follows. Consider two parallel metal plates spaced some small distance and placed in a vacuum. In general the secondary emission ratio for metals (with usual surface contamination) will be greater than one. That is, if an electron strikes the surface more than one electron will be emitted.

If an increasing r.f. voltage is established between the plates, there will be found one value of voltage such that an electron can just cross the gap in exactly one-half cycle. If this energy is of the correct order of magnitude more than one secondary electron will be released, and these electrons will see a voltage such as to accelerate them back across the gap again where they will make still more electrons. This process builds up very rapidly, and can dissipate a large amount of energy. It occurs only at low amplitudes in our geometry because the transit time must be very nearly right for multiplication to be cumulative, and it limits the amplitude to this value.

The straightforward cures are to make the electron transit time different in the two directions by a d.c. bias, or to raise the voltage so rapidly that there are not enough r.f. cycles in the critical region for the discharge to become large. The linear accelerator entrance end provides extremely favorable geometry for such a discharge between drift tubes. The spacings between drift tubes in this region are of the order of one inch and it can be shown that this gap will be resonant for multipactor action at around 2000 volts. In addition there are many such gaps, any one of which can be responsible.

This problem produced some difficulty in early tests, and it was decided to remove the effect by isolating every other drift tube from ground for d.c. and to apply a bias such as to make the transit time different in one direction from that in the other. This method worked, but brought with it many difficulties in providing a suitable bypass condenser from the stems to the liner. Later it was discovered experimentally that the cavity could be pre-excited at the high energy end where the drift tube spacings were long and the geometry was not suitable for multipactoring, and the d.c. bias provisions were removed. It turns out that sufficient energy can be put into the high energy end (taking advantage of the very low group velocity of propagation of the cavity as a waveguide at cut-off) to bring the rest of the cavity up through the critical region fast enough to eliminate the effect.

With the cavity fed as described, build-up occurs in about 100 microseconds after



00100605568

Fig. 33 Wave Shape of the Plate Voltage and Radio-frequency Voltage Pulses

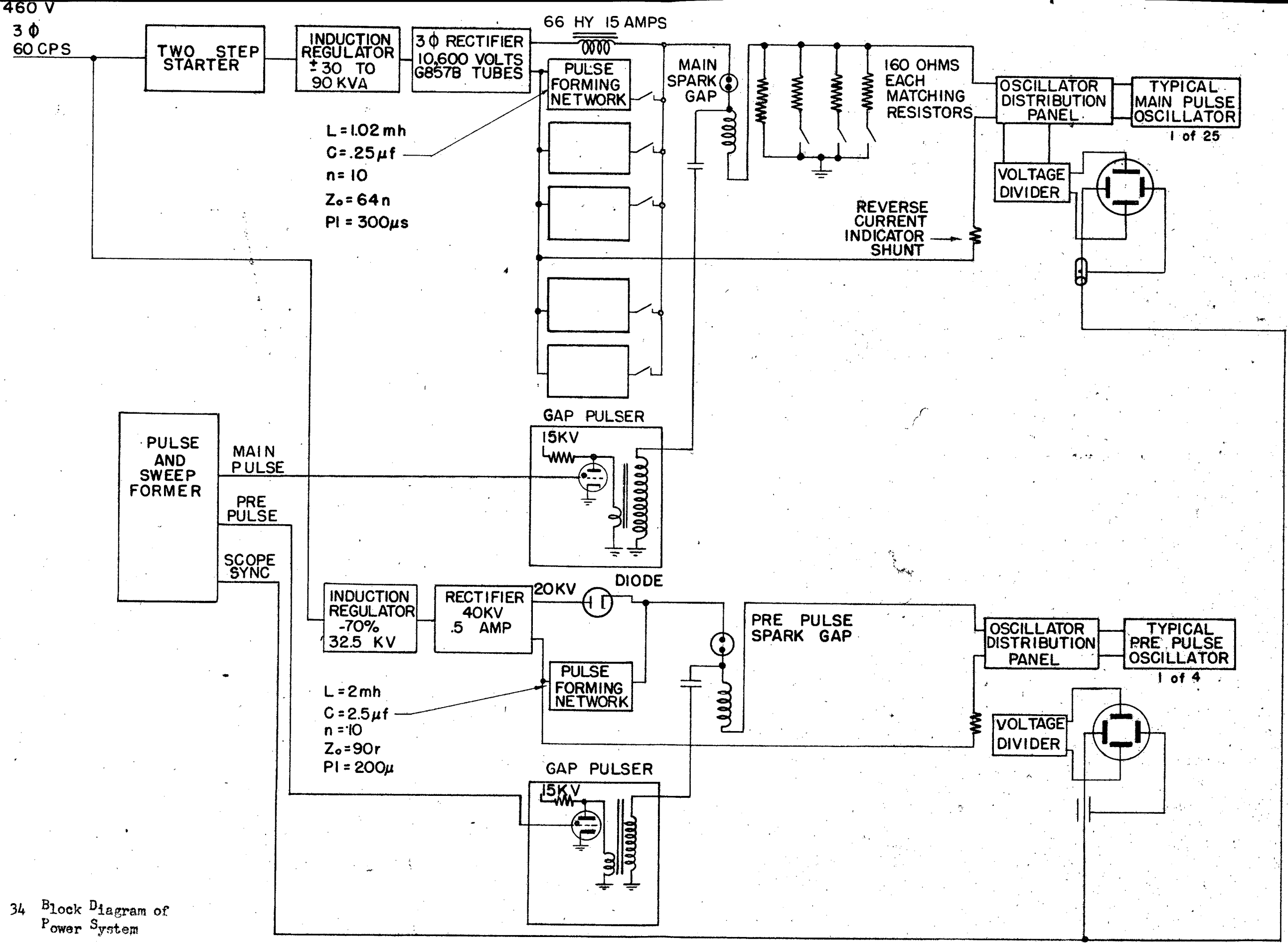


Fig. 34 Block Diagram of Power System

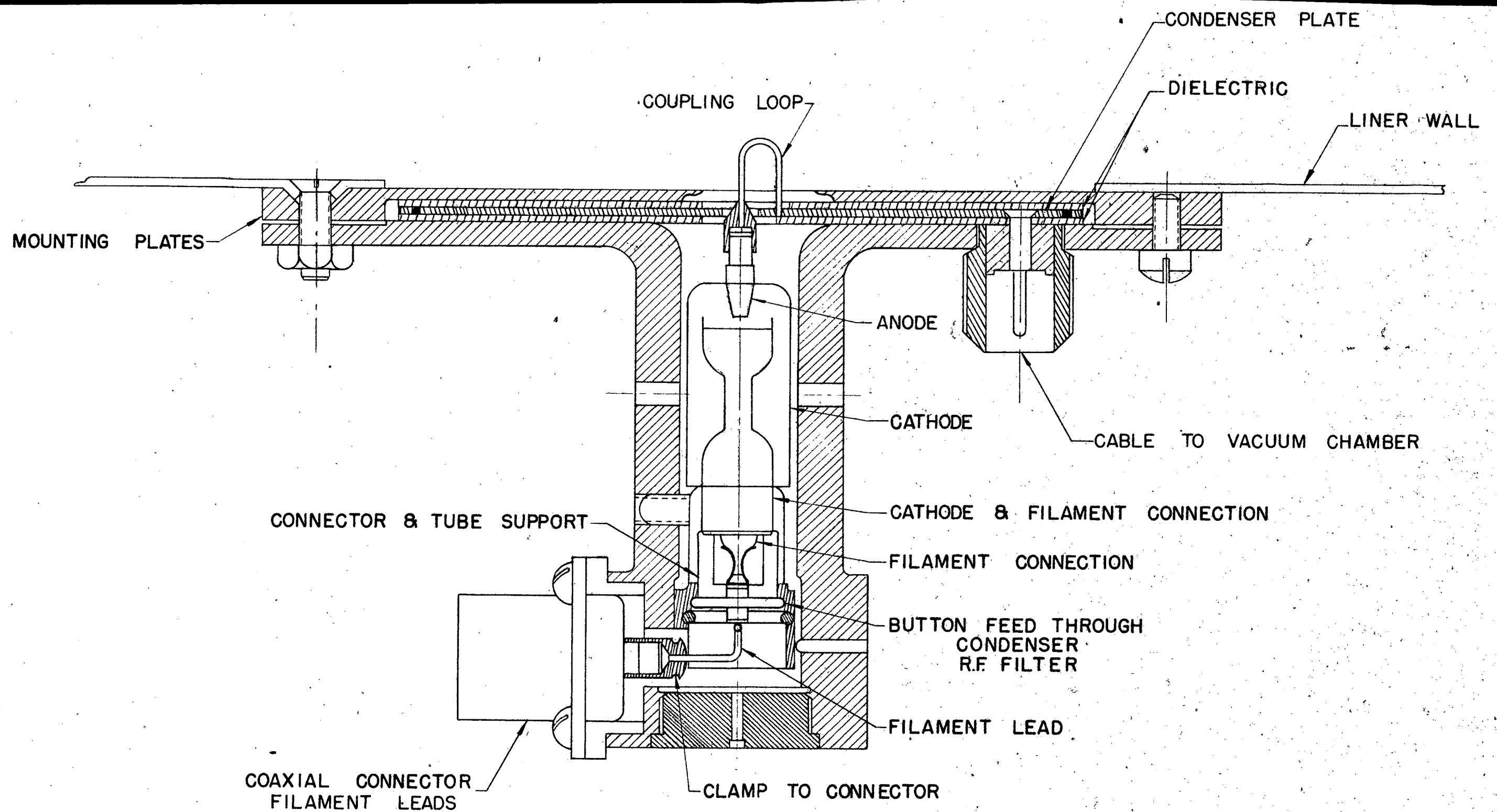


Fig. 41 Outline Drawing of Diode Voltmeter Pick-up Device

plate voltage is applied to the main power oscillators. The time sequence of operations and the plate voltage and r.f. pulse shapes are shown in Fig. 33.

VI. POWER SYSTEM

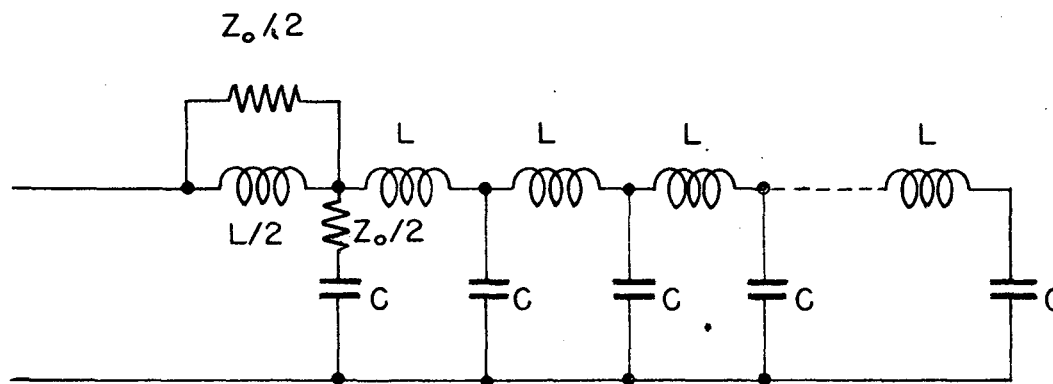
(1) Pulse Network - This section presents the general requirements of the power system of the linear accelerator and the design that was adopted to meet these requirements. Engineering details that are standard practice are omitted and the discussion is limited to those features of the machine that are unique. An over-all picture of the power system is given by a simplified block diagram, Fig. 34, that will be referred to frequently in the text.

Available electrical components, electron tubes, the problem of cooling, and other considerations, indicated that a pulsed power supply for the oscillators would be required. Until the final oscillator was developed, the exact impedance and load characteristics that this pulse system would have to drive were not known. However, it seemed that at most a system with the following specifications would be needed: a) 1,000 amperes peak current at 15,000 volts, with the voltage reasonably constant during the pulse. b) A 300 microsecond pulse with a pulse repetition rate of 15 cps, or a duty cycle of approximately 225. To fulfill these specifications it was decided to use a standard three-phase mercury vapor rectifier circuit followed by a pulse-forming network and spark gap switching. The five main pulse-forming networks shown in Fig. 34 were constructed as a result of this decision.

The development of the power oscillators used in the present design of the linear accelerator required that pre-exciters (oscillators which provide an initial field in the cavity before the main pulse) be used and that they be supplied with a pulse starting before the main pulse. This required that a separate system to the main system be installed and that it be triggered before the main system.

The final power system is shown in Fig. 34: this figure describes most of the important features of the power modulator. In the following we shall attempt to describe some of its more unusual features.

(2) Pulse-forming networks - Many types of modulators providing pulses were used



Z_0 = CHARACTERISTIC IMPEDANCE

$$= \sqrt{L/2}$$

V = VELOCITY, SECTION PER SECOND

$$= 1/\sqrt{LC}$$

N = NUMBER OF SECTIONS

T = PULSE LENGTH = $2N \sqrt{NC}$

Fig. 35 Schematic Diagram of Pulse-forming Line

19550900100

during the war in radar equipment¹⁴⁾¹⁵⁾; one of the better types developed during this time was the pulse-forming network type.¹⁵⁾¹⁶⁾ In it a synthetic transmission line, that is open circuited at one end, is charged up to a high voltage and then suddenly discharged through a load impedance at the other end. If the load impedance is equal to the characteristic impedance of the transmission line, the result is a voltage across the load equal to one-half the original line voltage and lasting for a time corresponding to twice the electrical length of the line. At the end of this time, the voltage on the line is zero and all of the energy has been taken from the line at a constant voltage. With regard to output voltages, reflections, and waveform, when the load impedance differs from the characteristic impedance Z_0 of the network, the network may be treated by conventional transmission line theory.

The original pulse-forming networks developed early in the war for radar applications¹⁵⁾¹⁶⁾ were made of four or five sections with mutual inductance between sections and the values of the L and C in each section different. Such a network is an excellent device if it is to be mass produced, but it is difficult to construct from standard components. The type of network we have used is illustrated in Fig. 35. The network is composed of identical lumped components, except for the $L/2$ in the first section, and is a very simple thing to make. The resistances of $Z_0/2$ in parallel and in series with the first section L and C respectively have been called "Gibbs suppressors", since they eliminate the "Gibbs phenomenon," which is the overshoot at a point of discontinuity when a function is synthesized from its Fourier components. This method is due to W. W. Hansen. Consider the initial impedance looking into the network; because the capacity initially acts as a short circuit and the inductance as an open circuit, the impedance will be infinite. With the Gibbs suppressors, the initial impedance is Z_0 , as it should be. We have had very excellent results with networks of more than six sections and have arbitrarily selected ten sections as a good number to use. By changing the values of the inductances (or the capacities) a voltage that varies with time in a specified manner may be obtained,¹⁷⁾ for example, to correct for pulse droop due to coil resistance.

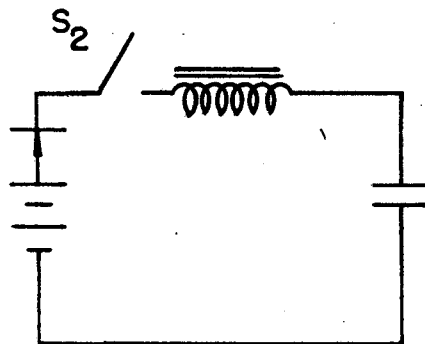
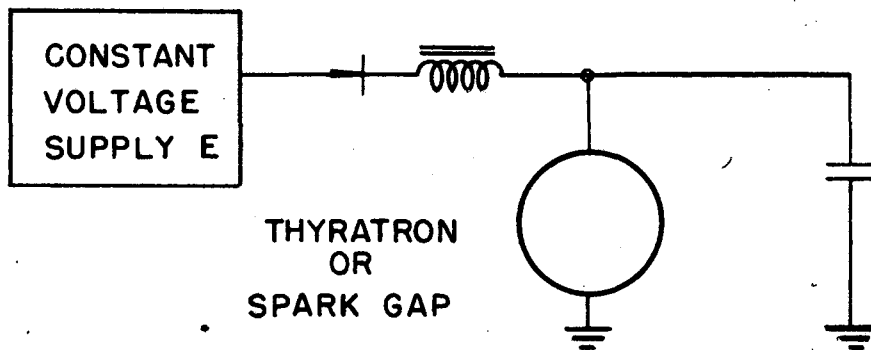
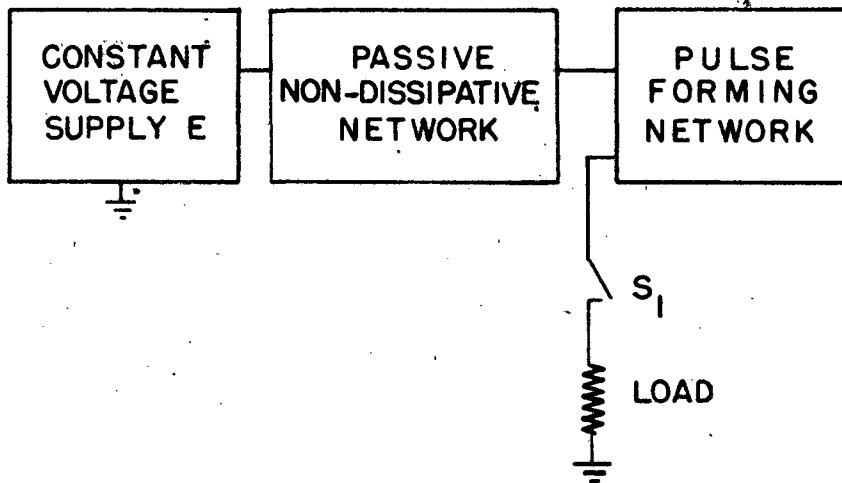


Fig. 36. Idealized Pulse-forming Line Charging and Discharging Networks

The values used for the main and pre-pulsed networks are shown in Fig. 35. If the five main pulse lines were run in parallel at 30 kv line voltage, there would be 5,600 joules stored in the capacities which corresponds to 18.7 megawatts peak power or 1,250 peak amperes. In operation, the machine normally uses four pulse lines at around 20 kv on the pulse line, corresponding to 6.6 megawatts output.

Let us consider the charging cycle of the circuit of Fig. 36a, which is an idealized pulse network. Let us assume: (a) All the energy is stored in the capacities of the pulse-forming network when S_1 is opened and closed. (b) No energy flows through the charging network during the time S_1 is closed. (c) The network is operating with repeating switch closures in a steady state. Equating the energy "in" to the energy "out" for one cycle;

$$\begin{aligned} \int E i dt = EQ = EC(V_1 - V_2) &= \frac{1}{2} C(V_1^2 - V_2^2) & \text{if } V_1 > 0 & \quad (58) \\ & & V_2 > 0 & \\ &= EC(V_1 - V_2) = \frac{1}{2} C(V_1^2 + V_2^2) & \text{if } V_1 > 0 & \\ & & V_2 < 0 & \end{aligned}$$

In Eq. (58), V_1 and V_2 are the voltages on the network when S_1 is closed and opened respectively. Solving for V_1 :

$$\begin{aligned} V_1 &= 2E - V_2 & \text{if } V_2 > 0 & \quad (59) \\ &= E + \sqrt{E^2 - V_2(2E + V_2)} & \text{if } V_2 < 0 & \end{aligned}$$

In most modulators $V_2 = 0$, i.e. the pulse line is fully discharged, and this line serves as a voltage doubler.

The coupling network is usually an inductance, as shown in Fig. 26b. The unilateral element is due to the rectifying tubes. The charging current may be studied by Circuit 36c, whose equation is:

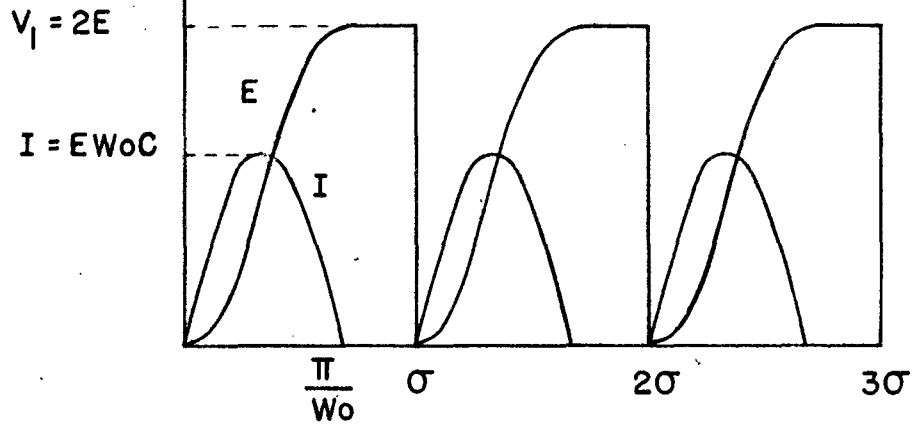
$$L \frac{di}{dt} + \frac{1}{C} \int i dt = E \quad (60)$$

Integrating (60), assuming that the line is discharged at $t = 0$, when E is applied:

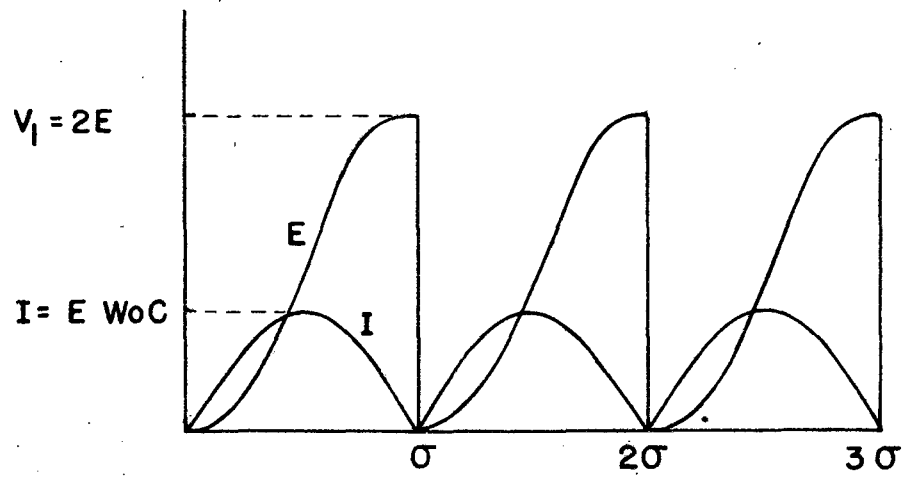
$$i(t) = \sqrt{\left(\frac{E}{\omega_0 L}\right)^2 + (i_0)^2} \sin(\omega_0 t + \phi) \quad (61)$$

where $\phi = \tan^{-1} \frac{i_0 L \omega_0}{E}$ and $\omega_0 = \frac{1}{\sqrt{LC}}$.

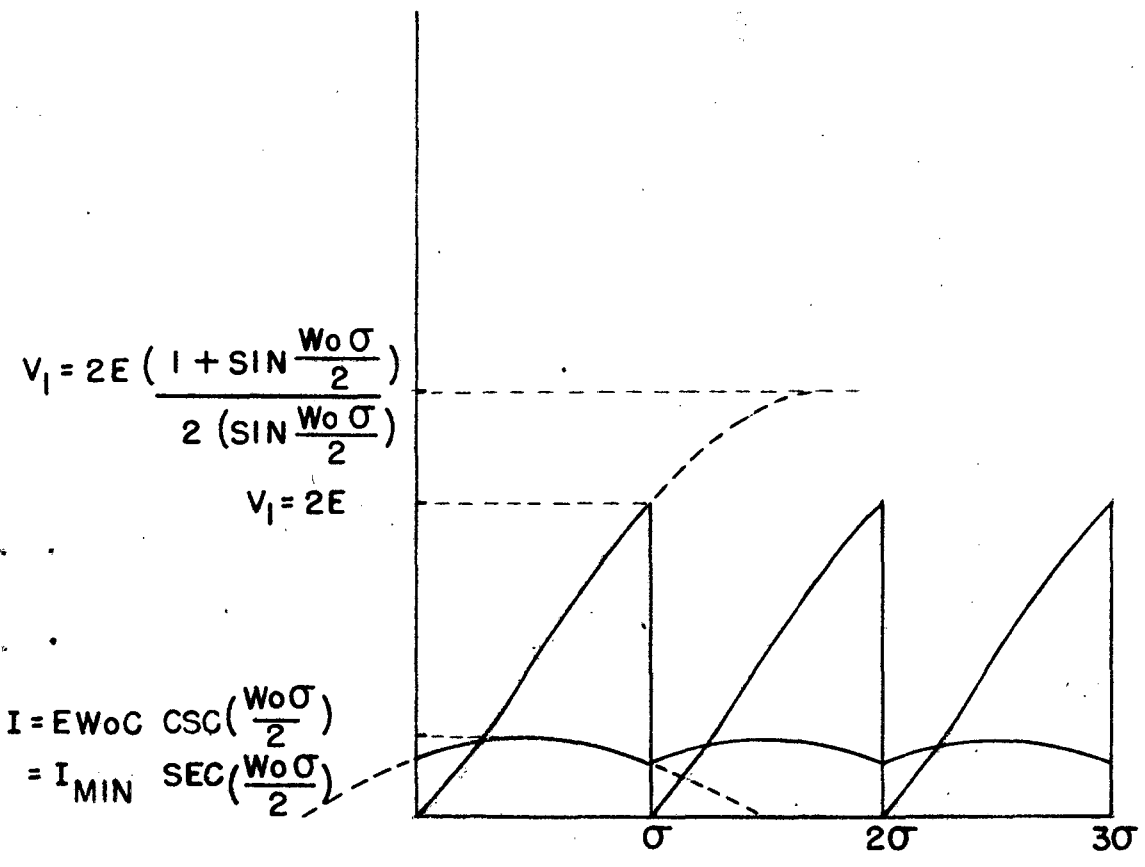
0 0 1 0 0 6 0 5 5 6 5



CASE I
 $\sigma > \frac{\pi}{W_0}$



CASE II
 $\sigma = \frac{\pi}{W_0}$



CASE III
 $\sigma < \frac{\pi}{W_0}$

Fig. 37 Pulse Shapes Obtained in Charging of Pulse-forming Line

Let σ be the time between the closings of S_1 . We then have three cases, if we have a unilateral circuit like Fig. 36b. These cases are plotted in Fig. 37.

Case I

$$\sigma > \frac{\pi}{\omega_0}$$

$$i(t) = \left[\frac{E}{\omega_0 L} \right] \left[\sin \omega_0 t \right] \quad , t < \frac{\pi}{\omega_0} \quad (62)$$

$$= 0 \quad , t > \frac{\pi}{\omega_0}$$

Case II

$$\sigma = \frac{\pi}{\omega_0}$$

This is a special case of Case I, and the condition usually called resonant charging.

Case III

$$\sigma < \frac{\pi}{\omega_0}$$

The current through the reactance L remains constant during the discharge interval, thus

$$\phi = \frac{\pi}{2} - \frac{\omega_0 \sigma}{2} \quad (63)$$

Then from (63) and (61)

$$i(0) = \frac{E}{\omega_0 L} \cot \frac{\omega_0 \sigma}{2} \quad (64)$$

And for (61)

$$i(t) = \left[(E \omega_0 C) \right] \left[\cos \left(\frac{\omega_0 \sigma}{2} \right) \right] \left[\sin \left\{ \omega_0 t + \left(\frac{\pi}{2} - \frac{\omega_0 \sigma}{2} \right) \right\} \right] \quad (65)$$

It is interesting to integrate (65) and divide by C :

$$V = 2E \csc \left(\frac{\omega_0 \sigma}{2} \right) \left[\cos \left\{ \omega_0 \sigma + \frac{\pi}{2} - \frac{\omega_0 \sigma}{2} \right\} \right] \quad (66)$$

This gives us the voltage at any time. The ratio between the voltage at the peak, if the switch fails to close, and the normal voltage is:

$$\frac{1 + \sin \omega_0 \sigma / 2}{2 \sin \omega_0 \sigma / 2} = \text{line voltage ratio}$$

From (65) the ratio of maximum to minimum current is:

$$\frac{\text{Max current}}{\text{Min current}} = \sec \frac{\omega_0 \sigma}{2}$$

In design a compromise must be made between the improved current ratio and the chances of a voltage overshoot; in case of misfire or shutting off the voltage

overshoot may be suppressed by a safety device. As can be seen from the constants on the block diagram, the linear accelerator is operated with $\sigma < \frac{\pi}{\omega_0}$ to reduce power supply ripple.

The pre-pulse network system is approximately the same, but on a much smaller scale. It puts out a pulse of about 200 microseconds which starts 100 microseconds before the main pulse. The pre-pulse line is charged through a temperature limited diode. This is a very convenient method of smoothing out the current ripple on a low power system where one can afford to throw away half of the power in the diode. It is easily seen that half of the power is lost in the diode by noting that during the charging time the current is constant and the average diode voltage is equal to the average line voltage. Voltage doubling is not obtained in this case because there is a power sink in the pulse generating system.

(3) Spark Gaps - The pulse networks are discharged through an air core choke that slows down the rate of rise of the voltage applied to the oscillators. The spark gaps are copper spheres with a jet of air blowing on them, mounted in a sound-proof box.

As indicated in Fig. 34, the spark gap is triggered by a thyatron that discharges a condenser into an iron core pulse transformer; the secondary of the pulse transformer applies a high voltage to the gap.

The pre-pulse system is similar. The electronic triggering circuit gives a flexible system in that the time spacing between the main and pre-pulse pulses may be changed by merely turning a knob.

(4) Matching, Interlocks, Etc. - Both the main and pre-pulse channels have resistor banks composed of 500 watt "glow coils" with the oscillators. These are switched in or out from the control desk and insure that the networks are always operating into a matched load. If a mismatch occurs, there will be reflections from the end of the network and a reverse current will pass through the ground connection to the networks. A small shunt is in series with this ground current and the reverse current causes an electronic device to open the trigger signal circuit before the next pulse. A good many possible faults on the load side of the spark gap will result in a mismatch and thus

prevent the next pulse.

The a.c. and d.c. parts of the power supply are interlocked and protected from overload in a standard fashion. Most of the fault protection on the load side of the gap, such as the individual oscillator overload relays, (see Section V) prevents the next pulse by opening the trigger circuit.

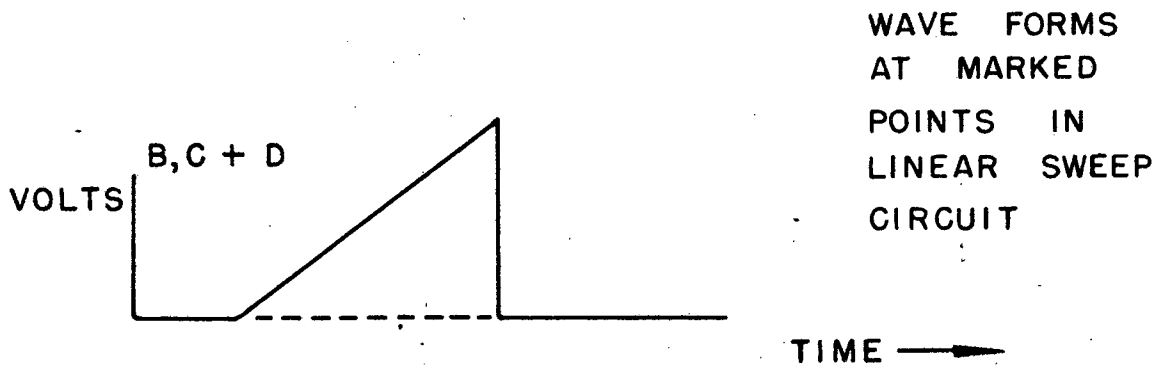
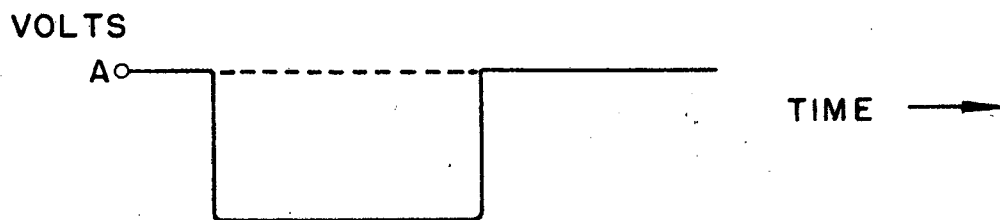
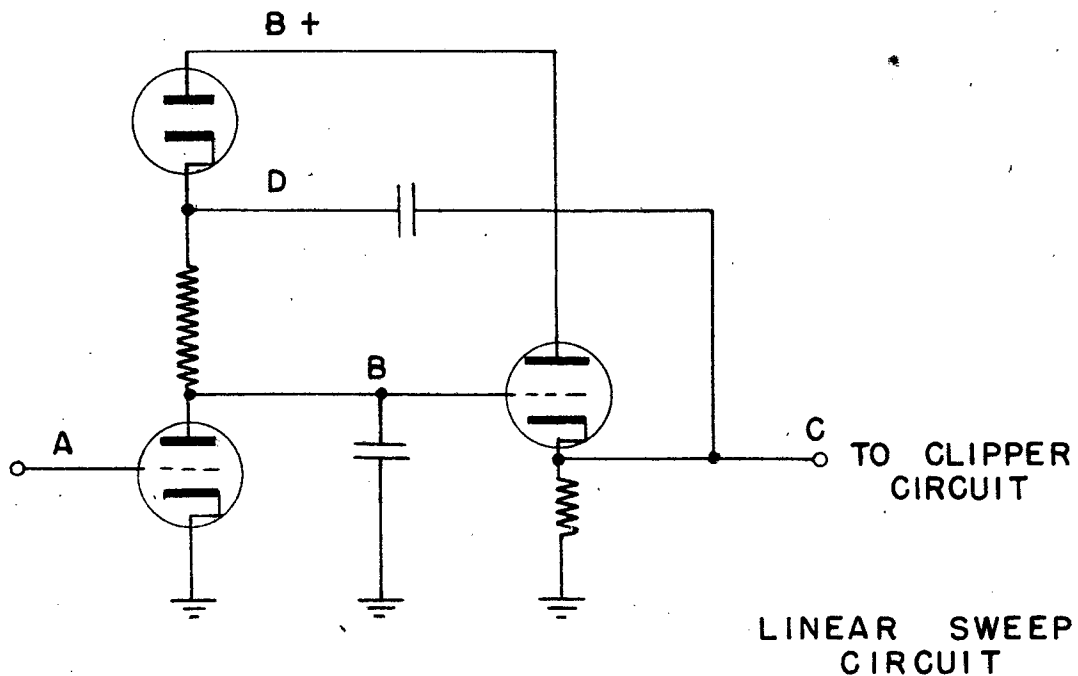
The high voltage pulse output is run directly to a distribution panel where knife switches are provided that connect to the individual oscillators. At this point there is also attached a voltage divider that provides an oscillograph picture of the d.c. pulse on the control panel. The high voltage wiring is RG-9U and RG-17U concentric cable, with the shield used as the ground return.

All high voltage equipment is interlocked for the protection of personnel. Interlocks and overload protective switches have indicating lights on the main control panel to facilitate the location of trouble.

VII. ELECTRONIC ACCESSORIES

(1) Time base for linear accelerator - The requirements for the time base are that it generate 4 pulses, to be used for turning on the sweep in an oscilloscope, for starting the pre-exciters, for starting the main oscillators, and for pulsing the Van de Graaff. It was considered desirable that there be considerable latitude in the adjustment of these, and that there be a trigger which is adjustable over about 600 microseconds for examining in detail any events taking place after the linear accelerator has been pulsed. It is also desirable to be able to obtain additional triggers from the same time base. The requirement on stability of the triggers is that they be stable with respect to each other within about 10 microseconds.

Since the desired repetition rate is approximately 15 cycles, it was decided to make it exactly one quarter of the 60 cycle line frequency. This causes the power for the oscillator pulses to be taken from the line at the same point in each cycle. It has the minor advantages that it produces freedom from hum troubles in associated equipment, and that it makes it possible to synchronize easily other equipment operating near the accelerator, in such a way that the linear accelerator pulses do not interfere.



WAVE FORMS
AT MARKED
POINTS IN
LINEAR SWEEP
CIRCUIT

Fig. 39 Linear Time Base Schematic Diagram

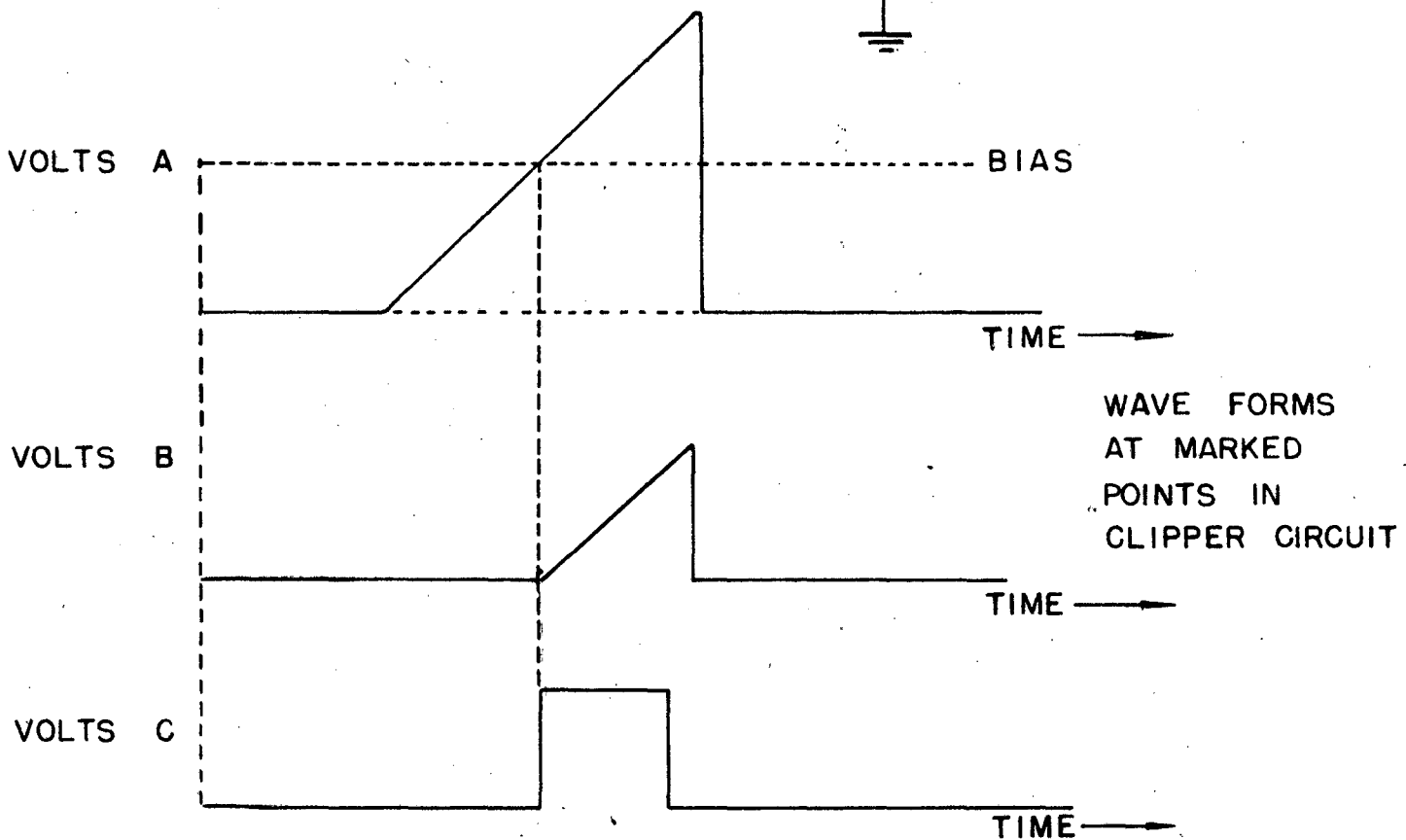
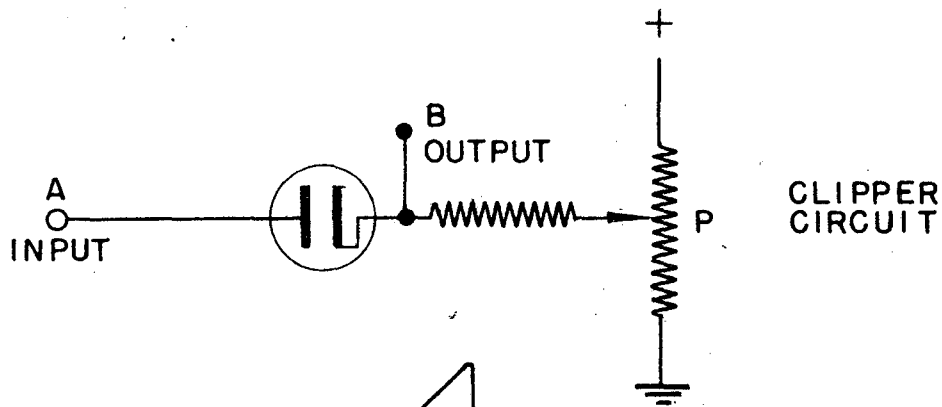


Fig. 40 Generation of Timing Pulses by Clips on Linear Time Bases.

A 15 cycle master timing pulse is obtained by squaring the 60 cycle input and frequency dividing with two scaling pairs. The 15 cycle trigger is used to generate a linear sweep using a circuit much as described in Puckles.¹⁸⁾ See Fig. 39. Actually, for the purposes used, the linearity is merely a convenience. This linear sweep is intercepted by a series of clipper circuits at various biases, and the discontinuities thus obtained are used to generate the triggers. (Fig. 40 and wave form A and B). The time of occurrence of trigger C can thus be varied by adjusting the bias at P. (Fig. 40).

Several channels can be taken from the same linear sweep if suitable means are used to keep the various channels decoupled. This decoupling problem is particularly accentuated by those channels which drive the thyatron triggers for the spark gap. Current fed back through these lines is sufficient to make it necessary to place the output circuits for these triggers in a separate chassis.

Although the general operation of the accelerator is at 15 cycles, some experiments have required a lower or higher repetition frequency. The only change required to operate at any desired frequency below 15 cycles is to replace the 60 cycle signal input by the output of an audio-oscillator.

(2) Vacuum tube voltmeter - If a loop of accurately known area is introduced into the linear accelerator cavity from the side wall, the voltage generated on this loop can be used to determine the voltage down the axis of the cavity, if the field distribution in the cavity is accurately known.

The shape of the r.f. envelope is as shown in Fig. 33. To measure the average voltage and extrapolate to the peak voltage is difficult, since the shape of the r.f. envelope is then important. As a result, a peak voltmeter is used. In the discussion of this, the fact that the top of the r.f. envelope is not perfectly flat will be neglected.

If the r.f. voltage is taken from the tank and measured at some distance from the loop, there are problems associated with matching the loop to the line, matching impedances in the line, and terminating the line properly. These difficulties are such that it appears easier to convert the a.c. to d.c. at the loop itself. To do this, a diode

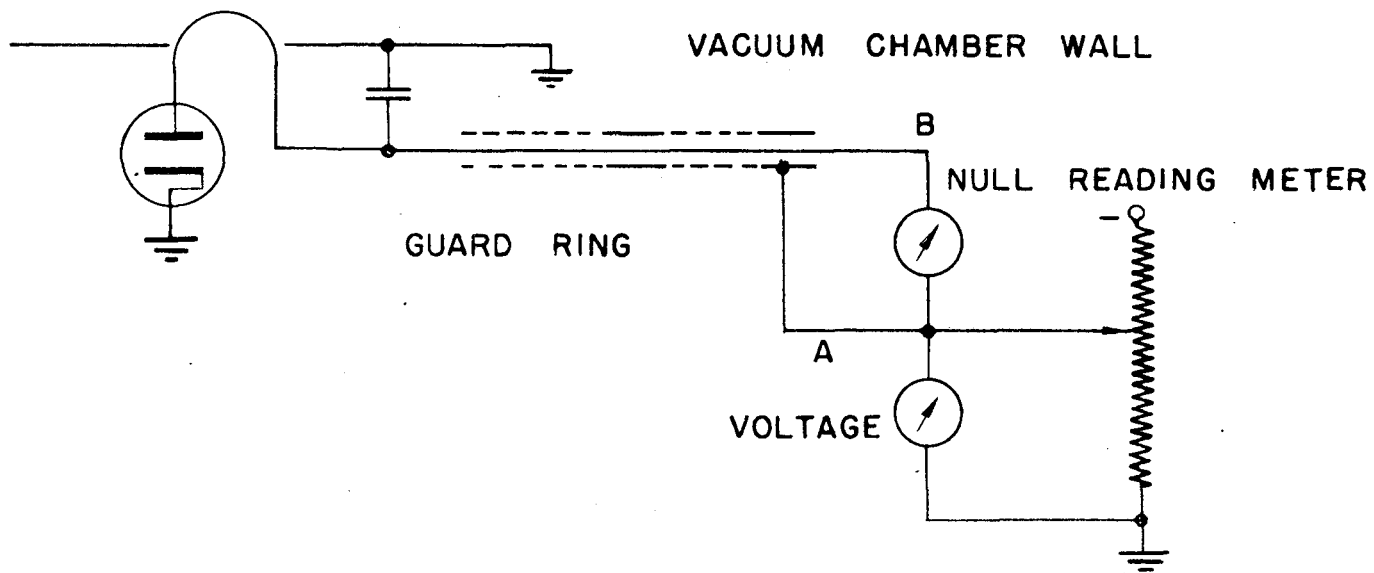


Fig. 42 Direct Current Slide-back Current

00100605572

is placed at the loop itself, inside of the vacuum system, but outside of the r.f. cavity. (Fig. 41)

To operate this as a peak voltmeter, the d.c. voltage at the diode plate must be just a small amount less negative than the height of the peak of the r.f. envelope. If the loop and the diode impedance are known, the peak voltage can be calculated. The duty cycle and the shape of the r.f. envelope must be taken into account. To avoid taking all of these factors into consideration, except as second order effects, the d.c. must be as close to the r.f. peak as the maximum allowable error. In this way, the actual d.c. voltage at the diode is treated as the r.f. peak voltage.

A design of approximately 1 percent accuracy is considered here, with one hundred volts the size of the r.f. voltage to be measured. At least -99 volts d.c. must then be at the diode. This gives one volt across the diode at the r.f. peak. The angle of conduction is approximately 16° out of 360° .

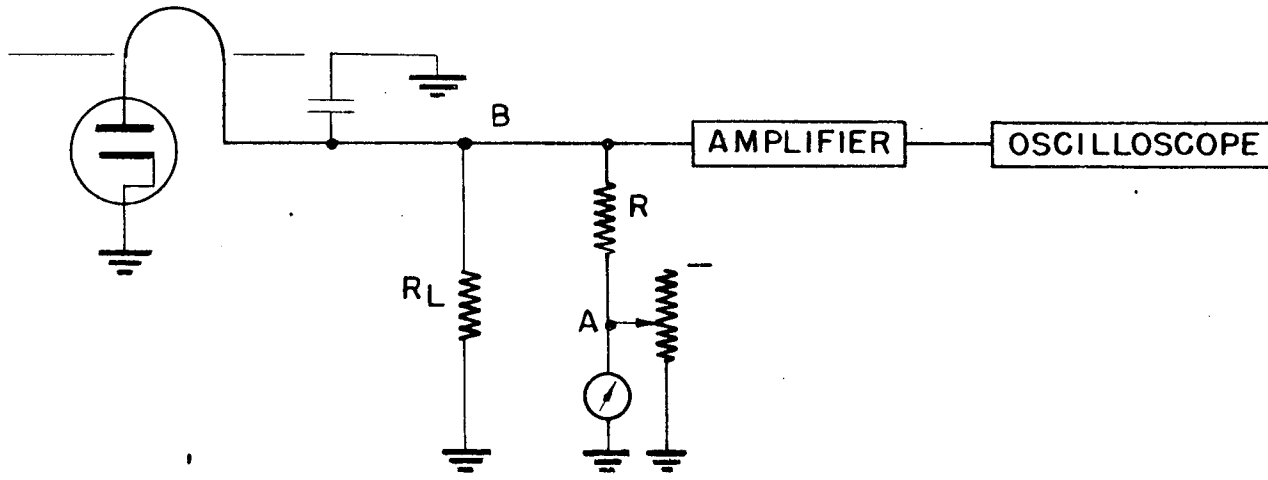
The average voltage across the diode is .58 volts during conduction. Over an r.f. cycle, the average voltage is $.58 \times 16/360 = 2.6 \times 10^{-2}$ volts. If the duty cycle is $1/200$, the voltage averaged over the entire $1/15$ second cycle is 1.3×10^{-4} volts. The average current through the 10 K resistance of the diode is 1.3×10^{-8} amps.

If we obtain the -99 volts at the diode by placing a high resistance to ground and then measuring with some type of electrometer circuit or galvanometer, an R of approximately 1.3×10^{10} ohms is required. This is the maximum leakage allowable. This can be obtained under ordinary circumstances quite easily, but making connections through the wall of a vacuum system would be quite difficult.

If a slide-back voltmeter of the ordinary type is used, the -99 volts is obtained from some outside source. All connections can be guard-ringed. (Fig. 42)

If the negative voltage at B exceeds the r.f. peak, no current flows through the diode and the null reading galvanometer. Therefore this null reading must be approached from one side. For one percent accuracy, the negative voltage at A can be at most 99 volts. This means that it must be possible to read the 1.3×10^{-8} amps previously calculated on the null reading galvanometer. Leakage resistances from B to A can be

COUPLING LOOP



VACUUM TUBE VOLTMETER WITHOUT AUTOMATIC FEEDBACK

00100605574

Fig. 43 Alternating Current Manual Slide-back Vacuum Tube Voltmeter

very small (they must be large compared to resistance of the galvanometer). However, leakage resistances from B direct to ground must be the same as previously calculated, over 1.3×10^{10} ohms. The chief disadvantages of such a system are the difficulties in finding a suitable guard ring, and the difficulty of obtaining a null reading from one side only.

To overcome these disadvantages, an automatic slide-back peak voltmeter was designed. This is similar in most respects to one described by Creveling and Mautner.¹⁹⁾ The operation of this voltmeter is automatic, but its operation can be best understood from a description of a manually-operated voltmeter of the same type. (Fig. 43) If there is 100 V peak r.f. and -99 V bias is applied at B, there is one volt of r.f. across the diode.

The current waveform through the diode will be integrated by the r.f. bypass condenser to give a square video waveform. This video pulse will have a peak 200 times as large as the corresponding d.c. voltage, when the duty cycle is 200. In the case considered,

$$R = 50 \text{ K}$$

$$i = 1.3 \times 10^{-8} \times 200 = 2.6 \times 10^{-6} \text{ amps}$$

$$V = 2.6 \times 10^{-6} \times 5 \times 10^4 = 13.0 \times 10^{-2} = .13 \text{ volts}$$

This voltage can be amplified by an amplifier of reasonable gain and applied to a cathode ray oscillograph. In operation potentiometer P can be adjusted until the waveform is just visible on the oscillograph. The voltage at A is the same as the peak voltage.

The actual circuit used differs from this only in that the voltage at A is obtained by using the detected amplified waveform. (Fig. 44) As a specific example, consider that with 100 volts r.f., if -99 volts is somehow placed at A, -.13 volts of video will be applied to the amplifier. With a gain of +762, this will give a rectified output of -99 volts, which can be applied to A. If less than -99 volts were applied to A, i.e., -98 volts, the output of the detector would be -198. If this were applied to A, it would cut the diode off. As this voltage decreased, at 100 volts the diode would start

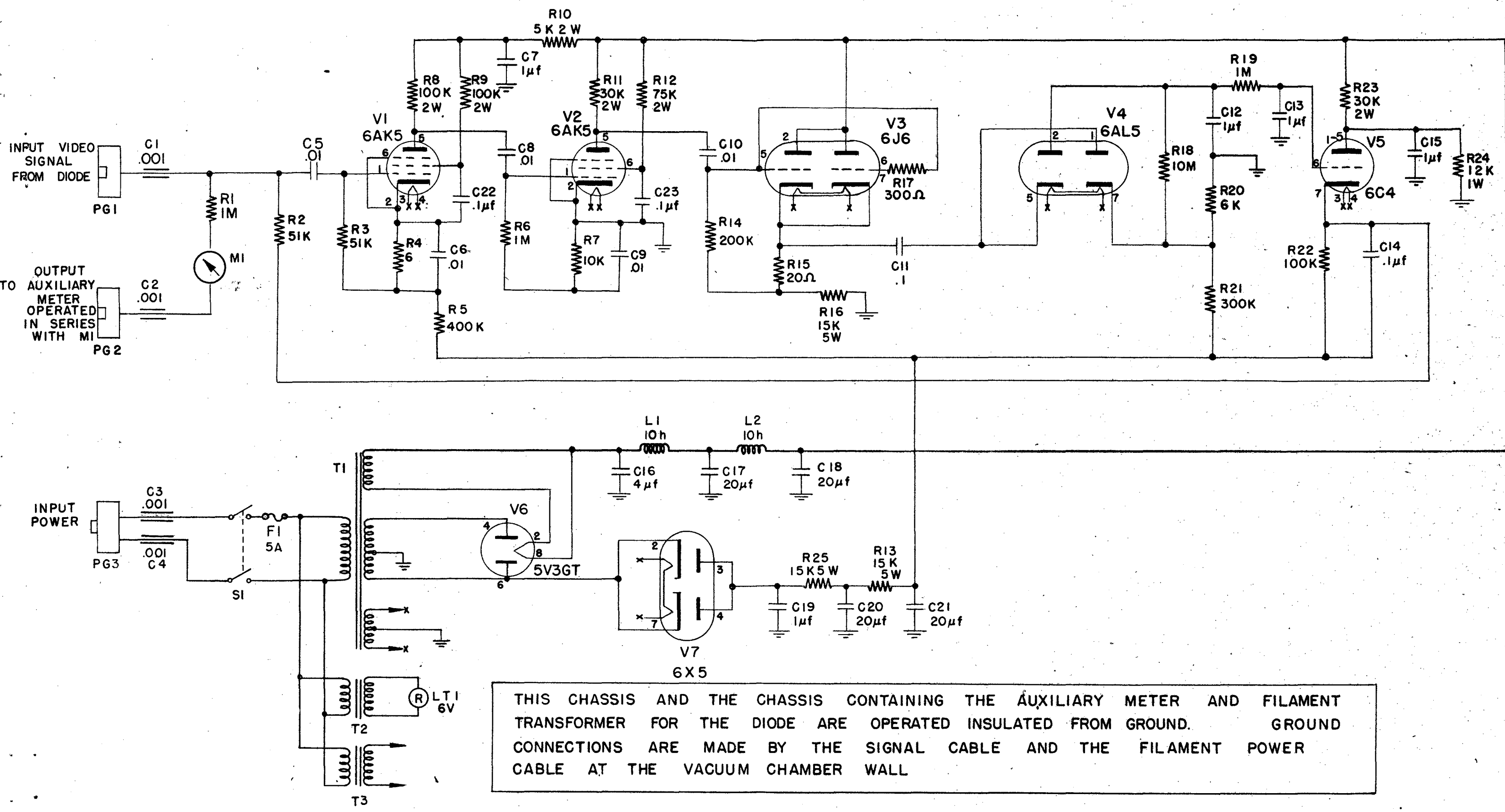


Fig. 45 Schematic of Electronic Slide-back Vacuum Tube Voltmeter

conducting, the voltage feed back would continue to be less than -99 volts until the voltage at B dropped to -99 volts. The schematic diagram of the instrument is shown in Fig. 45.

Since there is a feedback loop, the circuit must be such that the loop gain is less than unity for all frequency components for which the phase shift is zero. The feedback is effectively positive for the loop itself and negative for the signal. This consideration requires that a fairly long time constant be introduced in the attenuation circuit. It is not claimed that optimum conditions have been obtained in the design of the present circuit. It may be possible to achieve stability with a smaller time constant than that used if a different type of attenuation circuit is used. For an accuracy of one percent, it can be seen that a gain of approximately 800 is required. If an accuracy of .1 percent were required, a gain of 8000 would be necessary. The actual gain is unimportant as long as it is greater than the required value. If the voltmeter is placed at B, any leakage causes only a change in the gain. It will have three effects. One will be to reduce the size of the video pulse by reducing the load resistance across which it is formed. If R were infinite, a leakage resistance of 10,000 ohms would reduce the gain by a factor of 2 at this point. There will be an additional effect due to the attenuation of the d.c. signal feedback. If $R_L = R$ this will reduce the gain by a factor of 2. It can be seen that there will be no large loss of gain as long as $R_L > R$. The third effect is that leakage may cause saturation of the amplifier. The peak voltage that the detector can put out in the circuit used is -200 volts. If operated at -100 volts, a leakage resistance of $R_L < R$ would cause the amplifier to saturate. In the circuit used a practical limit to leakage resistance would be $R_L > 100,000$.

Any capacity across the input will also cause a loss of gain if its size is such as to cause an input time constant long compared with the width of the pulse being measured. In our case, the input pulse was approximately 300 microseconds and the input resistance 50,000 ohms. Hence:

$$C < \frac{300 \times 10^{-6}}{50 \times 10^3} = 6 \times 10^{-9} \text{ farad} = .006 \text{ microfarad}$$

Additional capacitance causes a corresponding loss in gain. If the gain obtained is high enough, then the only critical components in the circuit are the ammeter and the resistance in series with it. The total gain of the circuit can change without causing any effect. There is no provision for setting the zero of the instrument.

It is not possible to obtain arbitrarily high accuracy with this instrument under the conditions in which it is used here. Any increase in gain requires a correspondingly longer time constant. As the gain is increased, the r.f. must be filtered more effectively. The chief trouble obtained in operation was pick-up of the current pulse of the oscillators. The main frequency component of this pulse was approximately 3 kv. The skin depth of this is such that ordinary coaxial cables will not shield the center wire from it. The pick-up voltage on the cable ground and the center wire of the cable was of different amplitude, causing a signal to appear at the input. If the chassis containing the amplifier equipment was grounded, this signal could be large enough to throw the meter up to 200 volts. By isolating the chassis and cabling from the ground, this can be reduced to a volt or so on the output. It can be seen that any appreciable increase in gain would cause additional trouble from this source, possibly requiring the chassis to be mounted at the tank rather than at the end of a 30-foot cable.

The diode used is a 2-01C Eimac diode. Since this is located in the vacuum, it is necessary to operate this at half of its rated filament voltage because of insufficient cooling. The cut-off of this tube is effectively at $-1/2$ volt, the current being down to approximately 2 μ A at this point. The gain of the amplifier is greater than 1,000, making the error of the instrument of the order of one percent at the 100 V level. This has not taken into account the fact that the slope of the r.f. envelope being measured is about 5 percent. Taking this into account, and considering changes which might occur in the diode and meter circuits, the voltmeter is probably stable to about 5 percent in operation over a period of several months.

(3) Q measurements on the accelerator cavity - Q measurements were made on the linear accelerator cavity in order to determine its shunt impedance. At each step in the development of the copper liner, its Q was measured, and when Q was lower than

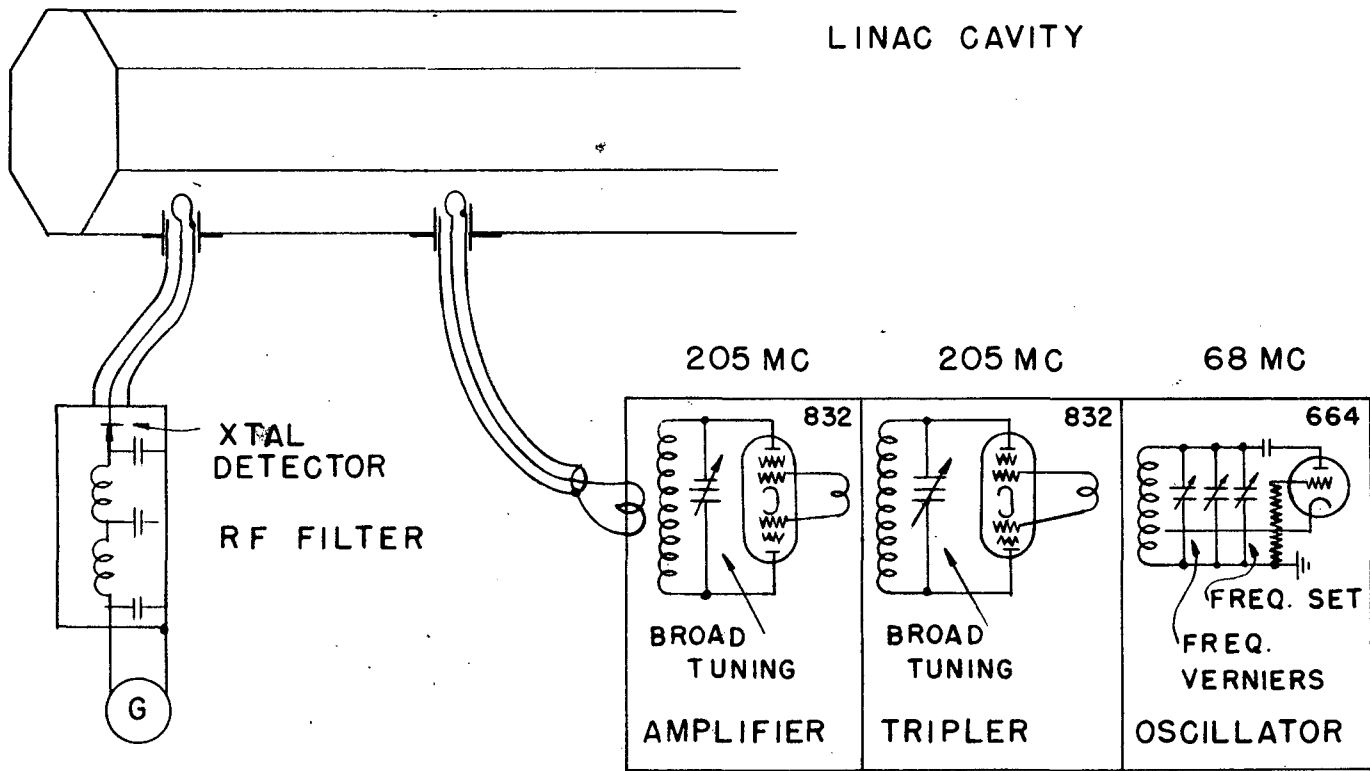


Fig. 46 Diagram of Q Meter

00100605379

anticipated, a search was made until the lossy element of the cavity was located and fixed, as indicated by a satisfactory Q reading. Most of these losses were found actually to lie in the joints of the drift tubes, and in the drift tube stems.

Several methods of Q measurement were tried, but the most satisfactory was the standard method of measuring the width of the r.f. resonance curve of the cavity, using a tunable CW oscillator. A diagram of the apparatus is shown in Fig. 46. R.f. energy from the oscillator is brought into the cavity by a small adjustable loop which couples into the magnetic field, and a similar loop takes energy out to the detector.

Oscillator - The oscillator for making a Q measurement must be sufficiently stable in frequency that it can be reproducibly tuned through frequency intervals equal to the resonance width of the cavity between half-power points, which is of the order of $\Delta f = 2.9$ kilocycles.

The oscillator is followed by two amplifier stages, and consists of a 6C4 triode self-excited oscillator, an 832 tripler, and an 832 power amplifier supplying about 20 watts of r.f. Actually, for reasons to be mentioned later, only a small fraction of the power is coupled into the cavity. It is never necessary to retune the tripler or amplifier stages during a measurement, since the Q of the tank circuits is small compared with the accelerator cavity. The plate power supply is electronically regulated, and in addition, the a.c. is supplied through a Sola line voltage regulator. The latter was added to stabilize filament temperatures.

Detector - A crystal rectifier and galvanometer measure the r.f. power which couples through the cavity; we used both 1N-21 and 1N-34 type crystals, the latter being preferable because of their high burn-out characteristic. A galvanometer of sensitivity of 0.3 microamperes full scale was found to be convenient and sufficiently sensitive. It is necessary to be sure that the crystal is being operated at a level sufficiently low that its characteristic is accurately a square law. This is easily verified by rotating the plane of the detector loop 45° from maximum in the cavity; for a square law detector, this reduces the galvanometer reading by $\cos^2 45^\circ$, which is $1/2$.

The detector must be well shielded so that r.f. reaches the crystal only from its pick-up loop; we used an LC filter of several stages in the crystal output, so that r.f. picked up by the galvanometer would not get back to the crystal and be rectified. No precautions were taken to shield the oscillator from radiating r.f. into the laboratory.

Procedure - It was necessary to isolate the desired mode of the cavity from several others which are close to it in frequency. The accurate frequency of this mode is read on a heterodyne frequency meter (Signal Corps No. TS-175/U).

When the oscillator has been aligned for the correct frequency, the input and output loops coupling the oscillator and detector to the cavity are adjusted to give a convenient reading on the galvanometer when the micrometer frequency vernier is adjusted for maximum energy transfer through the cavity. Noting the galvanometer deflection for the peak of resonance, the micrometer is turned quickly to find the two positions on either side of resonance where the galvanometer reads exactly $1/2$ of maximum; these two micrometer readings then represent the half-width of the resonance curve.

It now remains to determine accurately the frequency interval, Δf , which these two micrometer readings subtend. The No. TS-175/U frequency meter is used as a heterodyne oscillator and detector to produce an audio beat note against the frequency of the oscillator, and the resulting audio frequency is measured by comparison with a conventional audio oscillator. Q is then obtained from $Q = f/\Delta f$, where Δf is the full width of the resonance curve, to the half-power points. As an over-all check, we found it convenient to construct a standard cylindrical cavity of sheet copper, whose Q we measured once very carefully; thereafter it was our practice to measure the Q of this cavity after measuring an unknown Q , as a comparison on the calibration.

To insure that the act of measuring the Q of a cavity does not introduce extra losses and hence lower the measured Q , it is necessary to have both oscillator and detector so loosely coupled that: (1) Reducing either coupling does not change the measured Q . (2) The loading on the final stage of the oscillator is not appreciably

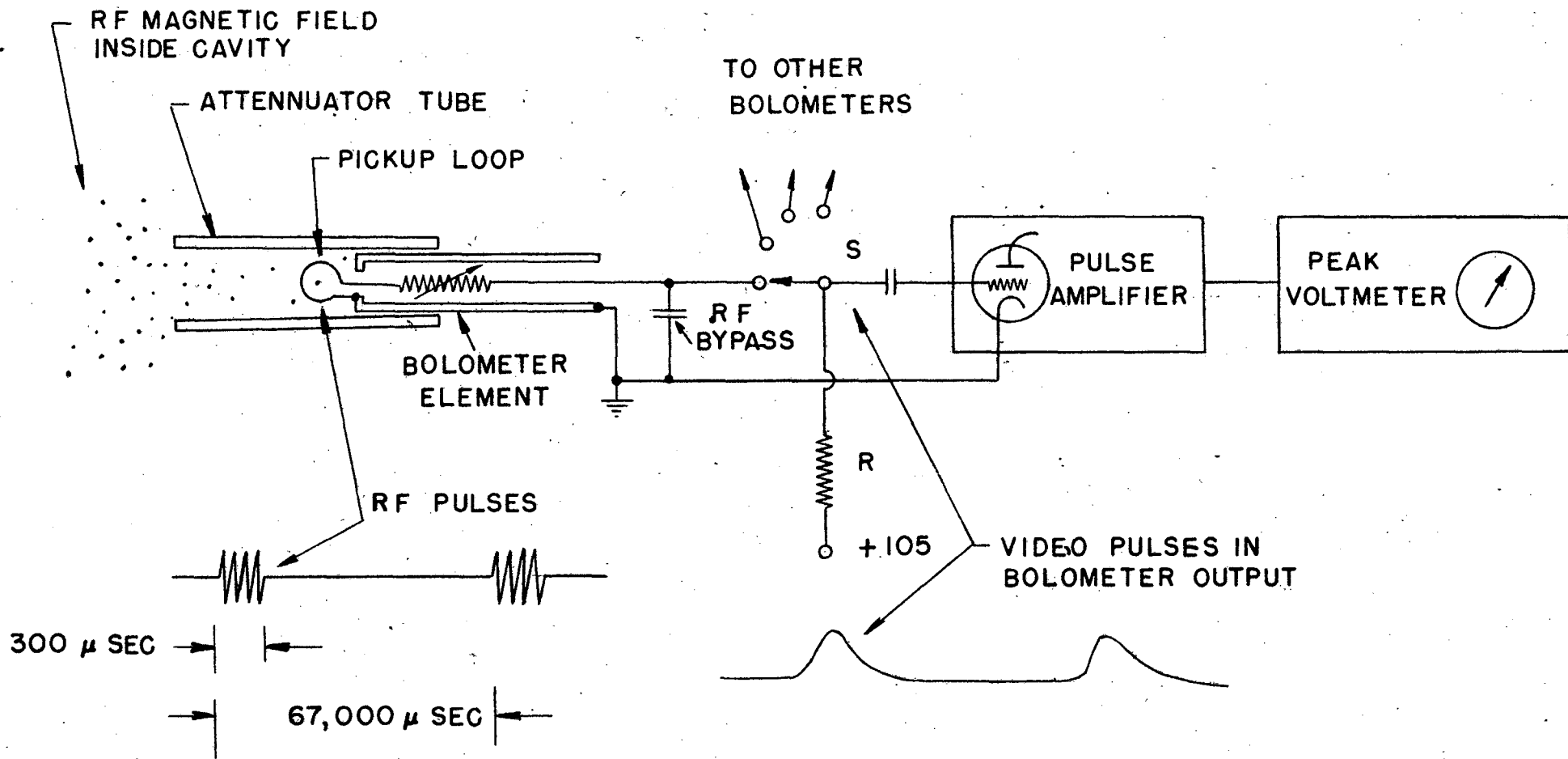
changed as the oscillator tunes through resonance. These conditions are realized, for our case, by using the loops in a position where their effective area is about $1/2 \text{ cm}^2$. If galvanometer readings are too small at the desired coupling conditions, either the oscillator power may be increased, or a more sensitive galvanometer can be used.

To test whether the coupling is sufficiently loose when a Q measurement has been made, one increases or decreases the coupling and re-measures Q ; if Q is independent of coupling, the coupling is loose enough.

The final result for the linear accelerator cavity was a Q of 72,000. This was for the copper liner with drift tubes and 27 transmitter coupling loops, but with the loops disconnected from the transmission lines and oscillators. We estimate the probable error of the measurements to be about 5 percent, due mainly to frequency drifts in the oscillator.

(4) Bolometer system for linear accelerator field distribution measurements - The bolometer system was developed in order to give a quick and accurate comparison of the r.f. magnetic field at a number of points along the copper liner. This function would ordinarily be accomplished by means of a single travelling probe moving the length of the cavity; however, because of the mechanical difficulty of controlling the motion of such a probe inside the linear accelerator vacuum tank, it was thought simpler to use a system of many fixed probes.

The most difficult requirement of the fixed-probe system is to produce a large number of r.f. detectors (this system uses twenty) all having the same sensitivity, and capable of holding their calibration over long periods of time. Bolometers were chosen as the detector element because they are very durable, and have an accurate square-law characteristic, even at high r.f. input levels. The actual elements used were taken from Buss fuse cartridges, type 8AG, rated at 10 milliamperes; and these follow a square law to within 5 percent, up to power levels $1/4$ of the burnout level. It was found that bolometers deteriorated and changed their calibration in a few weeks of operation, if they were operated higher than about 5 percent of the burnout level. The output under this condition is about 25 millivolts, with 5 milliamperes d.c. flow-



00100605583

Fig. 47 Schematic Diagram Showing Bolometer Operation

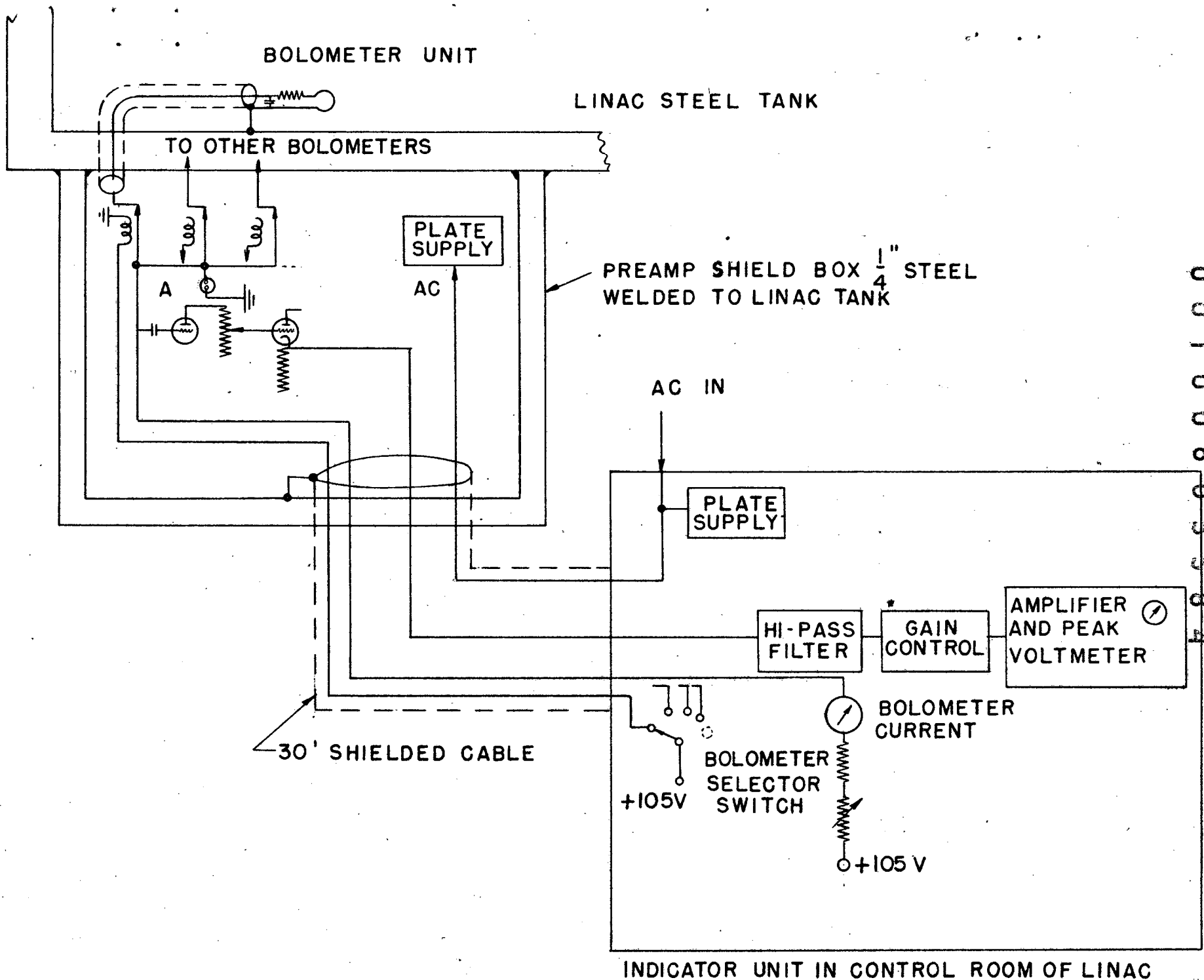
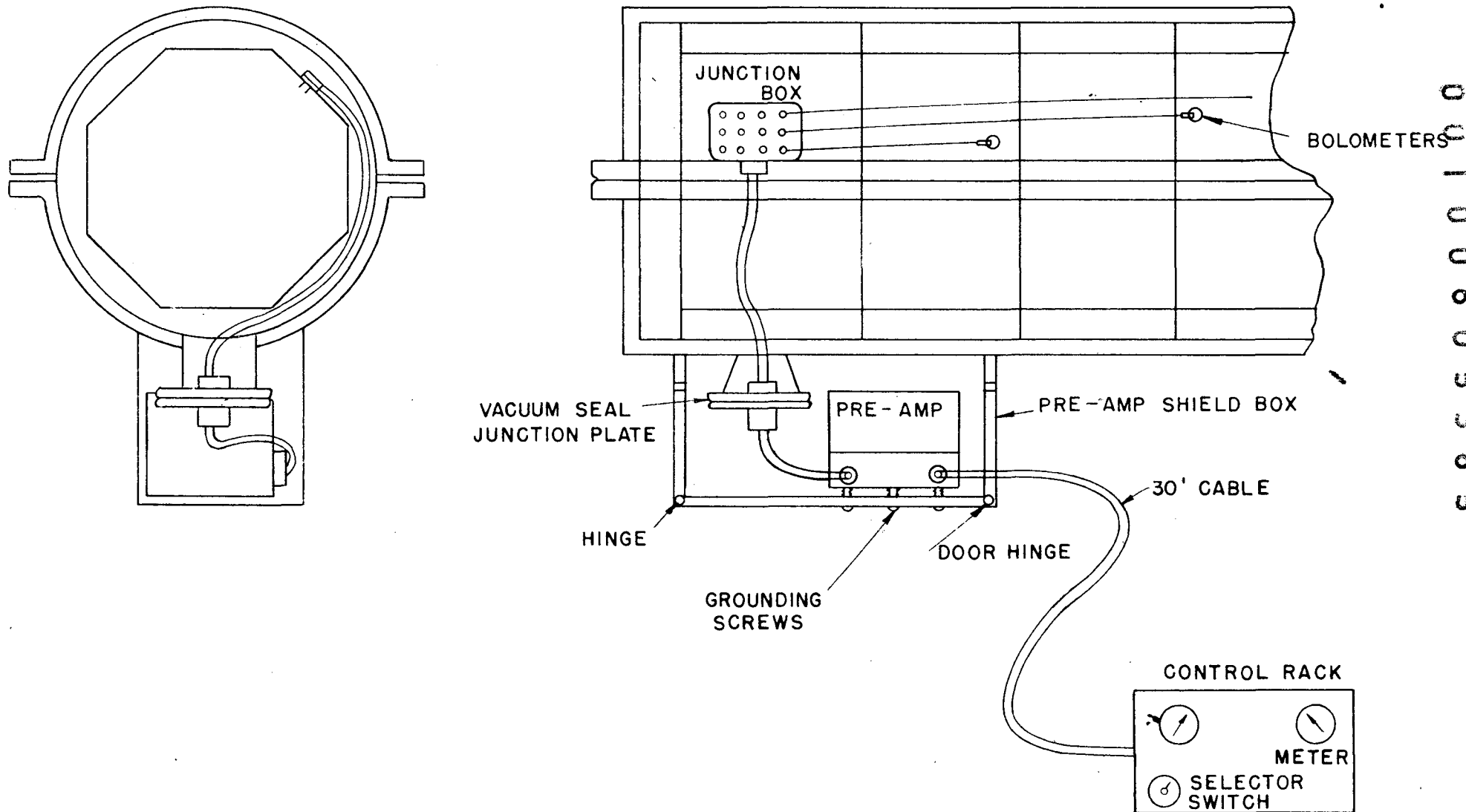


Fig. 48 Bolometer Preamplifier

001006000004



00100605385

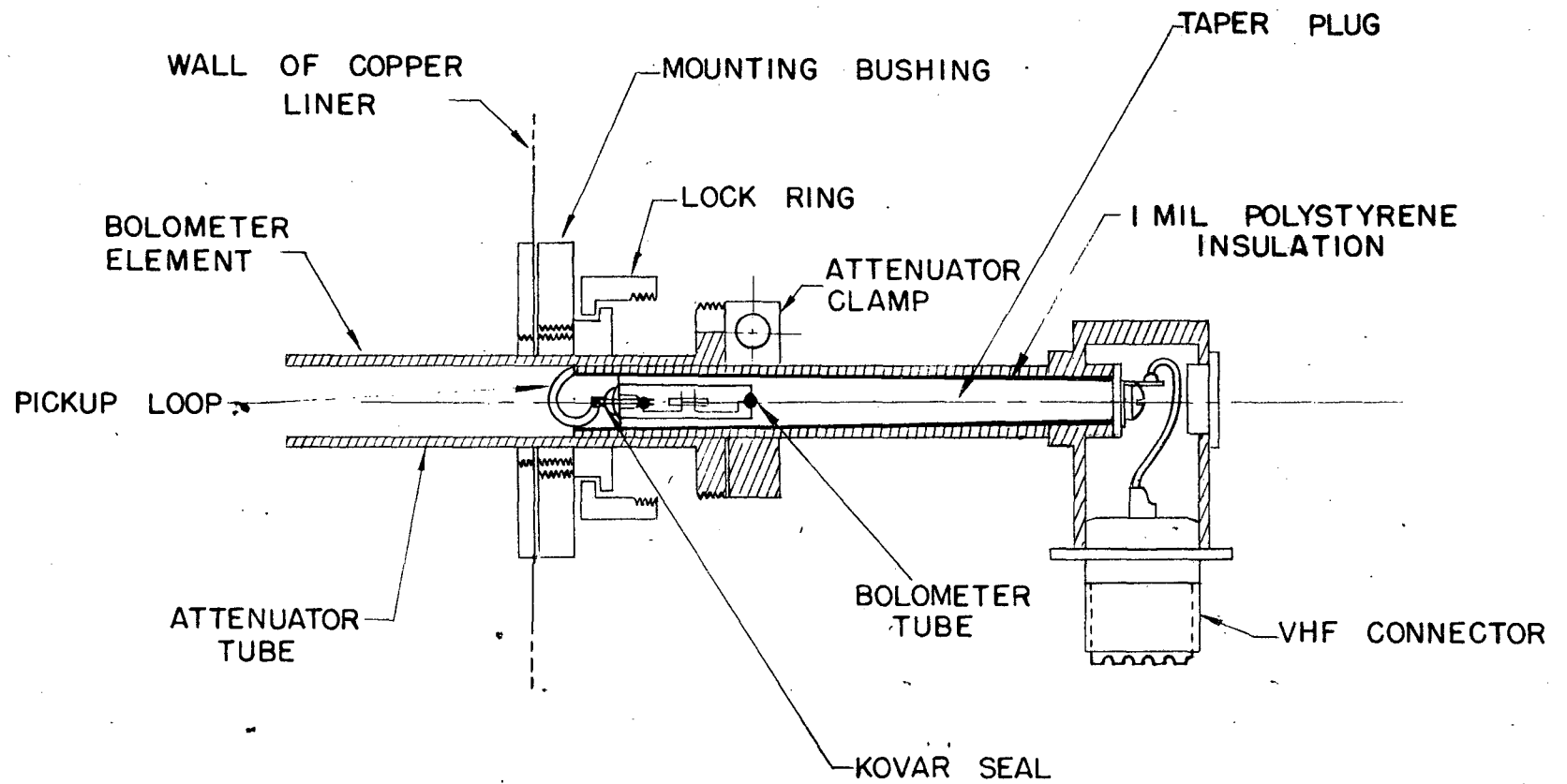
Fig. 49 Bolometer Schematic Wiring Diagram

ing in the wire.

Fig. 47 shows the basic circuit to operate a single bolometer. The bolometer element is a fine platinum fuse wire carrying a direct current, which gets heated by r.f. current pulses from the pick-up loop. The resistance of the platinum changes with the temperature, so the temperature change is reflected in a different IR drop in voltage at the point P. These voltage pulses are then amplified and measured on a peak voltmeter, the latter reading being proportional to the total r.f. energy per pulse; this is true because the thermal time constant of the bolometer is long compared to the pulse duration. Since the various bolometers which are to be used with the system have resistances varying as much as 30 percent, the load resistor R is made 100 times larger than the bolometer resistance (100 ohms) so that the current will always be the same, regardless of which bolometer is switched in.

Two kinds of pick-up were troublesome, namely 60 cycle a.c. and the 300 μ sec long video pulses fed to the transmitters. Both these arise from ground currents flowing from the oscillators to the steel tank; the video currents particularly cause magnetic fields which induce voltages of the order of tenths of a volt in any closed loop in the area. The solution was to install a preamplifier in a thick-walled steel box welded to the under side of the linear accelerator tank (see Fig. 48) in such a way that all leads from the bolometers to the preamplifier are shielded from the induction field by at least $1/4$ " of steel. The preamplifier chassis is heavily grounded to the inside of the box, so that currents flowing in the cable from the control rack to the preamplifier will not be carried to the bolometer cables. It was also necessary to thoroughly bond the copper liner to the steel tank by means of copper straps at both ends and in the middle of the cavity.

A block diagram of the entire system is shown in Fig. 49. The bolometer switching is done remotely by means of twenty individual relays, so that all low-level video lines stay within the shielding of the preamplifier. The preamplified pulse is put through a high-pass R-C filter at the control unit to get rid of 60-cycle pick-up, then it is amplified to about 100 volts and fed to the peak voltmeter. The pulses, shown on



00100605587

Fig. 50 Outline Drawing of Bolometer Probe

Fig. 33, have Fourier components only in the region from 3,000 to about 10,000 cycles so a great discrimination against 60 cycles is possible in the filter. A neon tube, shown at A in the preamplifier, is necessary to prevent capacitive surges from blowing out bolometer wires, during switching from one bolometer to the next.

Fig. 50 is a drawing of the bolometer probe assembly, showing it in relation to the cavity. The outer bushing is permanently screwed to the wall of the cavity, its function being to orient each probe correctly to the field inside the cavity. The bushing has a lock ring and an aligning pin to hold the probe in position. The probe consists of an attenuator tube with a bolometer tube which slides inside it, providing a waveguide beyond cutoff of adjustable length. The attenuation setting is locked by means of a screw and clamp, built into the right-hand end of the attenuator tube. The bolometer tube contains an r.f. pick-up loop, the bolometer element, and a tapered plug type of bypass condenser. The insulation around the plug is one mil thick polystyrene, which gives a capacity of 1,000 μfd .

The bolometer element is in a hole drilled in the end of the taper plug, and is hermetically sealed to contain one atmosphere of air. This prevents the element from having to operate surrounded by vacuum, which would give the bolometer wire a long thermal time constant. The time constant under 1 atmosphere pressure is about .05 seconds. The connection from the bolometer element to the pick-up loop is made through a small commercial Kovar-to-glass seal.

The calibration of the probes is done in such a way that any of the probes may be plugged into any one of the bushings on the linear accelerator liner, and give identical readings to within 5 percent in power. Fortunately, it turns out that we can excite a short copper cavity without drift tubes in air at the same high r.f. magnetic field as exists in the linear accelerator cavity during ordinary operation. This provides identically the same excitation for the bolometers as they would get in the linear accelerator tank, and so provides an ideal calibration. The test cavity is provided with two bushings and two bolometer amplifiers, one to monitor the power level and the other to calibrate an "unknown" bolometer probe. The regular bolometer amplifier system

for the linear accelerator is used for the latter. The calibration procedure is as follows:

1. The test cavity is excited to give approximately the same reading on a given bolometer as the same bolometer gives when installed in the linear accelerator. This level is then maintained by watching the monitor, while calibrating a whole set of probes.

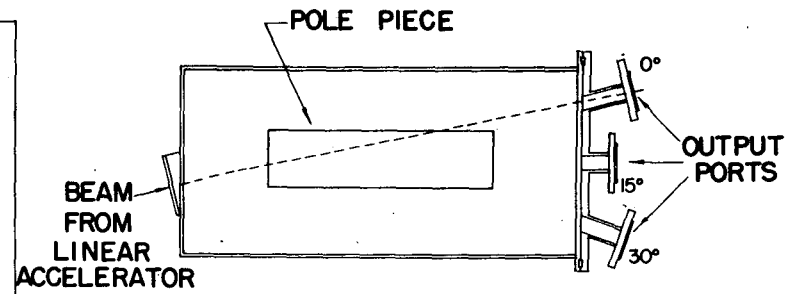
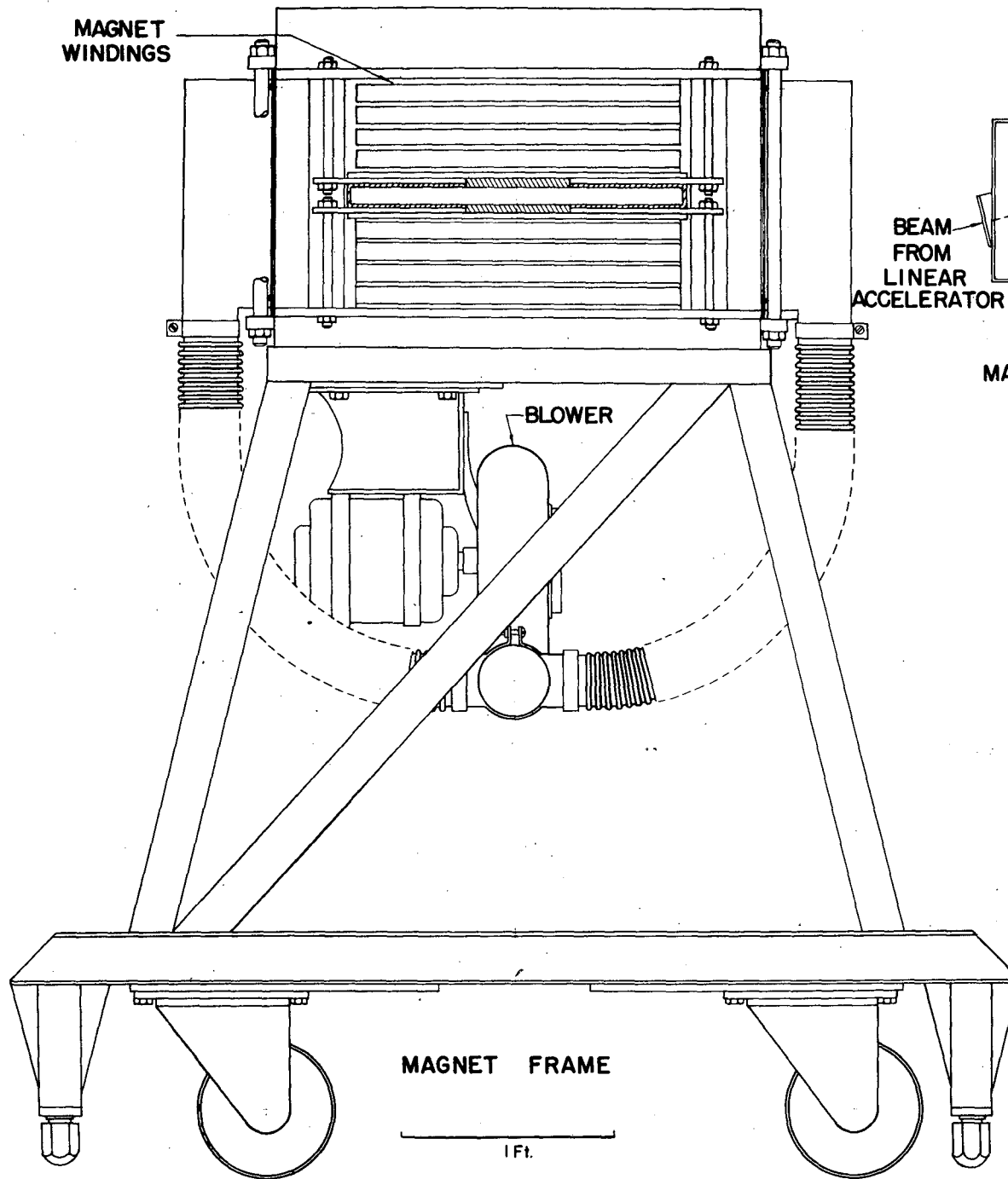
2. An unknown bolometer is installed in the second bushing, and connected to the amplifier. We now wish to determine roughly the power level at which the bolometer will operate. The criterion has been to operate at 5 percent of burn-out level, or at 20 percent of the level at which the probe characteristic deviates from square law. The latter point may be determined without destroying the bolometer, and hence was used as the reference point. To determine the characteristic, a bolometer probe is arranged so that it may be rotated relative to the r.f. magnetic field; in the square-law region, rotating the loop 45° from maximum gives exactly $1/2$ maximum reading on the meter. Having established the attenuator setting for the first bolometer, the gain control is now set to give a convenient reading (say 80 percent of full scale) and the other bolometers will be set for exactly this same sensitivity.

3. To calibrate the other bolometers, the gain setting is left at the value determined in (2) and each attenuator is set to give the same meter reading.

VIII. ACCESSORY EQUIPMENT

(1) Electron Catcher Magnet and Monochromatizing Magnet - The high axial r.f. electric fields existing in the resonant cavity can accelerate any free electrons, formed between drift tubes, to considerable energies, approximately 60 percent of the voltage across the gap. Electrons formed near the exit end of the No. 46 drift tube by secondary electron multiplication or gas ionization can be accelerated to an energy of 1.1 Mev. These electrons constitute an appreciable personnel hazard and also interfere with certain experimental equipment.

A small electromagnet, producing approximately 3,000 gauss between pole pieces $2\frac{1}{2}$ " in diameter and 2" apart, is provided to deflect these electrons vertically, so



MAGNET VACUUM CHAMBER

1 Ft.

MAGNET FRAME

1 Ft.

FIG. 38

FRONT VIEW OF BEAM ANALYZING MAGNET & PLAN VIEW OF MAGNET VACUUM CHAMBER

06550900100

that they strike a carbon cylinder, thus producing only soft x-rays which are absorbed in a three-inch-thick lead shield around the cylinder. This magnet can also be used for small-angle vertical steering of the proton beam.

(2) Monochromatizing magnet - An 8,000 gauss deflecting magnet is used to deflect the 32 Mev proton beam horizontally through an angle of 30° and thus separate it from the lower components of 4 and 8 Mev. The latter are produced by protons spending 2 r.f. cycles in each drift tube space. The magnet also removes the 16 Mev H_2 component if a $1/4$ mil aluminum stripping foil is inserted ahead of the field. This magnet has a plan view and cross section as shown in Fig. 38. Output ports are provided at the 0° , 15° , and 30° positions.

(3) Bombardment facilities - The facilities available at this time are the following:

4 Mev Beam - A 90° horizontal deflecting magnet inserted between the Van de Graaff generator and the linear accelerator permits use of either pulsed or d.c. proton beams up to approximately 4.5 Mev. Energy stabilization circuits for the Van de Graaff generator are not yet completed.

32 Mev Beam - Proton beam current monitors, consisting of r.f. shielded parallel plate ion chambers feeding into conventional d.c. amplifier circuits, are wired to indicate both at the bombardment area and the control board. Chambers with $1/4$ mil aluminum plates are used when it is desired to monitor ahead of the target. Solid backed ones are available for use when it is possible to monitor the beam after it has passed through the target. There are two amplifiers, each with range variable from 5×10^{-8} to 10^{-13} amps of protons with the ionization chamber.

A current integrating chamber has been specially constructed for absolute cross section experiments. Proton current is measured in a Faraday cup, and integrated either by a condenser or by an adjustable RC circuit which can be set to the same time constant as the half-life being investigated, and hence eliminates any error due to fluctuations in beam current.

Other Energies - Aluminum absorbers can be put ahead of the 30° horizontal deflect-

ing magnet, so that beams of energy less than 32 Mev can be obtained. The 30° deflecting magnet chambers can be removed, leaving a pole gap of 2", with pole faces 6" x 20" in which fields up to 9 kilogauss can be obtained. A 30-foot-long evacuated tube can be attached to the exit end of the machine to bring the beam out through a concrete wall in a region of reduced background. The beam there has increased in diameter to approximately 1/2 inch compared to 1/4 inch at the exit of the linear accelerator. Cloud chambers can be used at the end of the 30-foot pipe.

A special bombardment chamber has been constructed for the investigation of half-lives of a few seconds to a few minutes. The chamber which is a 2-inches thick lead house, contains the target holder, a thin-walled Eck and Krebs Geiger counter, and a parallel plate ion chamber to monitor the beam. Provision is made for flowing helium through the chamber. Provision is also made for placing absorbers in the beam, to vary the incident proton energy.

There is a special bombardment chamber for investigating absorption of β 's from short-lived emitters. It consists of a target holder and parallel plate beam monitor functioning like the lead house mentioned above, but having two thin walled Geiger tubes approximately equally spaced 1 inch from the "count" position of the target. Absorbers can be placed in front of one Geiger tube, while the other serves as monitor of the target activity.

An automatic sequence circuit* which controls the operation of the two chambers mentioned above has been constructed. It activates a solenoid to place the target in the beam for a predetermined time, then swings it over adjacent to the counter, and records the counts on one pen of a Brush recorder for a predetermined length of time. The other pen of the recorder gives 1/15 second and 10 second time marks or records a second Geiger counter. The automatic circuit can be switched to turn off the linear accelerator at the beginning of the counting period, in order to reduce the counter background.

* Constructed by Mr. Donald R. Cone.

Delayed gate circuits, giving an "on" time adjustable in width from 0 to 1,000 microseconds and delayed from 0 to 1/15 seconds after the r.f. pulse are available for study of very short half-lives.

IX. PERFORMANCE

(1) Voltage - The output voltage of the linear accelerator has been measured by:

(a) Total range measurement in aluminum, using the range energy relation as computed by Smith²⁰); (b) Absorbing the beam²¹) from the output of the accelerator to the threshold of the reaction $B^{11}(p,n)C^{11}$ which is accurately known²²); and (c) By measuring the threshold²¹) of the reaction $C^{12}(p,d)C^{11}$ and correcting for barrier effect. All these measurements are in excellent agreement and give

$$32.0 \pm .1 \text{ Mev}$$

as the central energy of the beam when the machine is operated in the normal manner. It was shown that shifts up to 150 Kev could be produced by operating the oscillators at an abnormally high value.

The energy spread of the beam can only be inferred at present from the sharpness of the threshold of the reaction²¹) $C^{12}(p,d)C^{11}$. When the resulting excitation curve is corrected for barrier and absorber straggling, the R.M.S. energy width of the beam can be shown to be

$$\Delta E < 100 \text{ Kev}$$

In addition to the principal 32 Mev beam, there are two other beam components (usually removed by the analyzing magnet, Section VIII).

a) 16 Mev H_2^+

b) 8 Mev H^+

caused by particles spending two r.f. cycles in each drift tube space.

(2) Current - Present output current of the machine as observed by the current integrals (Section VIII) and check of the absolute cross section²³) of $C^{12}(p,pn)C^{11}$ is approximately 4×10^{-9} amps. This is accounted for as follows:

a) Injection current: 50 μA

b) Phase angle loss: 15

- c) Grid loss: 2.5
- d) Effective duty cycle: 300

Improvement in this figure is anticipated, due to: a) Ion source improvements; b) Grid redesign; c) Bunching of ion beam prior to entering the linear accelerator; d) Improved duty cycle.

(3) Beam geometry - About 85 percent of the beam will pass through a circular hole 1/8 inch in diameter. The beam divergence is 10^{-3} radians.

(4) Reliability - The mean tube life of the 434-A tubes when used in the accelerator has been 300 hours, corresponding to one tube change per three hours of bombardment time. Since the time loss for the exchange of an oscillator for tube repair is less than 2 minutes, this has not resulted in appreciable time loss. There have only been three openings of the tank for repairs involving leaks, etc., during the first year of operation.

X. ACKNOWLEDGMENTS

The design and construction of the linear accelerator was in every sense a cooperative affair, and contributions from a large number of men are involved. The list of authors of this article has been arbitrarily restricted to those who had the responsibility for the major design features, and who were members of the group for the period of two years during which the most intensive work was done. (The first 32 Mev beam was observed less than two years after the decision to build the machine, and another six months elapsed before reasonably steady operation was reached. At the moment, the beam is used on the average of 12 hours per day.) Much of the work was done by graduate students in the Department of Physics, and major contributions were made by the electrical and mechanical design groups of this laboratory.

We are indebted to Professor E. O. Lawrence for encouraging us to embark on the project. The Manhattan District of the U.S. Army Engineers gave us strong backing in the early days, and the Atomic Energy Commission continued this support. The Signal Corps generously donated large quantities of radar equipment, without which we probably would not have been able to build the accelerator.

Dr. Lauriston C. Marshall and Dr. Frank Oppenheimer contributed greatly to the success of the project, but had to leave the work before the machine was in operation. Mr. William Baker is responsible for the redesign of the radar oscillators, without which there is a good possibility that the accelerator would never have produced a beam. In this work, he was ably assisted by Jack Frank and Donald Gow. Among the graduate students, special acknowledgments must be made of the valuable electronic contributions of Lawrence H. Johnston, Robert Mozley, Bruce Cork, Ernest Martinelli, Robert Phillips, Lee Aamodt, Thomas Parkin, Richard Shuey, William Toulis, Val J. Ashby, and Donald R. Cone. In the field of mechanical design, the following made important contributions: A. W. Chesterman, A. E. Kaehler, E. A. Day, R. L. Olson, D. A. Vance, Virginia McClain, Florence Mosher. The laboratory Electrical Design Group was of the greatest assistance, and we would like to acknowledge the work of Saul Lissauer, J. C. Kilpatrick, Walter Sessions, Porter Evans, and C. A. Harris.

A group of former radar technicians played an important role in the building of the machine, and some of these men are operating and servicing it at the present time. We wish to thank especially Phillip Carnahan, Albert J. Bartlett, Alva Ray Davis, Jr., Wilfred P. Kimlinger, James A. McFaden, Wendell W. Olson, and Frank Grobelch. Finally, we wish to acknowledge the important contributions in various fields, of Dr. Robert Serber, who developed the mathematical theory of beam stability, Richard Crawford, David Garbellano, Velma Turner, Leonard Deckard, and Craig Nunan.

REFERENCES

- 1) Sloan and Lawrence, Phys. Rev., 38, 2021, 1931.
- 2) Kinsey, Phys. Rev. (A), 50, 386, 1936, and private communication.
- 3) Sloan, W. J., Patent No. 2,398,162.
- 4) Hansen, R.S.I., 19, 89, 1948.
- 5) McMillan, Phys. Rev., 68, 1943, 1945.
Veksler, Journ. Phys. U.S.S.R., 9, 153, 1945.
- 6) Slater, L. C., Rev. Mod. Phys., 20, 473, 1948.
- 7) Bradner, H., R.S.I., 19, 662, 1948.
- 8) Serber, R., Phys. Rev. (A), 73, 535, 1948.
- 9) Sperry Gyroscope Co., "Microwave Transmission Design Data."
- 10) Oppenheimer, F., Johnston, L. H., Richman, Chaim; Phys. Rev. (A), 70, 447, 1946.
- 11) Slater, L. C., Microwave Electronics, Rev. Mod. Phys., 18, 441, 1946, Section 7.
- 12) Gabor, Nature, 159, 303, 1947.
- 13) Smythe, "Static and Dynamic Electricity," McGraw-Hill, 1939.
- 14) Schneider, E. G., "Radar," Proc. I.R.E., Vol. 34, No. 8, Pg. 536-540.
- 15) Glasce, G. N., Lebacqz, J., "Pulse Generators," McGraw-Hill, 1948.
- 16) Radiation Laboratory, MIT, "Colloquium on Pulse Forming Networks," Report No. 692, March 14, 1945.
- 17) Shuey, R. L., "Pulse Forming Networks of Non-uniform Voltage Output," M.S. Thesis, Department of Electrical Engineering, University of California.
- 18) Puckle, "Time Bases," Wiley, 1943.
- 19) Creveling and Mautner, Proc. I.R.E., 35, 208, 1947.
- 20) Smith, J. H., Phys. Rev., 71, 32, 1947.
- 21) Panofsky, W. K. H., and Phillips, R., Phys. Rev., 74, 1732, 1948.
- 22) Haxby, Shoupp, Stephen, and Wells, Phys. Rev., 58, 1035, 1940.
- 23) McMillan and Miller, Phys. Rev., 73, 80, 1948.

This report was done with support from the Department of Energy. Any conclusions or opinions expressed in this report represent solely those of the author(s) and not necessarily those of The Regents of the University of California, the Lawrence Berkeley Laboratory or the Department of Energy.

TECHNICAL INFORMATION DEPARTMENT
LAWRENCE BERKELEY LABORATORY
UNIVERSITY OF CALIFORNIA
BERKELEY, CALIFORNIA 94720